METHODS OF WIDEBAND SIGNAL DESIGN FOR RADAR AND SONAR SYSTEMS

by

Richard A. Altes

DISCLAIMER NOTICE

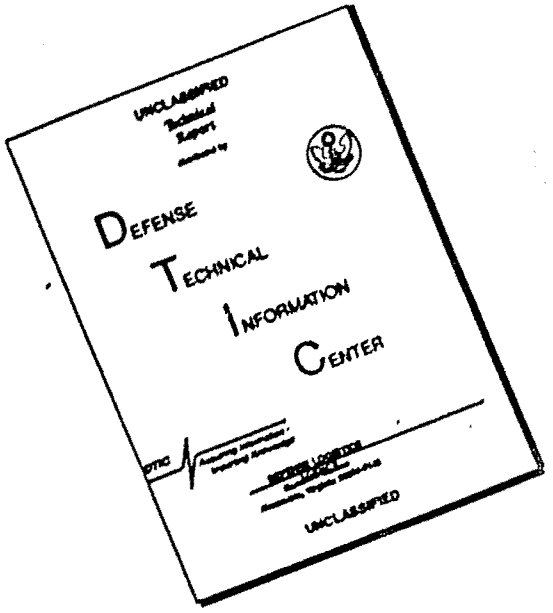

THIS DOCUMENT IS BEST QUALITY AVAILABLE. THE COPY FURNISHED TO DTIC CONTAINED A SIGNIFICANT NUMBER OF PAGES WHICH DO NOT REPRODUCE LEGIBLY.

Statement A per R. Todd, Naval URDC. No contract involved,
11 Oct 71

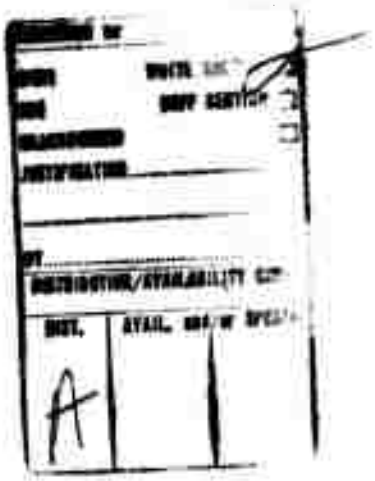

METHODS OF WIDEBAND SIGNAL DESIGN FOR RADAR AND SONAR SYSTEMS

by

Richard Alan Altes

Submitted in Partial Fulfillment
of the
Requirements for the Degree

DOCTOR OF PHILOSOPHY

Supervised by Edward L. Titlebaum
Department of Electrical Engineering
The University of Rochester
Rochester, New York

1970

VITAE

The author was born [redacted]. He attended Cornell University from 1959 to 1965, receiving a B.E.E. degree in 1964 and an M.E.E. degree in 1965. He is a member of Tau Beta Pi and Eta Kappa Nu.

PII Redacted

Mr. Altes first matriculated at the University of Rochester in 1965 for the purpose of earning an advanced degree in biomedical engineering. After receiving an M.S. degree in 1966, he took a fourteen-month leave of absence. During his absence from Rochester, he worked for the Raytheon Company Equipment Division and the Raytheon Company Research Division, both in Massachusetts. He returned to Rochester in 1967 as an advisee of Dr. E. L. Titlebaum. His graduate work was supported by NASA Traineeships and by a research assistantship from the Naval Undersea Research and Development Center. In 1969, Mr. Altes married [redacted]

PII Redacted

ACKNOWLEDGMENTS

The author wishes to express his appreciation to his wife, [redacted]; to his advisor, Edward L. Titlebaum; and to his parents. He is also grateful to Aristedes Requicha and L. R. Morris for their helpful advice concerning computer programming, and to J. J. G. McCue and D. R. Griffin for their detailed responses to his inquiries concerning bats.

The author acknowledges the financial support of the National Aeronautics and Space Administration and the Naval Undersea Research and Development Center.

PII Redacted

ABSTRACT

The radar problem is generalized to wideband signals and receivers. This generalization necessitates consideration of a wideband ambiguity function and of distributed targets. System design methods, using newly-discovered properties of the wideband ambiguity function, the trajectory diagram, and computerized clutter suppression techniques, are established. The application of these methods, combined with distributed target and accelerating target considerations, reveals signals that are optimally tolerant to doppler, acceleration, and distributed target effects. These signals are compared with those used by several species of bats.

TABLE OF CONTENTS

LIST OF FIGURES

LIST OF TABLES

"One walks step by step into the darkness. The motion itself is the only truth."

Ingmar Bergman, The Magician

"We set out from a dark point, we proceed toward another dark point--honest, clean, good--and are consoled."

Nikos Kazantzakis, in a letter to his first wife

"He can see in the dark--no small power this, in a world which is one-half shut from the light."

Bram Stoker, Dracula

CHAPTER I

INTRODUCTION

1.1 General Statement of the Problem.

This dissertation considers a fundamental question of radar or active sonar system design:

For a given environment and system constraints, what is the best signal-filter pair to use in order to gain information about an object via its echo?

It will be worthwhile to examine the meaning of this question in some detail.

The "environment" refers to the channel through which the signal must propagate and to all possible spurious echoes that can occur when the target is surrounded by wave-reflecting "clutter" or is located in a reverberation-prone setting.

"System constraints" are the limitations inherent in any physical system. An example is found in bats; by virtue of finite lung capacity, bat waveforms are subject to a constraint on signal energy. Other examples might be maximum power, mean square bandwidth, and system noise level.

The word "best" can be translated into many mathematical measures of "goodness" such as minimum mean square error, maximum signal to interference ratio, or maximum probability of detection for a given false alarm probability.

The signal is a transmission used to induce echoes. The filter is a system designed to receive these echoes and to process them in such a way as to extract information descriptive of a target (including its presence or absence). A "signal-filter pair" (as opposed to a signal or filter taken alone) is considered because of the inherent dependence of the receiver upon the signal which it is designed to process. This is why the discipline of radar signal design might justly be called "radar system design".

"Information" not only includes the inevitable question about the presence or absence of the target (detection), but may also include acquisition of knowledge about the shape or number of targets present (range resolution), their speeds (velocity resolution) and even higher time derivatives of range (acceleration, etc.).

Finally the "object" or target is an important part of any problem specification. The cross-sectional area of an object determines what frequencies are needed in order to receive a strong return (above the Rayleigh scattering region). The depth or range-extent of an object determines whether it can be treated as a point target (negligible thickness in range) or whether it must be treated as a distributed target. Finally, if the target is indeed distributed in range, one must consider the dependence of reflected energy and power upon the transmitted waveform.

The fundamental question, although simply phrased, is thus seen to contain many nuances and complications. The various complications and their effects on the problem will be the major topics of discussion.

1.2 The Correlation Process.

It has been demonstrated [1,2] that a correlation process is a sufficient statistic for the detection of a signal in additive white Gaussian noise. Thus, if a detector correlates all received signals with the waveform that was transmitted (or a hypothetical version of the echo), the result of this correlation can be used as the basis for a decision concerning the presence or absence of the target (likelihood ratio test).

If the transmitted waveform is u(t) and the received waveform is r(t), then the correlation between the two signals is

$$\int_{-\infty}^{\infty} u(t)\, r^*(t)\, dt \tag{1.1}$$

where the asterisk indicates complex conjugation. It is assumed throughout this dissertation that the filter used to receive radar-sonar echoes performs a correlation operation.

1.3 The Wideband Assumption and the Waveform Design Problem.

In contrast to much past radar research, the signals used in this thesis are not necessarily confined to a small band of frequencies around a large carrier frequency. That is, signals are not narrowbanded per se. This departure from previous work is motivated by the recent development of wideband radar and sonar systems.

An immediate consequence of the wideband assumption is that the effect of target velocity can no longer be approximated by a simple translation or "shift" in frequency. The doppler effect is, in reality, a compression

(or stretching) of the signal, mathematically described by a scale factor in time or frequency. This more general model of the received signal r(t) results in a version of Equation (1.1) that is different from the correlation of narrowband waveforms using a "doppler shift" assumption.

The new version of Equation (1.1) for constant velocity point targets is known as the wideband ambiguity function. It is a function of two variables, range and velocity, and is a mathematical description of the behavior of a radar-sonar system for a particular signal-filter pair. Specifically, the ambiguity function describes the reaction of a correlation processor to all possible delayed and doppler compressed versions of the transmitted signal. It therefore determines the ability of a radar system to unambiguously measure range and velocity of a given target, to recognize a time-scaled version of the transmitted signal, to resolve targets on the basis of their differing ranges and/or velocities, and to distinguish a target within a cluttered environment.

If the ambiguity function is indeed descriptive of the above system capabilities, its characteristics should be studied. The relations between these characteristics and signal parameters (such as various time-spectral moments) are particularly important. Properties of the wideband ambiguity function are therefore investigated in Chapter III.

The analysis in Chapter III is first concerned with a Taylor series expansion of the wideband function about the origin of the range-velocity plane. This expansion reveals origin properties that are particularly relevant

to discussions of signal resolving capability. A comparison of wideband origin properties with their narrowband counterparts helps to illustrate the nature of the narrowband assumption. The relation between wideband and narrowband ambiguity functions is then made even more explicit by the derivation of an integral transformation between them. Volume properties are studied. The effect upon the wideband function of certain fundamental operations on the signal (e.g., time scaling, differentiation) are investigated. The behavior of the function along certain curves on the range-velocity plane is written in terms of autocorrelation functions. Symmetry and separability properties are discussed. Finally, the consequences of narrowbandedness (i.e., ambiguity function dependence upon the ratio of signal bandwidth to carrier frequency) are examined from a wideband viewpoint.

All of the above properties are investigated in Chapter III; not all of them are used in the sequel, but they are included for completeness. The reader may therefore wish to skip Chapter III on first perusal, since subsequent chapters refer back to previous results as they are utilized.

It is easy to casually observe that radar system capabilities depend upon the ambiguity function; it is more difficult to mathematically define the desired capabilities in such a way as to derive an optimal signal-filter pair. It is therefore important to demonstrate how ambiguity function characterization can be used to derive signal-filter functions that satisfy a particular need. Such a demonstration is given in Chapter IV, where the desired property is designated to be doppler tolerance. A doppler tolerant signal is

defined as one which, when correlated with a time-scaled (energy normalized) version of itself, produces a maximum correlator response which is nearly as large as that obtained by autocorrelation.

As already indicated in Section 1.1, constant velocity point targets alone in space do not exemplify most practical radar-sonar problems. The interaction of a signal with accelerating targets, distributed targets, and reverberatory (or cluttered) environments must be considered. These problems are investigated in Chapters V and VI. In Chapter VI, optimal signal-filter pairs are again derived, this time using a computer algorithm for clutter suppression (with wideband waveforms).

A useful description of signal-target interaction is found in Altar's trajectory diagram. These diagrams are applicable not only to modelling echoes from point targets with nonlinear trajectories; they are also descriptive of general time-varying-delay effects, and can be used to depict the echoes of certain distributed targets (viz., those that can be represented as arrays of point targets). Each of these applications is investigated in its appropriate context.

CHAPTER II

CONSTANT VELOCITY POINT TARGET: MODELS OF THE RETURNED SIGNAL AND CORRESPONDING VERSIONS OF THE AMBIGUITY FUNCTION

In order to utilize the sufficient statistic (1.1) one must have an expression for r(t), the received signal, in terms of the transmitted waveform u(t). In general, r(t) will depend not only upon u(t) but also upon the environment, the shape of the target, and how the target is moving. In this chapter exceedingly simple assumptions are made concerning these echo-determining factors.

Assume first that the environment is free of clutter (spurious reflections) and that the channel contributes no signal distortions other than additive white Gaussian noise. Secondly, assume that the object is a point target. The point target assumption insures that a perfect replica of the transmitted signal would be reflected from the object if it were held motionless. This implies not only negligible thickness in range but also a large reflecting area (relative to maximum signal wavelength) so that reflectivity is not frequency dependent. Finally, the point target is assumed to be moving at a constant velocity (or not moving at all).

The situation described by the above assumptions is admittedly oversimplified, but it provides a basis for the consideration of more complicated problems that will be discussed later.

2.1 The Narrowband (Woodward) Model.

In addition to the assumptions already set forth, P.M. Woodward [1] also assumed that the transmitted signal was narrowbanded. That is, practically all of the signal energy is assumed to be contained in a narrow range of frequencies distributed around the carrier frequency. The carrier frequency (defined here as the centroid of the analytic signal's power spectral density function) is many times greater than the width of the frequency band within which almost all the signal's energy is to be found.

Under these conditions, the echo has the form:

$$r(t) = u(t + \tau) \exp(-j \phi t) \tag{2.1}$$

where $\tau \equiv$ negative of time delay

and $\phi \equiv -(2 \omega_o v)/\tilde{v}$ = frequency "shift" caused by the doppler effect.

The narrowband idea is so prevalent in introductory physics that one usually hears the effect of target velocity described as a " doppler shift".

In the foregoing definitions, ω_o is carrier frequency in radians, $\tilde{v}$ is speed of signal propagation and v is radial component of target velocity ($v = -\dot{R}$), taken to be positive for motion toward the receiver and negative away from it.

Almost all radar signal design has been concerned with the narrowband model until quite recently. As a result, a great many properties are known for the corresponding correlation response (or ambiguity function):

$$\chi_{uu}^{(1)}(\tau, \phi) = \int_{-\infty}^{\infty} u(t)\, u^*(t + \tau)\, e^{j \phi t}\, dt. \tag{2.2}$$

Many of these properties have been summarized in a recent book by C. E. Cook and M. Bernfeld [4]. Although a discussion of ambiguity function properties should be relegated to the next chapter, one rather important characteristic will be mentioned here for motivation purposes: The ability of a signal to resolve between two point targets with slightly different ranges and/or velocities is dependent upon the signal's time-bandwidth product. In particular, accurate range resolution is associated with large bandwidth. One therefore expects the designer of sophisticated high-resolution radar signals to become dissatisfied with the narrowband assumption as available system bandwidth increases. At the same time, sonar signals must violate the narrowband assumption quite often, since the carrier frequencies involved are on the order of 10^{+4} to 10^{+8} lower than those used for radar. More will be said about this in Chapter III.

2.2 The Wideband (Kelly-Wishner) Model.

A 1965 paper by E. J. Kelly and R. P. Wishner [5] has led to a generally accepted version of the ambiguity function for wideband signals. For uniform-velocity point targets the Kelly-Wishner argument may be phrased as follows:

The returned signal is $v(t) = u(t - \tau(t))$ before energy normalization. Consider the differential part of signal (or the "photon") that returns at

time $t - \tau(t)$; this bit of signal must have been reflected from the target at time $t - \tau(t)/2$. But the range of the target at the time of reflection is $\tilde{v}\tau(t)/2$, by definition. That is,

Range of target at time of reflection

$$= R(t - \tau(t)/2)$$

$$= \tilde{v}\tau(t)/2 \qquad (2.3)$$

Expanding $\tau(t)$ in Taylor series about some reception time t_o and expanding $R(t)$ about the corresponding reflection time $t_o/2$ gives

$$\tau(t) = t_o + \zeta(t - t_o) \qquad (2.4a)$$

$$R(t) = R(t_o/2) - v(t - t_o/2) \qquad (2.4b)$$

where the higher order terms in the expansion are zero by the assumption of uniform target velocity. Notice that

$$\tau(t_o) = t_o \; ; \quad \dot{\tau}(t_o) = \zeta \; ; \quad \dot{R}(t_o/2) = -v \; . \qquad (2.5)$$

Substituting (2.5) into (2.3) yields $\tilde{v}t_o/2 = R(t_o/2)$.

Differentiating (2.3) with respect to t:

$$\tilde{v}\dot{\tau}(t)/2 = (1 - \dot{\tau}(t)/2)\dot{R}(t - \tau(t)/2) \; . \qquad (2.6)$$

Evaluating (2.6) at $t = t_o$ by using (2.5):

$$(\zeta/2)(\tilde{v} - v) = -v \; ; \quad \zeta = (-2v)/(\tilde{v} - v) \; . \qquad (2.7)$$

Notice that

$$t - \tau(t) = t - t_o - \zeta(t - t_o) = (1 - \zeta)(t - t_o), \tag{2.8}$$

so that

$$\begin{aligned} r(t) &= u(t - \tau(t)) \\ &= u[(1 - \zeta)(t - t_o)] \\ &= u\left[\frac{\tilde{v} + v}{\tilde{v} - v} \cdot (t - t_o)\right] \\ &= u[s(t - t_o)] \quad . \end{aligned} \tag{2.9}$$

Here s, which will be called the "doppler stretch (or compression) factor," equals $(1 + \beta)/(1 - \beta)$, where $\beta = v/\tilde{v}$.

Since the derivation of the correlation process is based upon the assumption that all signals are normalized to some energy, one must multiply u(st) by the factor $s^{1/2}$:

$$E = \int_{-\infty}^{\infty} |u(t)|^2 dt = \int_{-\infty}^{\infty} |s^{1/2} u(st)|^2 dt. \tag{2.10}$$

The resulting ambiguity function is then:

$$\chi_{uu}^{(2)}(\tau, s) = s^{1/2} \int_{-\infty}^{\infty} u(t)\, u^*[s(t + \tau)]\, dt. \tag{2.11}$$

2.3 Description of the Returned Signal Obtained from Altar's Trajectory Diagrams.

In Chapter 11 of his book, Rihaczek [6] introduces the Altar trajectory diagram* as a useful concept for qualitative visualization of the interaction between signal and point target. It will be shown, however, that the trajectory

diagram can be used to obtain quantitative results as well. This idea will be further discussed in Chapter IV. For now, the trajectory diagram is introduced as a graphical method to derive the doppler stretch factor, s.

The trajectory diagram of a point target is a plot of target range (in seconds) versus measured time lapse between transmitted and received signals. If range as a function of time is written R(t), then the trajectory of the target is traced out on the graph of $R(t)/\tilde{v}$ versus t, as shown in Figure 2.1 for a constant velocity target.

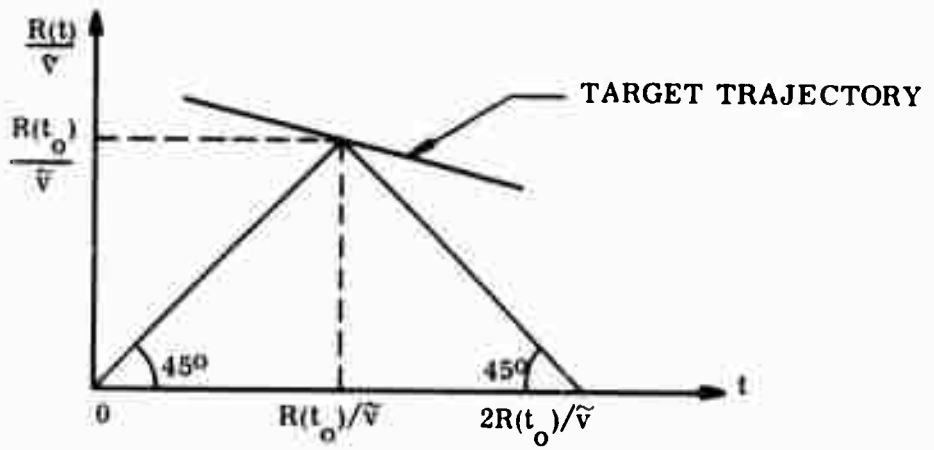

Figure 2.1. Trajectory Diagram for a Single "Photon".

---

* The author has tried to obtain Altar's original paper, but at the time of his inquiry it was still classified "Confidential."

With reference to Figure 2.1, consider a "photon" of energy radiated toward the target at t= 0. The time taken for this photon to reach the target is $R(t_o)/\tilde{v}$, so that the reflected photon is received after a time $2R(t_o)/\tilde{v}$. Here, t_o is the instant at which the photon is reflected. Thus $t_o = R(t_o)/\tilde{v}$. The "path" of the photon on the trajectory plot may therefore be represented as the legs of a 45^o right triangle with apex at the trajectory, as shown by the construction lines in Figure 2.1.

The trajectory diagram of Figure 2.1 can be used to show that the doppler stretch factor is $(1 + \beta)/(1 - \beta)$, where $\beta = v/\tilde{v}$. The argument is as follows.

Consider two photons transmitted at t = 0 and $t = t_1$, respectively. The construction lines associated with these two photons are shown on the trajectory diagram of Figure 2.2.

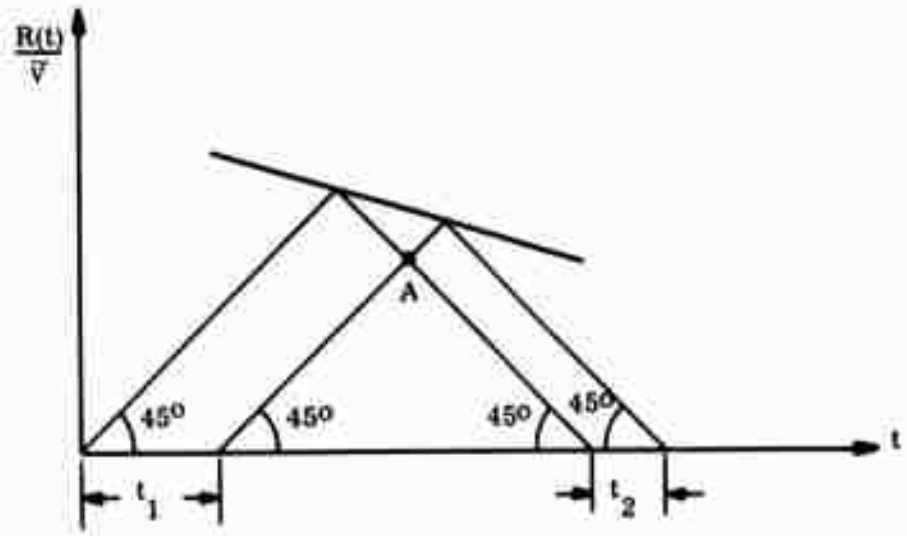

Figure 2.2. Trajectory Diagram for Two "Photons".

If $t_1 = st_2$, then what is s? To answer this question, draw a more detailed picture of the trajectory (Figure 2.3) with a horizontal line through the point A on Figure 2.2.

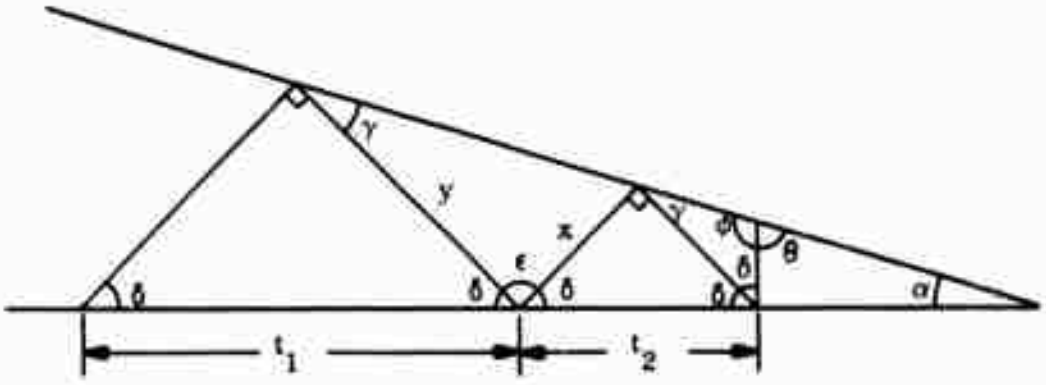

Figure 2.3. Trajectory Diagram Determination of the Doppler Factor, s.

From the trajectory diagram and the 45^o construction lines, it is evident that $\delta = 45^o$ and $\epsilon = 90^o$, where δ and ϵ are angles as shown in Figure 2.3. Furthermore, the slope of the trajectory $= -\dot{R}/\tilde{v} = v/\tilde{v} = \beta = \tan\alpha$. Since the sum of the interior angles of a triangle must be 180^o, it follows that $\theta = 90^o - \alpha$. But $\phi + \theta = 180^o$, so $\phi = 90^o + \alpha$. From this it follows that $\gamma = 180^o - \delta - \phi = 45^o - \alpha$. Since x is one leg of a 45^o right triangle with hypotenuse t_2, it must be that $x = t_2/2^{1/2}$. Similarly, $y = t_1/2^{1/2}$. But $x/y = \tan\gamma$; $\tan(45^o - \tan^{-1}\beta) = x/y = t_2/t_1$. Now

$$\tan(A+B) = (\tan A + \tan B)/(1 - \tan A \cdot \tan B)$$

so that

$$s = 1/\tan(45^o - \tan^{-1}\beta) = (1+\beta)/(1-\beta) .$$

Trajectory diagrams yield a description of the reflected waveform in terms of easily recognized attributes of the signal. Examples of easily recognized attributes are the signal's zero crossings (real zeros), its maxima and minima (zero crossings of its first derivative), etc. Figure 2.4 illustrates a trajectory diagram derivation of reflected real zero locations, given the transmitted signal and the target trajectory.

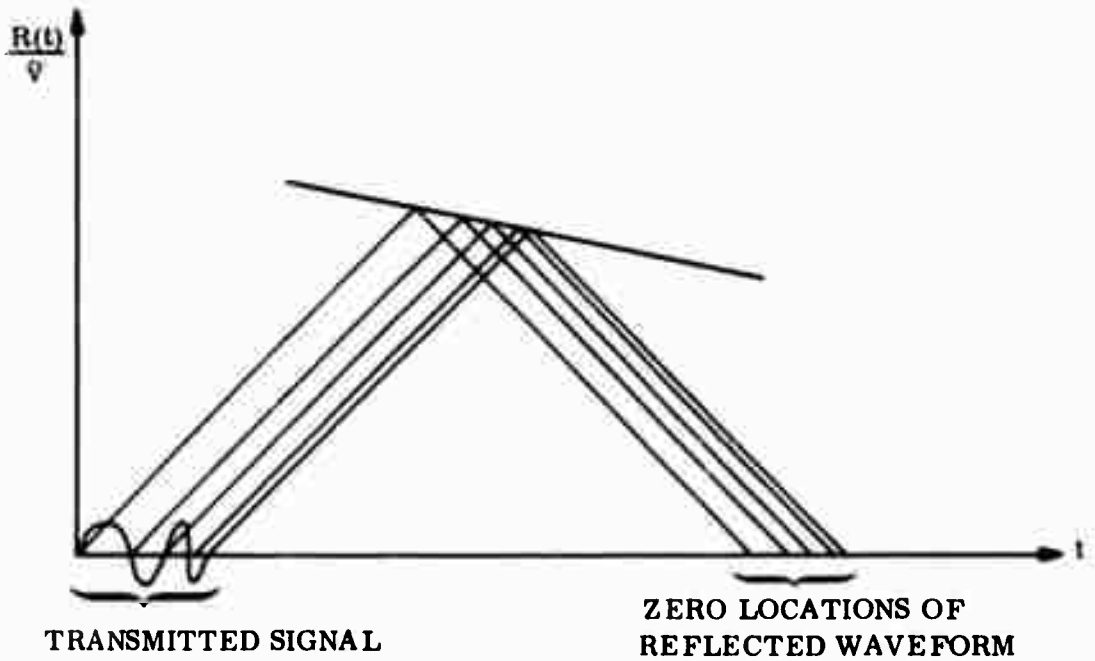

Figure 2.4. Trajectory Diagram for an Arbitrary Signal.

2.4 Another Version of the Ambiguity Function.

There is one model of the received signal that has not yet been mentioned. This model leads to a wideband ambiguity function that has often appeared in the literature [7,8,9]. It conceives of the energy-normalized echo as

$$r(t) = s^{1/2} u(st - t_o) \tag{2.12}$$

where t_o corresponds to the delay of the first transmitted photon. Then

$$\chi^{(3)}_{uu}(\tau, s) = s^{1/2} \int_{-\infty}^{\infty} u(t)\, u^*(st + \tau)\, dt \quad . \tag{2.13}$$

The three versions of the ambiguity function will be compared and discussed in future chapters. A table summarizing the above definitions is to be found in Section 3.1.

III. Properties and Interrelationships of the Various Versions of the Ambiguity Function

The constant velocity point target ambiguity function is in fact a correlation of hypothetical and actual target returns. The hypotheses are in this case limited to range and target velocity. If a given mismatch between guessed and actual parameters results in a small correlator response (compared with the response to a correct guess), then the system will be sensitive to such an error and will be capable of resolving between point targets whose ranges and velocities differ by the given amount. On the other hand, if the mismatch results in a correlator response that is nearly as large as that obtained for a correct guess, the system will be incapable of determining whether the parameter hypotheses were indeed correct. Even so, a large correlator response to a poor guess will at least inform the radar of a target's presence.

To always detect a target (regardless of its range and velocity) one must use a whole set of correlators such that at least one correlator has a large response (exceeding a threshold that is set in accordance with a given false alarm probability) for each point on the range-velocity plane.*

---

* If the correlators are realized as matched filters, then a continuous or running hypothesis on time delay is automatically implemented. For this case, at least one matched filter should have a large response (exceeding threshold) for every possible target velocity.

An excellent resolving signal (with what is visualized as a "thumb-tack" ambiguity function, i.e., with a small correlator response to all bad guesses) will therefore require many correlators for foolproof target detection. The price of resolution capability is thus paid in system complexity.

The above considerations are introduced in order to illustrate the dependence of radar-sonar system capability upon ambiguity function characteristics. In order to intelligently design a radar system that uses correlation processing, it is necessary to determine the behavior of the ambiguity function in terms of hypothetical and actual target parameters. This behavior, in turn, is generally dependent upon the signal waveform.

The purpose of this chapter is to amass knowledge about the ambiguity function and about any signal characteristics that can alter the behavior of this function in some straightforward fashion. The chapter is organized as follows:

After finding expressions for (τ, s) in terms of hypothetical and actual target parameters, the behavior of the ambiguity function, in the neighborhood of an accurate hypothesis, is examined via a two dimensional Taylor series. This examination reveals the dependence of resolution capability upon certain time-spectral moments of the signal. Important similarities between the wideband and narrowband functions are then demonstrated, and an integral transformation between the two functions is derived. Ambiguity volume is also found to depend upon the signal's time-spectral moments, particularly mean-square time duration and carrier frequency. Some signal

transformations are then investigated to reveal their effects upon the ambiguity function. It is demonstrated that, when the ambiguity function is evaluated along certain curves in the (τ,s) plane, it can be written as an autocorrelation function. Separability tests are then discussed; such tests are important to determine whether a given function (perhaps suggested as an ideal ambiguity function for a given situation) is indeed an ambiguity function. Finally, the dependence of wideband ambiguity function behavior upon the ratio of bandwidth to carrier frequency (and the ratio of timewidth to mean time) is investigated.

5.1 Hypothesis Testing

The argument leading to the correlation process (1.1) is generally applicable to the detection of a known signal $u(t)$ immersed in additive white noise: $r(t) = u(t) + n(t)$. In many radar/sonar problems, however, certain parameters of the received signal are unknown a priori. For the simple case of a constant velocity point target, the range parameter τ and the Doppler factor s are, in general, unknown. The known signal $u(t)$ then actually becomes a guessed or hypothesized signal to be correlated with received data $r(t)$, and the magnitude of correlator response is indicative of the goodness, in the sense of maximum a posteriori estimation, of the guess. If the signal is such that the ambiguity function is negligible for a bad guess, then correlation of received data with a bad guess will not even indicate the presence of the target.

As a result of this uncertainty concerning the echo, it behooves the radar system to make many simultaneous guesses about target parameters. The signal corresponding to each guess would then be correlated with received data. The largest magnitude of correlator response would indicate the best guess (assuming that there is actually a target present). Such a system not only detects the target but also makes maximum a posteriori (MAP) estimates of the parameters associated with its trajectory. The system is usually implemented as a bank of matched filters in parallel (Figure 3.7 in Rihaczek [6]).

It is possible to have a large-negative correlator output if, for example, τ is guessed with just a small error and the signal is nearly monochromatic. But it is mathematically convenient to have a measure which is a positive function of the accuracy of parameter estimation. Most of this dissertation will therefore concern itself with the quantities $|\chi_{uu}^{(i)}|^2$, $i = 1,2,3$, the magnitude-squared correlator responses.

It is easily demonstrated that the correlation of received data with a hypothetical version of the echo does not affect the general forms of the magnitude-squared ambiguity functions.

Let s_h (or ϕ_h) and τ_h be the hypothesized Doppler and time delay parameters, respectively. Let s_T (or ϕ_T) and τ_T be the actual parameters of a constant velocity point target. Then

$$|\chi_{uu}^{(1)}(\tau_h,\tau_T,\phi_h,\phi_T)|^2 = \left| \int u(t+\tau_h)e^{-j\phi_h t} u^*(t+\tau_T)e^{j\phi_T t}\,dt \right|^2$$

where unlabelled limits of integration are hereafter taken to be $(-\infty, \infty)$. Changing variables,

$$|\chi_{uu}^{(1)}(\tau,\phi)|^2 = \left|\int u(t)u^*(t+\tau)e^{j\phi t}\,dt\right|^2$$

where

$$\phi = \phi_T - \phi_h; \qquad \tau = \tau_T - \tau_h . \tag{3.1}$$

In the narrowband case, then, τ and ϕ are simply the differences between hypothetical and actual parameters.

Similarly,

$$|\chi_{uu}^{(2)}(\tau_h,\tau_T,s_h,s_T)|^2 = \left|\int s_h^{1/2}u[s_h(t+\tau_h)]s_T^{1/2}u^*[s_T(t+\tau_T)]dt\right|^2.$$

Changing variables:

$$|\chi_{uu}^{(2)}(\tau,s)|^2 = \left|s^{1/2}\int u(t)u^*[s(t+\tau)]dt\right|^2$$

where

$$s = s_T/s_h; \qquad \tau = s_h(\tau_T - \tau_h). \tag{3.2}$$

For the third version of the ambiguity function:

$$|\chi_{uu}^{(3)}(\tau,s)|^2 \quad \text{has} \quad s = s_T/s_h;\ \tau = \tau_T - (s_T/s_h)\tau_h . \tag{3.3}$$

The above results are summarized in Table 3.1.

Ambiguity function	Definition	τ	s (or ϕ)
$\chi_{uu}^{(1)}(\tau,\phi)$	$\int u(t)u^*(t+\tau)e^{j\phi t}dt$	$\tau_T - \tau_h$	$\phi_T - \phi_h$
$\chi_{uu}^{(2)}(\tau,s)$	$s^{1/2}\int u(t)u^*[s(t+\tau)]dt$	$s_h(\tau_T - \tau_h)$	s_T/s_h
$\chi_{uu}^{(3)}(\tau,s)$	$s^{1/2}\int u(t)u^*(st+\tau)dt$	$\tau_T-(s_T/s_h)\tau_h$	s_T/s_h

Table 3.1 The three point-target ambiguity functions with τ and s (or ϕ) in terms of hypothesized (τ_h,s_h) and actual (τ_T,s_T) target parameters.

3.2 Origin Properties

3.2.1 Taylor Series Expansion

As a consequence of equations (3.1 - 3.4), one sees that a good guess about target parameters would make $s_h \approx s_T$ ($\phi_h \approx \phi_T$) and $\tau \approx 0$. It is thus desirable to know the properties of the magnitude-squared ambiguity function near the origin ($s = 1$ or $\phi = 0$, $\tau = 0$). Also, the shape of the constant amplitude contours near the origin is somewhat indicative of the volume distribution of the central lobe of $|\chi|^2$. The shape of these contours is dependent upon certain moments of the signal. The radar engineer can thus approximately estimate the effect upon the ambiguity function of a particular change in his signal if he knows the behavior of $|\chi|^2$ near the origin.

Consider, then, a two-dimensional Taylor series expansion of $|\chi_{uu}^{(2)}(\tau,s)|^2$ around the point $(\tau,s) = (0,1)$:

$$|\chi_{uu}^{(2)}(\tau,s)|^2 = |\chi_{uu}^{(2)}(0,1)|^2 + \tau \left.\frac{\partial|\chi_{uu}^{(2)}(\tau,s)|^2}{\partial\tau}\right|_{(0,1)} + (s-1)\left.\frac{\partial|\chi_{uu}^{(2)}(\tau,s)|^2}{\partial s}\right|_{(0,1)} + \frac{\tau^2}{2}\left.\frac{\partial^2|\chi_{uu}^{(2)}(\tau,s)|^2}{\partial\tau^2}\right|_{(0,1)}$$

$$+ \tau(s-1)\left.\frac{\partial^2|\chi_{uu}^{(2)}(\tau,s)|^2}{\partial\tau\,\partial s}\right|_{(0,1)} + \frac{(s-1)^2}{2}\left.\frac{\partial^2|\chi_{uu}^{(2)}(\tau,s)|^2}{\partial s^2}\right|_{(0,1)}$$

$$+ \text{higher order terms.} \qquad (3.5)$$

With $\int_{-\infty}^{\infty} u(t)u^*(t)dt \equiv 1$ and $\chi_{uu}^{(2)}(\tau,s)$ defined as in (2.8), the derivatives on the right side of (3.5) are calculated in Appendix A. It is assumed here that $u(t) = a(t)\exp(j\theta(t))$ is complex and analytic [10,11], i.e., that $a(t)$ and $\theta(t)$ satisfy the relation

$$a(t)\cos\theta(t) = H\{a(t)\sin\theta(t)\} \tag{3.6}$$

where $H\{\cdot\}$ denotes Hilbert transformation. See the discussion preceding equation A.6 in Appendix A.

Application of the Schwarz inequality to $|\chi_{uu}^{(2)}|^2$ gives*

$$|\chi_{uu}^{(2)}(\tau,s)|^2 \leq \int|u(t)|^2dt \cdot s\int|u[s(t+\tau)]|^2dt = |\chi_{uu}^{(2)}(0,1)|^2 = 1 \tag{3.7}$$

with equality if and only if

$$u(t) = ks^{\frac{1}{2}}u[s(t+\tau)]; \quad (\tau,s) = (0,1). \tag{3.8}$$

Therefore, $|\chi_{uu}^{(2)}(\tau,s)|^2 \leq 1$, with maximum value at the origin (0,1). In the immediate neighborhood of the origin a constant amplitude contour of $|\chi|^2$ can then be written in terms of a constant δ^2:

$$|\chi_{uu}^{(2)}(\tau,s)|^2 = 1 - \delta^2 \qquad \text{where} \quad \delta^2 \ll 1. \tag{3.9}$$

---

* Some of the following discussion is modelled after a similar analysis of the narrowband ambiguity function by C. H. Wilcox [12].

The fact that $|X|^2$ has a maximum at the origin would seem to imply that the contour (3.9) is usually an ellipse for δ^2 sufficiently small. Proof of this conjecture follows.

3.2.2 Contour Shape Near $(\tau,s) = (0,1)$

Within a very small neighborhood of the origin, the higher order terms of equation (3.5) may be neglected, so that (3.5) and (3.9) become identical. Using the fact that the first partial derivatives at (0,1) are zero (Appendix A):

$$1 + \frac{1}{2}\left[\tau^2 \left.\frac{\partial^2 |X_{uu}^{(2)}(\tau,s)|^2}{\partial\tau^2}\right|_{(0,1)} + 2\tau(s-1)\left.\frac{\partial^2 |X_{uu}^{(2)}(\tau,s)|^2}{\partial s\,\partial\tau}\right|_{(0,1)}\right.$$

$$\left. + (s-1)^2 \left.\frac{\partial^2 |X_{uu}^{(2)}(\tau,s)|^2}{\partial s^2}\right|_{(0,1)}\right] = 1 - \delta^2 \,. \qquad (3.10)$$

If

$$\lambda^2 \equiv -\frac{1}{2}\left.\frac{\partial^2 |X_{uu}^{(2)}(\tau,s)|^2}{\partial\tau^2}\right|_{(0,1)} \qquad (3.11a)$$

$$\eta^2 \equiv -\frac{1}{2}\left.\frac{\partial^2 |X_{uu}^{(2)}(\tau,s)|^2}{\partial s^2}\right|_{(0,1)} \qquad (3.11b)$$

$$\gamma \equiv -\frac{1}{2}\left.\frac{\partial^2 |X_{uu}^{(2)}(\tau,s)|^2}{\partial\tau\,\partial s}\right|_{(0,1)} \qquad (3.11c)$$

then the constant amplitude contour is described by the equation

$$\lambda^2 \tau_1^2 + 2\gamma\tau_1(\Delta s_1) + \eta^2(\Delta s_1)^2 = \delta^2 \qquad (3.12)$$

where $\Delta s_1 = s - 1$. If this is truly the equation of an ellipse, then there should exist a rotation of axes:

$$\begin{bmatrix} \tau \\ \Delta s \end{bmatrix} = \begin{bmatrix} \cos\theta & \sin\theta \\ -\sin\theta & \cos\theta \end{bmatrix} \begin{bmatrix} \tau_1 \\ \Delta s_1 \end{bmatrix} \qquad (3.13)$$

such that

$$\frac{\tau^2}{a^2} + \frac{(\Delta s)^2}{b^2} = \delta^2 \quad , \qquad (3.14)$$

a more familiar form of the equation for an ellipse.

Writing $(\tau, \Delta s)$ in terms of $(\tau_1, \Delta s_1, \theta)$ in (3.14) and comparing the resulting equation with (3.12), it is found that

$$\lambda^2 = (\cos^2\theta/a^2) + (\sin^2\theta/b^2) \qquad (3.15a)$$

$$\gamma = \sin\theta\cos\theta\,[(1/a^2) - (1/b^2)] \qquad (3.15b)$$

$$\eta^2 = (\sin^2\theta/a^2) + (\cos^2\theta/b^2) \quad . \qquad (3.15c)$$

An illustration of the relation between the quantities in equations (3.15) is shown in Figure 3.1.

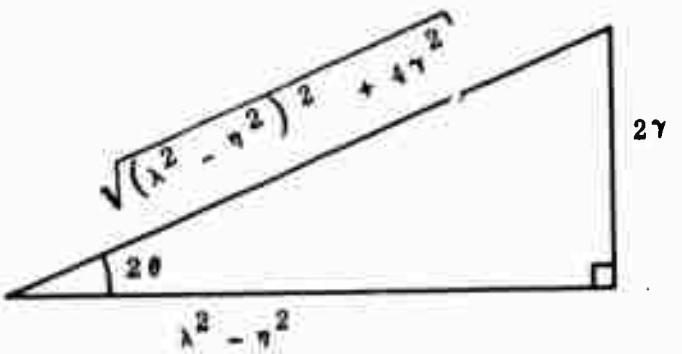

Figure 3.1. Right-Triangle Relationship of Origin Derivatives and Tilt of Wideband Uncertainty Ellipse

The triangle of Figure 3.1 is of immediate importance to the radar signal designer, as it illustrates the ways in which the angle of tilt (with respect to the τ-axis) of the wideband ambiguity ellipse depends upon the signal.

Equations (3.15) can be solved for a^2 and b^2 (with the help of Figure 3.1):

$$a^2 = \frac{2}{\lambda^2 + \eta^2 + \sqrt{(\lambda^2 - \eta^2)^2 + 4\gamma^2}} \tag{3.16a}$$

$$b^2 = \frac{2}{\lambda^2 + \eta^2 - \sqrt{(\lambda^2 - \eta^2)^2 + 4\gamma^2}} \tag{3.16b}$$

$$\text{Area} = \pi ab = \frac{\pi}{\sqrt{\lambda^2\eta^2 - \gamma^2}} \tag{3.16c}$$

For all the quantities in (3.16) to be positive, real, and finite, the following inequalities must be true:

$$\lambda^2 > 0 \tag{3.17a}$$

$$\eta^2 > 0 \tag{3.17b}$$

$$\lambda^2\eta^2 > \gamma^2 \tag{3.17c}$$

If these inequalities hold true, then the transformation (3.13) will give an equation of the form (3.14) and the contour $|\chi_{uu}^{(2)}|^2 = 1 - \delta^2$ will indeed be elliptical. In fact, the inequalities (3.17) can all be verified by the Schwarz inequality, although the proof of (3.17c) requires a special version of it.

From Appendix A and equations (3.11):

$$\lambda^2 = \int |u'(t)|^2 dt - \left| \int u(t)u^{*\prime}(t)dt \right|^2 \tag{3.18a}$$

$$\eta^2 = \int t^2 |u'(t)|^2 dt - \left| \int tu(t)u^{*\prime}(t)dt \right|^2 \tag{3.18b}$$

$$\gamma = \int t|u'(t)|^2 dt - \text{Re}\left\{ \int u'(t)u^*(t)dt \int tu(t)u^{*\prime}(t)dt \right\} \tag{3.18c}$$

As remarked in Appendix A, these quantities are the same for both $|\chi_{uu}^{(2)}|^2$ and $|\chi_{uu}^{(3)}|^2$.

Proof of (3.17a):

For unit energy signals,

$$\int |u'(t)|^2 dt = \int |u'(t)|^2 dt \int |u(t)|^2 dt \geq \left| \int u(t)u^{*\prime}(t)dt \right|^2 ,$$

with equality if and only if

$$u(t) = ku'(t) \ . \tag{3.19}$$

It would appear that an exponential is a counter-example to the inequality, since a solution to (3.19) is $u(t) = k_1 \exp(k_2 t)$ where k_1 and k_2 can be complex, e.g., $u(t) = k_1 \exp[(b + j\omega_o)t]$. But in order for the exponential to be of finite energy, it must have one of the forms:

$$u(t) = \begin{cases} k_1 e^{(b + j\omega_o)t} , & t \geq 0 \\ 0 , & t < 0 \end{cases} \tag{3.20a}$$

or

$$u(t) = k_1 e^{(b + j\omega_o)|t|} \ . \tag{3.20b}$$

The first form (3.20a) results in an undefined (delta function) derivative at $t = 0$, so that λ^2 will also be undefined. Such a signal is inadmissible per se. For the second form (3.20b),

$$u'(t) = k_1(b + j\omega_o)\exp[(b + j\omega_o)|t|]\cdot[\operatorname{sgn} t] \text{ , where}$$

$$\operatorname{sgn} t = \begin{cases} +1, & t > 0 \\ 0, & t = 0 \\ -1, & t < 0 \end{cases} .$$

But then $u(t) \neq ku'(t)$ for a consistent value of k, so that (3.19) is no longer satisfied.

Proof of (3.17b):

$$\int t^2|u'(t)|^2dt \int|u(t)|^2dt \geq \left|\int tu(t)u^{*\prime}(t)dt\right|^2 ,$$

with equality if and only if

$$u(t) = ktu'(t) \quad \text{or} \quad u(t) = k_1 t^{k_2} . \tag{3.21}$$

Once again, sudden truncation results in undefined moments, so that (3.21) must be satisfied for all t. Since there exists no value of k_2 such that $k_1 t^{k_2}$ has finite energy, (3.21) defines a set of inadmissible functions. Thus (3.17b) is verified.

Proof of (3.17c):

Given the standard form of the Schwarz inequality:

$$\int|u(t)|^2dt \int |v(t)|^2dt - \left|\int u(t)v^*(t)dt\right|^2 \geq 0, \tag{3.22}$$

one can derive a special version involving more functions by letting $u(t) = rf(t) + cg(t)$, where r and c are real scalars. This procedure has been suggested by E. F. Beckenbach and R. Bellman in their book, Inequalities [13]. Then (3.22) becomes

$$r^2\left[\int ff^*dt \int vv^*dt - \int fv^*dt \int vf^*dt\right]$$

$$+ rc\left\{\int vv^*dt\left[\int fg^*dt + \int gf^*dt\right] - \int fv^*dt\int vg^*dt\right.$$

$$\left. - \int gv^*dt \int vf^*dt\right\} + c^2\left[\int gg^*dt \int vv^*dt - \int gv^*dt \int vg^*dt\right]$$

$$\geq 0 \qquad (3.23)$$

for all r,c.

Equation (3.23) may be written $xr^2 + 2yrc + zc^2 \geq 0$, where $x \geq 0$ and $z \geq 0$ by the usual Schwarz inequality. But (3.23) is then a special case of Hermitian form [14]. Accordingly, the inequality always holds provided $xz - y^2 \geq 0$, or

$$\left[\int |f|^2dt \int |v|^2dt - \left|\int fv^*dt\right|^2\right]\left[\int |g|^2dt \int |v|^2dt - \left|\int gv^*dt\right|^2\right]$$

$$\geq \left[\int |v|^2dt \cdot \mathrm{Re}\left\{\int fg^*dt\right\} - \mathrm{Re}\left\{\int fv^*dt \int vg^*dt\right\}\right]^2 \qquad (3.24)$$

Letting $v(t) = u(t)$, $\quad g(t) = tu'(t)$, $\quad f(t) = u'(t)$ (3.25)

in (3.24) gives $\lambda^2\eta^2 \geq \gamma^2$, with equality if and only if $rf + cg = kv$, or

$$ru' + ctu' = ku; \quad u = k_1(r+ct)^{k_2} . \tag{3.26}$$

But (3.26) is inadmissible for the same reason that (3.21) was, so that the validity of (3.17c) has been demonstrated.

It has been shown that the constant-amplitude contours of $|\chi_{uu}^{(2)}|^2$ near (0,1) are indeed elliptical in shape, with axes determined by equations (3.16) and tilt-of-ellipse determined by Figure 3.1, in conjunction with equations (3.18).

3.2.3 Average Curvature of $|\chi_{uu}^{(2)}(\tau,s)|^2$ at the Origin

If the ambiguity function were expressed in terms of polar coordinates (ρ,θ) with $\rho = 0$ at $(\tau,s) = (0,1)$, then a measure of sharpness of the peak at the origin would be the quantity

$$\left.\frac{\partial^2 |\chi_{uu}^{(2)}|^2}{\partial \rho^2}\right|_{\rho=0}$$

averaged over all $\theta \epsilon (0,2\pi)$:

$$C \equiv \frac{1}{2\pi} \int_0^{2\pi} \left.\frac{\partial^2}{\partial \rho^2} |\chi_{uu}^{(2)}(\rho,\theta)|^2\right|_{\rho=0} d\theta . \tag{3.27}$$

C is then the average curvature of $|\chi_{uu}^{(2)}(\tau,s)|^2$ at (0,1). For good target resolution in both range and radial velocity, $|C|$ should be as large as possible. C may be found from earlier results by use of the chain rule:

$$\frac{\partial^2|X(\rho,\theta)|^2}{\partial\rho^2} = \frac{\partial^2|X(\tau,s)|^2}{\partial\tau^2}\left(\frac{\partial\tau}{\partial\rho}\right)^2 + \frac{\partial^2|X(\tau,s)|^2}{\partial s^2}\left(\frac{\partial s}{\partial\rho}\right)^2$$

$$+ 2\,\frac{\partial^2|X(\tau,s)|^2}{\partial\tau\,\partial s}\,\frac{\partial\tau}{\partial\rho}\,\frac{\partial s}{\partial\rho}$$

$$+ \frac{\partial|X(\tau,s)|^2}{\partial\tau}\,\frac{\partial^2\tau}{\partial\rho^2} + \frac{\partial|X(\tau,s)|^2}{\partial s}\,\frac{\partial^2 s}{\partial\rho^2} \qquad (3.28)$$

where

$$\tau = \rho\cos\theta \text{ and } s - 1 = \rho\sin\theta\ . \qquad (3.29)$$

Using equations (3.11) in conjunction with the results of Appendix A and (3.15):

$$\left.\frac{\partial^2|X(\rho,\theta)|^2}{\partial\rho^2}\right|_{\rho=0} = -2\lambda^2\cos^2\theta - 2\eta^2\sin^2\theta - 2\gamma\cos\theta\sin\theta \qquad (3.30)$$

and

$$|C| = (\lambda^2 + \eta^2) \qquad (3.31a)$$

$$= \int t^2|u'(t)|^2dt - \left|\int tu(t)u^{*\prime}(t)dt\right|^2$$

$$+ \int|u'(t)|^2dt - \left|\int u(t)u^{*\prime}(t)dt\right|^2 \qquad (3.31b)$$

$$= 1/a^2 + 1/b^2. \qquad (3.31c)$$

3.2.4 Comparison of the Origin Properties of Narrowband and Wideband Ambiguity Functions on the (τ,ϕ) Plane

In a small neighborhood about $s = 1$,

$$s = (1 + v/\tilde{v})/(1 - v/\tilde{v}) \approx 1 + 2v/\tilde{v} = 1 - 2\dot{R}/\tilde{v} = 1 - \phi/\omega_o . \qquad (3.32)$$

It follows that

$$\frac{\partial}{\partial s}|\chi_{uu}^{(2)}(\tau,s)|^2\Big|_{(0,1)} = -\frac{\partial}{\partial(\phi/\omega_o)}|\chi_{uu}^{(2)}(\tau,\phi)|^2\Big|_{(0,0)}$$

$$= -\omega_o \frac{\partial}{\partial\phi}|\chi_{uu}^{(2)}(\tau,\phi)|^2\Big|_{(0,0)} \qquad (3.33)$$

$$\frac{\partial^2}{\partial s^2}|\chi_{uu}^{(2)}(\tau,s)|^2\Big|_{(0,1)} = \frac{\partial^2|\chi_{uu}^{(2)}(\tau,\phi)|^2}{\partial(\phi/\omega_o)^2}\Big|_{(0,0)}$$

$$= \omega_o^2 \frac{\partial^2}{\partial\phi^2}|\chi_{uu}^{(2)}(\tau,\phi)|^2\Big|_{(0,0)} \qquad (3.34)$$

The behavior of the wideband and narrowband functions near the origin of the $\tau - \phi$ plane may now be compared. The comparisons are made in Table 3.2 (next page), where the derivatives are written in terms of $U(\omega)$, the Fourier transform of $u(t)$.

TABLE 3.2

Derivatives of $|\chi_{uu}^{(1)}(\tau,\phi)|^2$ at (0,0)

$$\left.\frac{\partial|\chi_{uu}^{(1)}(\tau,\phi)|^2}{\partial\tau}\right|_{0,0} = 0 \; ; \quad \left.\frac{\partial|\chi_{uu}^{(1)}(\tau,\phi)|^2}{\partial\phi}\right|_{0,0} = 0$$

$$\frac{1}{2}\left.\frac{\partial^2|\chi_{uu}^{(1)}|^2}{\partial\phi^2}\right|_{0,0} = \left|\frac{1}{2\pi}\int U(\omega)U^{*\prime}(\omega)d\omega\right|^2 - \frac{1}{2\pi}\int|U'(\omega)|^2d\omega$$

$$\frac{1}{2}\left.\frac{\partial^2|\chi_{uu}^{(1)}|^2}{\partial\tau\,\partial\phi}\right|_{0,0} = -\mathrm{Im}\left\{\frac{1}{2\pi}\int\omega UU^{*\prime}d\omega\right\} + \frac{1}{2\pi}\int\omega|U|^2d\omega\cdot\mathrm{Im}\left\{\frac{1}{2\pi}\int UU^{*\prime}d\omega\right\}$$

$$\frac{1}{2}\left.\frac{\partial^2|\chi_{uu}^{(1)}|^2}{\partial\tau^2}\right|_{0,0} = \left|\frac{1}{2\pi}\int\omega|U|^2d\omega\right|^2 - \frac{1}{2\pi}\int\omega^2|U|^2d\omega$$

Derivatives of $|\chi_{uu}^{(2)}(\tau,\phi)|^2$ at (0,0)

$$\left.\frac{\partial|\chi_{uu}^{(2)}(\tau,\phi)|^2}{\partial\tau}\right|_{0,0} = 0 \; ; \quad \left.\frac{\partial|\chi_{uu}^{(2)}(\tau,\phi)|^2}{\partial\phi}\right|_{0,0} = 0$$

$$\frac{1}{2}\left.\frac{\partial^2|\chi_{uu}^{(2)}|^2}{\partial\phi^2}\right|_{0,0} = \left|\frac{1}{2\pi}\int\left(\frac{\omega}{\omega_o}\right)UU^{*\prime}d\omega\right|^2 - \frac{1}{2\pi}\int\left(\frac{\omega}{\omega_o}\right)^2|U'|^2d\omega$$

$$\frac{1}{2}\left.\frac{\partial^2|\chi_{uu}^{(2)}|^2}{\partial\tau\,\partial\phi}\right|_{0,0} = -\mathrm{Im}\left\{\frac{1}{2\pi}\int\left(\frac{\omega}{\omega_o}\right)\omega UU^{*\prime}d\omega\right\} + \frac{1}{2\pi}\int\omega|U|^2d\omega\cdot\mathrm{Im}\left\{\frac{1}{2\pi}\int\left(\frac{\omega}{\omega_o}\right)UU^{*\prime}d\omega\right\}$$

$$\frac{1}{2}\left.\frac{\partial^2|\chi_{uu}^{(2)}|^2}{\partial\tau^2}\right|_{0,0} = \left|\frac{1}{2\pi}\int\omega|U|^2d\omega\right|^2 - \frac{1}{2\pi}\int\omega^2|U|^2d\omega$$

Table 3.2 helps to illustrate the nature of the narrowband assumption. The $|\chi_{uu}^{(2)}|^2$ expressions become nearly equal to their $|\chi_{uu}^{(1)}|^2$ counterparts only when the signal energy is concentrated within a small band of frequencies around a large carrier (ω_o).

3.3 An Integral Transformation Between Wideband and Narrowband Ambiguity Functions

From the comparison (Table 3.1) of narrowband and wideband ambiguity functions at the origin of the (τ,ϕ) plane, one sees that an easy transformation exists between corresponding derivatives. One may then wonder about the existence of a global operation that maps $\chi_{uu}^{(1)}$ into $\chi_{uu}^{(2)}$ and vice versa.

3.3.1 Symmetrical Forms

Application of Parseval's theorem to the narrowband function (3.2) yields

$$\chi_{uu}^{(1)}(\tau,\phi) = \frac{1}{2\pi}\int U(\omega)U^*(\omega+\phi)e^{-j\omega\tau}d\omega \ . \tag{3.35}$$

Letting $\omega = \omega' - \phi/2$:

$$\chi_{uu}^{(1)}(\tau,\phi) = \frac{e^{j\phi\tau/2}}{2\pi}\int U(\omega'-\phi/2)U^*(\omega'+\phi/2)e^{-j\omega'\tau}d\omega' . \tag{3.36}$$

It was pointed out in section 3.1 that the magnitude-squared ambiguity function will be used as a measure of correlation.

This means that the phase factor $\exp(j\phi\tau/2)$ in equation (3.36) may be neglected, so that an equivalent version of $\chi_{uu}^{(1)}$ is:

$$\chi_{uu}^{(1)}(\tau,\phi) = \frac{1}{2\pi} \int U(\omega - \phi/2)U^*(\omega + \phi/2)e^{-j\omega\tau}\, d\omega \ . \qquad (3.37)$$

(3.37) is then a symmetrical form of the narrowband ambiguity function [4]. Once again, $\phi \equiv -2\omega_o\beta$ and $\beta \equiv v/\tilde{v}$, where v is positive toward the receiver.

The Kelly-Wishner function also has a symmetrical form on the (τ,β) plane: Let $\hat{\chi}_{uu}^{(2)}(\tau,\beta) \equiv \chi_{uu}^{(2)}(\tau,s)\Big|_{s=\frac{1+\beta}{1-\beta}}$. Then,

$$\hat{\chi}_{uu}^{(2)}(\tau,\beta) = \left(\frac{1+\beta}{1-\beta}\right)^{1/2} \int u(t)u^*\left[\frac{1+\beta}{1-\beta}(t+\tau)\right]dt. \qquad (3.38)$$

Let $t = t'/(1+\beta)$:

$$\hat{\chi}_{uu}^{(2)}(\tau,\beta) = \frac{1}{[(1+\beta)(1-\beta)]^{1/2}} \int u\left(\frac{t'}{1+\beta}\right) u^*\left(\frac{t'}{1-\beta} + \frac{1+\beta}{1-\beta}\,\tau\right) dt' \ . \qquad (3.39)$$

Applying Parseval's theorem:

$$\hat{\chi}_{uu}^{(2)}(\tau,\beta) = \frac{(1-\beta^2)^{1/2}}{2\pi} \int U[\omega(1+\beta)]U^*[\omega(1-\beta)]\, e^{-j\omega(1+\beta)\tau}\, d\omega. \qquad (3.40)$$

Similarly, it can be shown that

$$\hat{\chi}^{(3)}_{uu}(\tau,\beta) = \frac{(1-\beta^2)^{1/2}}{2\pi} \int U[\omega(1+\beta)]U^*[\omega(1-\beta)]e^{-j\omega(1-\beta)\tau}d\omega. \quad (3.41)$$

Equations (3.40 - 41) are symmetrical forms of the wideband ambiguity functions, analogous to equation (3.37) for the narrowband function.

3.3.2 Integral Transformations

Theorem*:

Integral transformations between wideband and narrowband ambiguity functions are as follows:

$$(1) \quad \hat{\chi}^{(2)}_{uu}(\tau,\beta) = \frac{(1-\beta^2)^{1/2}}{2\pi} \iint \chi^{(1)}_{uu}(\tau',-2\beta\omega)\, e^{j\omega[\tau'-(1+\beta)\tau]}d\tau'd\omega \quad (3.43)$$

$$(2) \quad \chi^{(1)}_{uu}(\tau,\beta) = \iint \frac{\hat{\chi}^{(2)}_{uu}[\tau'/(1-\beta/2\omega),-\beta/2\omega]}{2\pi[1-(\beta/2\omega)^2]^{1/2}} e^{j\omega(\tau'-\tau)}d\tau'd\omega . \quad (3.44)$$

Proof:

Consider the τ-integration of the Woodward function

$$\chi^{(1)}_{uu}(\tau',-2\beta\omega) \equiv \chi^{(1)}_{uu}(\tau,\phi)\Big|_{(\tau,\phi)=(\tau',-2\beta\omega)} .$$

Using equation (3.37):

---

* Although this theorem is original with the author, the type of transformation involved here was briefly mentioned in a paper by E. L. Titlebaum and N. DeClaris [14].

$$\int \chi_{uu}^{(1)}(\tau', -2\beta\omega) e^{j\omega\tau'} \, d\tau'$$

$$= \frac{1}{2\pi} \iint U\left(x + \frac{2\beta\omega}{2}\right) U^*\left(x - \frac{2\beta\omega}{2}\right) e^{-jx\tau'} e^{j\omega\tau'} \, dx \, d\tau' .$$

The τ-integration results in the function $2\pi\delta(x - \omega)$, so that

$$\int \chi_{uu}^{(1)}(\tau', -2\beta\omega) e^{j\omega\tau'} d\tau' = \int U(x + \beta\omega) U^*(x - \beta\omega) \, \delta(x - \omega) dx$$

$$= U[\omega(1 + \beta)] U^*[\omega(1 - \beta)] . \qquad (3.45)$$

By equation (3.40),

$$\hat{\chi}_{uu}^{(2)}(\tau, \beta) = \frac{(1 - \beta^2)^{1/2}}{2\pi} \int U[\omega(1 + \beta)] \, U^*[\omega(1 - \beta)] \, e^{-j\omega(1+\beta)\tau} \, d\omega$$

so that

$$\hat{\chi}_{uu}^{(2)}(\tau, \beta) = \frac{(1 - \beta^2)^{1/2}}{2\pi} \int \left[\int \chi_{uu}^{(1)}(\tau', -2\beta\omega) e^{j\omega\tau'} \, d\tau' \right] e^{-j\omega(1+\beta)\tau} d\omega.$$

This is the first transformation (3.43).

Similarly, by (3.40),

$$\frac{\hat{\chi}_{uu}^{(2)}\left(\frac{\tau'}{1-\beta/2\omega}, \frac{-\beta}{2\omega}\right)}{\left[1 - (\beta/2\omega)^2\right]^{1/2}} = \frac{1}{2\pi} \int U[x(1-\beta/2\omega)] \, U^*[x(1+\beta/2\omega)] \, e^{-jx\tau'} \, dx ,$$

so that

$$\int \frac{\hat{\chi}_{uu}^{(2)}(\tau'/(1-\beta/2\omega),-\beta/2\omega)}{[1-(\beta/2\omega)^2]^{1/2}} \cdot e^{j\omega\tau'} d\tau' = U(\omega-\beta/2)U^*(\omega+\beta/2). \quad (3.46)$$

But,

$$\frac{1}{2\pi} \int U(\omega-\beta/2)U^*(\omega+\beta/2)e^{-j\omega\tau} d\omega = \chi_{uu}^{(1)}(\tau,\beta) .$$

Therefore,

$$\chi_{uu}^{(1)}(\tau,\beta) = \iint \frac{\hat{\chi}_{uu}^{(2)}(\tau'/(1-\beta/2\omega),-\beta/2\omega)}{2\pi[1-(\beta/2\omega)^2]^{1/2}} e^{j\omega(\tau'-\tau)} d\tau' d\omega ,$$

which is the second transformation (3.44).

These transforms are similar in form to Fourier's integral formula [15] for the regeneration of a function by means of a double integration (repeated Fourier transform):

$$f(t) = \frac{1}{2\pi} \iint f(\tau)e^{-j\omega(\tau-t)} d\tau \, d\omega . \quad (3.47)$$

The difference is that the above Theorem involves kernels that are dependent upon ω as well as τ. The only exception to this difference occurs when $\beta \equiv 0$:

$$\hat{\chi}_{uu}^{(2)}(\tau,0) = \chi_{uu}^{(1)}(\tau,0) , \quad (3.48)$$

an obvious result .

3.4 Volume Properties

3.4.1 Woodward's Result for the Narrowband Case.

Woodward [1] has pointed out that the volume under the narrowband function $|\chi_{uu}^{(1)}(\tau,\phi)|^2$ is constant. This is easily shown by writing

$$V_{\tau,\phi}^{(1)} = \frac{1}{2\pi}\iint |\chi_{uu}^{(1)}(\tau,\phi)|^2 d\tau\, d\phi$$

$$= \frac{1}{2\pi}\iiiint u(x)u^*(x+\tau)e^{j\phi x}u^*(y)u(y+\tau)e^{-j\phi y}\,dx\,dy\,d\phi\,d\tau\,. \tag{3.49}$$

Since

$$\frac{1}{2\pi}\int e^{-j(y-x)\phi}d\phi = \delta(y-x), \tag{3.50}$$

$$V_{\tau,\phi}^{(1)} = \iint |u(x)|^2|u(x+\tau)|^2 dx\,d\tau$$

$$= 1, \text{ for unit-energy signals.} \tag{3.51}$$

3.4.2 The Kelly-Wishner Volume Calculation [5].

The volume under $|\chi_{uu}^{(2)}(\tau,s)|^2$ on the τ,s plane may be written:

$$V_{\tau,s}^{(2)} = \int_{-\infty}^{\infty}\int_{0}^{\infty}|\chi_{uu}^{(2)}(\tau,s)|^2 d\tau\,ds \tag{3.52}$$

$$= \frac{1}{2\pi}\int_{0}^{\infty}\iiint_{-\infty}^{\infty} u(t)u^*[s(t+\tau)]U^*(\omega)U(\omega/s)e^{j\omega\tau}d\omega\,dt\,d\tau\,ds,$$

where use has been made of the identity (using Parseval's theorem):

$$\chi_{uu}^{(2)}(\tau,s) = \frac{1}{2\pi s^{1/2}} \int U(\omega)U^*(\omega/s)e^{-j\omega\tau}\, d\omega \,. \tag{3.53}$$

$$\int u^*[s(t+\tau)]e^{j\omega\tau}d\tau = \frac{1}{s}\, U^*(\omega/s)e^{-j\omega t} \tag{3.54}$$

and

$$\int u(t)e^{-j\omega t}dt = U(\omega) \tag{3.55}$$

so that

$$V_{\tau,s}^{(2)} = \frac{1}{2\pi} \int_0^{\infty}\int_{-\infty}^{\infty} \frac{|U(\omega/s)|^2}{s}\, |U(\omega)|^2 d\omega\, ds \tag{3.56}$$

We can now make one of two reasonable assumptions:

(1) u(t) is real, which implies that $|U(\omega)|^2 = |U(-\omega)|^2$, or

(2) u(t) is complex with real and imaginary parts a Hilbert pair (analytic), which implies that $|U(\omega)|^2 = 0$, $\omega < 0$.

For assumption (2) with $\omega = \omega$'s:

$$\begin{aligned} V_{\tau,s}^{(2)} &= \frac{1}{2\pi}\int_0^{\infty}\int_0^{\infty} |U(\omega')|^2 |U(s\omega')|^2 ds\, d\omega' \\ &= \int_0^{\infty} \frac{|U(\omega')|^2}{\omega'} \left[\frac{1}{2\pi}\int_0^{\infty} \omega' |U(\omega' s)|^2 ds\right] d\omega' \\ &= \int_0^{\infty} \frac{|U(\omega)|^2}{\omega}\, d\omega \,. \end{aligned} \tag{3.57}$$

Assumption (1) would, of course, give a similar answer.

Kelly and Wishner did not energy normalize the returned waveform, so the original Kelly-Wishner ambiguity function lacks the factor of $s^{1/2}$ in front of the expression for $\chi_{uu}^{(2)}$. For this reason their volume result is somewhat different from the one obtained above.

If the signal were narrowband, one could evaluate (3.57) in the manner indicated by Table 3.1, yielding

$$V_{\tau,s}^{(2)} \approx \frac{2\pi}{\omega_o} \quad . \tag{3.58}$$

Even though the volume of the Woodward function is apparently constant, the volume of $|\chi_{uu}^{(2)}|^2$ decreases with larger carrier frequency. This apparent contradiction will be resolved in the next section.

3.4.3 A More Realistic Approach to Narrowband Volume.

Cursory observation of Woodward's volume theorem indicates that the ϕ-integration is, per se, unrealistic. In Chapter II, ϕ was defined as

$$\phi \equiv - \frac{2\omega_o v}{\tilde{v}} \quad . \tag{3.59}$$

To integrate ϕ form $-\infty$ to $+\infty$ would violate the theory of relativity for a radar signal, and would violate the implicit assumption that $|v| < |\tilde{v}|$ for sonar. But this objection is eclipsed by further problems when one considers the validity of Woodward's model of the returned signal.

Let us, for the sake of argument, assume a transmitted signal with linear phase:

$$u(t) = a(t)\exp(j\omega_o t) \ . \tag{3.60}$$

This signal may be wideband or narrowband, depending upon $a(t)$ and ω_o. Using the model of returned signal leading to (2.11):

$$r(t) = s^{1/2}u[s(t+\tau)] = s^{1/2}a[s(t+\tau)]\cdot\exp\{j\omega_o[s(t+\tau)]\} \ . \tag{3.61}$$

In the narrowband argument, this retuned signal is assumed to have the form:

$$r(t) = u(t+\tau)\exp(-j\phi t) = a(t+\tau)\exp(j\omega_o(t+\tau))\exp(-j\phi t). \tag{3.62}$$

Let us investigate the conditions under which (3.61) and (3.62) are equal.

It was shown in Chapter II that

$$s = (1+\beta)/(1-\beta) \tag{3.63}$$

where $\beta = v/\tilde{v}$, a relative velocity factor.

Since $\beta < 1$,

$$1/(1-\beta) = 1+\beta+\beta^2+\beta^3+\ldots \tag{3.64}$$

so that

$$s = (1+\beta+\beta^2+\beta^3+\ldots) + (\beta+\beta^2+\beta^3+\beta^4+\ldots) \ . \qquad (3.65)$$

Therefore (3.61) becomes

$$r(t) = (1+2\beta+2\beta^2+\ldots)^{1/2}\ a[(1+2\beta+2\beta^2+\ldots)(t+\tau)]$$

$$\exp[j\omega_o(1+2\beta+2\beta^2+\ldots)(t+\tau)] \ . \qquad (3.66)$$

If $\beta \ll 1$ and $\omega_o\beta^2 \ll 1$, ($\omega_o\beta$ need not be so small), then

$$r(t) = a(t+\tau)\exp[j\omega_o(t+\tau)]\cdot\exp[j2\omega_o\beta(t+\tau)]. \qquad (3.67)$$

By substituting (3.59) into (3.62), the narrowband model becomes

$$r(t) = a(t+\tau)\exp(j\omega_o(t+\tau))\exp(j2\omega_o\beta t). \qquad (3.68)$$

Since the quantity $|\chi|^2$ is of ultimate importance, phase factors that are not time dependent may be neglected. Thus the narrowband model (3.68) is nearly identical to the Kelly-Wishner echo provided that:

$$\begin{aligned} &(1) \qquad |\beta| \ll 1 \\ &(2) \qquad \omega_o\beta^2 \ll 1 \ . \end{aligned} \qquad (3.69)$$

Observe that neither of the above conditions requires that $\omega_o\beta \ll 1$.

In the calculation of narrowband ambiguity volume, even those limits commensurate with relativity theory are therefore

generally unacceptable (or, at least, unrealistic). Limits that take conditions (3.69) into account would be

$$-\frac{1}{\omega_o} < \beta < \frac{1}{\omega_o}, \qquad \text{where } \omega_o \gg 1.$$

A volume calculated with such limits would generally vary as $1/\omega_o$, as in equation (3.58) for $V_{\tau,s}^{(2)}$.

3.4.4 Upper Bounds to Wideband Ambiguity Volume

Theorem: The volume of the wideband ambiguity function $|\hat{\chi}_{uu}^{(2)}|^2$ on the τ, β plane is less than or equal to $2\pi^2(D_t^2/3)^{1/2}$, where $D_t^2 \equiv \int t^2|u(t)|^2dt$, the mean-squared time duration.

Proof: Let $V_{\tau,\beta}^{(2)}$ = ambiguity volume on the τ, β plane

$$= \int_{-1}^{1}\int_{-\infty}^{\infty} |\hat{\chi}_{uu}^{(2)}(\tau,\beta)|^2 d\tau\, d\beta \tag{3.70}$$

where $\hat{\chi}_{uu}^{(2)}(\tau,\beta)$ is given by (3.40), so that

$$V_{\tau,\beta}^{(2)} = \frac{(1-\beta^2)}{(2\pi)^2}\int_{-1}^{1}\iiint_{-\infty}^{\infty} U[x(1+\beta)]U^*[x(1-\beta)]U^*[y(1+\beta)]U[y(1-\beta)] \tag{3.71}$$

$$e^{-j[(1+\beta)(x-y)\tau]}\, dx\, dy\, d\tau\, d\beta .$$

Performing the τ-integration and making use of the relation:

$$\int e^{-j(1+\beta)(x-y)\tau} d\tau = \frac{2\pi}{1+\beta}\,\delta(x-y) \tag{3.72}$$

and then performing the y-integration, one is left with

$$V^{(2)}_{\tau,\beta} = \int_{-1}^{1} \frac{(1-\beta)}{2\pi} Z(\beta)d\beta \tag{3.73}$$

where

$$Z(\beta) = \int |U[x(1+\beta)]|^2 |U[x(1-\beta)|^2 dx \ . \tag{3.74}$$

Since $Z(\beta) = Z(-\beta)$, it follows that,

$$\int_{-1}^{1} \beta Z(\beta)d\beta \equiv 0. \tag{3.75}$$

Applying the Schwarz inequality:

$$(1-\beta^2)^{1/2} Z(\beta) \leq [(1+\beta)\int |U[x(1+\beta)]|^4 dx \cdot (1-\beta)\int |U[x(1-\beta)]|^4 dx]^{1/2}$$

$$= \int |U(\omega)|^4 d\omega \ . \tag{3.76}$$

Combining (3.73), (3.75), and (3.76):

$$V^{(2)}_{\tau,\beta} \leq \frac{1}{2\pi} \int_{-1}^{1} \frac{d\beta}{(1-\beta^2)^{1/2}} \int |U(\omega)|^4 d\omega \ . \tag{3.77}$$

Letting $\beta = \sin\theta$, $d\beta = \cos\theta\, d\theta$:

$$\int_{-1}^{1} \frac{d\beta}{(1-\beta^2)^{1/2}} = \int_{-\pi/2}^{\pi/2} d\theta = \pi \ . \tag{3.78}$$

Therefore,

$$V_{\tau,\beta}^{(2)} \leq \frac{1}{2}\int |U(\omega)|^4 d\omega \ . \qquad (3.79)$$

We now utilize an inequality of B. v. Sz.Nagy [16, 17] as given in Appendix B. Invoking the second part of Nagy's inequality with a = 2, b = 2, p = 2, r = 2, gives, for a unit energy signal:

$$\int \left| \frac{U(\omega)}{\sqrt{2\pi}} \right|^4 d\omega \leq \frac{(\frac{3}{2})^{-3/2} \cdot \frac{3}{2}\Gamma(\frac{3}{2})}{(\frac{1}{2})^{-1/2}\Gamma(\frac{3}{2})}(1) \left[\frac{\int |U'(\omega)|^2 d\omega}{2\pi} \right]^{1/2}$$

$$= (\tfrac{1}{3}D_t^{\,2})^{1/2} \ . \qquad (3.80)$$

Therefore, $V_{\tau,\beta}^{(2)} \leq 2\pi^2 (D_t^{\,2}/3)^{1/2}$. QED .

It is therefore evident that a signal with small mean square time duration will have comparatively small ambiguity volume on the τ, β plane.

By the RMS uncertainty relation (Appendix C):

$$D_t^{\,2} \geq 1/4 D_\omega^{\,2} \ .$$

If it is desired to make the volume small, one method would be to make $D_t^{\,2}$ small. But in order that $D_t^{\,2}$ be small,

$$D_\omega^{\,2} \equiv (\frac{1}{2\pi})\int \omega^2 |U(\omega)|^2 d\omega$$

must be made large. This is conveniently done by shifting $U(\omega)$

away from $\omega = 0$, i.e., by adding a large carrier frequency. In fact, for the special case wherein u(t) is Gaussian and narrowbanded,

$$D_t^2 \approx 1/4\omega_o^2 \quad \text{and} \quad V_{\tau,\beta}^{(2)} \leq \frac{\pi^2}{\sqrt{3}} \cdot \frac{1}{\omega_o} \quad .$$

This is in excellent agreement with (3.58).

Theorem: If a signal is strictly time limited with duration T ($u(t) \equiv 0$ for t outside $[-T/2, T/2]$) then $V_{\tau,\beta}^{(2)} \leq \pi[T \cdot \max_{-T/2 \leq t \leq T/2} |u(t)|]^2$. That is, the volume upper bound varies as T^2 times the maximum instantaneous signal power.

Proof: From (3.79), $V_{\tau,\beta}^{(2)} \leq \frac{1}{2}\int |U(\omega)|^4 d\omega$.

For the strictly time limited signal,

$$U(\omega) = \int_{-T/2}^{T/2} u(t)e^{-j\omega t}dt \leq \int_{-T/2}^{T/2} |u(t)|dt \leq \max_{-T/2 \leq t \leq T/2} |u(t)| \cdot T. \quad (3.81)$$

$$\frac{1}{2\pi} \int |U(\omega)|^4 d\omega \leq |\max_t |u(t)| \cdot T|^2 \cdot \frac{1}{2\pi} \int |U(\omega)|^2 d\omega \quad (3.82)$$

so that, for a unit energy signal,

$$V_{\tau,\beta}^{(2)} \leq \pi[T \cdot \max_t |u(t)|]^2 \quad . \qquad \text{QED} \; .$$

To minimize $\max_t |u(t)|$ for a given duration T and constant energy, it is evident that the best signal will have constant amplitude.

Corollary: The amplitude of the time limited signal (with given duration) that minimizes the upper bound (3.81) is a rectangular pulse.

Although volume on the (τ,β) plane is more meaningful than (τ,s) plane results in terms of comparisons with narrowband properties, the following result for the (τ,s) plane will prove useful.

Theorem: The volume under the $|\chi_{uu}^{(2)}(\tau,s)|^2$ function in the strip $(s_1 \geq s \geq s_2)$ of the τ,s plane is less than or equal to $4\pi(D_t^2/3)^{1/2}(s_1^{1/2} - s_2^{1/2})$.

Proof: Using the expression (3.53):

$$|\chi_{uu}^{(2)}(\tau,s)|^2 = \frac{1}{(2\pi)^2 s}\iint U(x)U^*(x/s)U^*(y)U(y/s)e^{-j(x-y)\tau}\,dx\,dy\,. \quad (3.83)$$

Integrating with respect to τ and then with respect to y:

$$\int_{-\infty}^{\infty}|\chi_{uu}^{(2)}(\tau,s)|^2 d\tau = \frac{1}{2\pi s}\int_{-\infty}^{\infty}|U(x)|^2|U(x/s)|^2 dx\,. \quad (3.84)$$

Applying the Schwarz inequality:

$$\frac{1}{2\pi s}\int |U(x)|^2|U(x/s)|^2 dx \leq \frac{1}{2\pi s^{1/2}}\left[\int |U(x)|^4 dx \int |U(x/s)|^4 d(x/s)\right]^{1/2}$$

$$= \frac{1}{2\pi s^{1/2}}\int |U(x)|^4 dx\,.$$

Using Nagy's inequality as in (3.80):

$$V_{\Delta s}^{(2)} = \int_{s_2}^{s_1}\int |\chi_{uu}^{(2)}(\tau,s)|^2 d\tau ds \leq (2\pi)(\tfrac{1}{3}D_t^{\,2})^{1/2} \int_{s_2}^{s_1} s^{-1/2}\, ds$$

$$= 4\pi(\tfrac{1}{3}D_t^{\,2})^{1/2}(s_1^{1/2} - s_2^{1/2}). \quad \text{QED.} \tag{3.85}$$

3.4.5 Distribution of Volume of the Unsquared Function Above and Below the Plane $\hat{\chi}_{uu}^{(2)}(\tau,\beta) = 0$.

Theorem: If u(t) has no d.c. component, then $\int_{-1}^{1}\int_{-\infty}^{\infty} \hat{\chi}_{uu}^{(2)}(\tau,\beta)d\tau d\beta = 0$. That is, the volume of $\hat{\chi}_{uu}^{(2)}(\tau,\beta)$ is equally distributed above and below the plane $\hat{\chi}_{uu}^{(2)} = 0$.

Proof: From (3.40) and (3.72),

$$\int_{-\infty}^{\infty} \hat{\chi}_{uu}^{(2)}(\tau,\beta)d\tau = \frac{1}{2\pi}\left(\frac{1-\beta}{1+\beta}\right)^{1/2} |U(0)|^2 \tag{3.86}$$

$$\int_{-1}^{1}\left(\frac{1-\beta}{1+\beta}\right)^{1/2} d\beta = \int_{0}^{1}\left(\frac{1+x}{1-x}\right)^{1/2} dx + \int_{0}^{1}\left(\frac{1-x}{1+x}\right)^{1/2} dx$$

$$= 2\int_{0}^{1}\frac{dx}{(1-x^2)^{1/2}} = \pi\,,$$

by changing variables as in (3.78). Therefore,

$$\int_{-1}^{1}\int_{-\infty}^{\infty} \chi_{uu}^{(2)}(\tau,\beta)d\tau d\beta = \tfrac{1}{2}|U(0)|^2 \equiv 0\,. \quad \text{QED.} \tag{3.87}$$

A similar argument shows that narrowband volume is also equally distributed above and below the plane $\chi_{uu}^{(1)} = 0$, provided that U(o) = 0 or u(o) = 0.

3.5 Bounds on Ambiguity Function Amplitude

The first part of Sz.-Nagy's inequality can be used to find an upper bound on the wideband ambiguity function along a constant s profile.

Theorem:
$$\max_{-\infty < \tau < \infty} |\chi_{uu}^{(2)}(\tau,s)|^2$$

$$\leq \left[2\pi \left(\frac{D_t^2}{3s}\right)^{1/2}\right]^{1/2} \left[\int_{-\infty}^{\infty} \left|\frac{\partial}{\partial\tau} \chi_{uu}^{(2)}(\tau,s)\right|^2 d\tau\right]^{1/2} \tag{3.88}$$

Proof: For a = 2, p = 2, r = 2, and s fixed, the first part of Sz.-Nagy's inequality (Appendix B) gives*

$$\max_{\tau} |\chi_{uu}^{(2)}(\tau,s)| \leq \left[\int |\chi_{uu}^{(2)}(\tau,s)|^2 d\tau\right]^{1/4} \left[\int \left|\frac{\partial}{\partial\tau}\chi_{uu}^{(2)}(\tau,s)\right|^2 d\tau\right]^{1/4} \tag{3.89}$$

In the proof of Theorem 5 it was shown that

$$\int |\chi_{uu}^{(2)}(\tau,s)|^2 d\tau \leq 2\pi(D_t^2/3s)^{1/2} \tag{3.90}$$

and this proves the theorem. QED.

---

* where $\max_{\tau} \equiv \max_{-\infty < \tau < \infty}$

Corollary:

$$\max_{\tau} |\chi_{uu}^{(2)}(\tau,s)|^2 \leq s^{-1/2}\left[\frac{1}{2\pi}\int |U(\omega)|^4 d\omega\right]^{3/4}\left[\frac{1}{2\pi}\int \omega^4 |U(\omega)|^4 d\omega\right]^{1/4}$$

$$\leq s^{-1/2}(2\pi)^{3/4}\left(\frac{1}{3}D_t^2\right)^{3/8}\left[\frac{1}{2\pi}\int \omega^4 |U|^4 d\omega\right]^{1/4} \qquad (3.91)$$

Proof: $\int |\chi_{uu}^{(2)}(\tau,s)|^2 d\tau \leq \frac{1}{2\pi s^{1/2}} \int |U(\omega)|^4 d\omega$, from (3.85).

$$\int \left|\frac{\partial}{\partial\tau}\chi_{uu}^{(2)}(\tau,s)\right|^2 d\tau = \frac{1}{2\pi s}\int \omega^2 |U(\omega)|^2 |U(\omega/s)|^2 d\omega$$

$$\leq \frac{1}{2\pi s^{1/2}}\left[\int \omega^4 |U(\omega)|^4 d\omega \int |U(\omega/s)|^4 d(\omega/s)\right]^{1/2}. \qquad (3.92)$$

Substituting (3.92) and (3.85) into (3.89) gives the first inequality of the corollary. Substituting (3.80) into the first inequality gives the second. QED.

Finally, one can find a <u>lower</u> bound on $\max_{\tau} |\chi_{uu}^{(2)}(\tau,s)|^2$ for strictly time limited signals.

<u>Theorem</u>: $\max_{\tau} |\chi_{uu}^{(2)}(\tau,s)|^2 \geq \frac{s^2 \int R_u(\tau) R_u^*(s\tau) d\tau}{T(s+1)}$

where $u(t) \equiv 0$ for $|t| > T/2$

and $R_u(\tau) = \chi_{uu}^{(2)}(\tau,1)$.

Proof: The theorem is a consequence of the inequality

$$\int_{\tau_1}^{\tau_2} |\chi_{uu}^{(2)}(\tau,s)|^2 d\tau \leq \max_{\tau} |\chi_{uu}^{(2)}(\tau,s)|^2 \cdot (\tau_2 - \tau_1)_{max} \qquad (3.93)$$

where $(\tau_2 - \tau_1)_{max}$ is the maximum support in τ of the ambiguity function. For a strictly time limited signal with duration T,

$$\chi_{uu}^{(2)}(\tau,s) = s^{1/2} \int u(t) u^*[s(t+\tau)] dt$$

is the correlation of a signal with duration T and a signal with duration T/s. The quantity $s\tau$ can therefore have a maximum range of $T + T/s$ over which $\chi_{uu}^{(2)}$ is not identically zero. Then the maximum support in τ is $(1/s)(T + T/s) = T(s+1)/s^2$.

Since
$$|U(\omega)|^2 \longleftrightarrow R_u(\tau) \qquad (3.94)$$

and
$$\frac{|U(\frac{\omega}{s})|^2}{s} \longleftrightarrow R_u(s\tau) \qquad (3.95)$$

where $R_u(\tau) = \chi_{uu}^{(2)}(\tau,1)$ = the autocorrelation function of u(t) and "$\longleftrightarrow$" denotes a Fourier transform pair, Parseval's theorem applied to (3.84) yields:

$$\int_{-\infty}^{\infty} |\chi_{uu}^{(2)}(\tau,s)|^2 d\tau = \int_{-\infty}^{\infty} R_u(\tau) R_u^*(s\tau) d\tau \, . \qquad (3.96)$$

Substituting (3.96) into (3.93) and utilizing the fact that

$$(\tau_2 - \tau_1)_{max} = T(s+1)/s^2 \tag{3.97}$$

gives the required inequality. QED.

3.6 Some Transformations of the Signal and Their Effects on the Ambiguity Function

Theorem: If $u(t) \Longrightarrow \hat{\chi}_{uu}^{(2)}(\tau,\beta)$

$$\text{then } u(t+d) \Longrightarrow \hat{\chi}_{uu}^{(2)}\left(\tau - \frac{2d\beta}{1+\beta}, \beta\right) . \tag{3.98}$$

Proof: $u(t+d) \longleftrightarrow U(\omega)\exp(jd\omega)$. (3.99)

Substituting (3.99) into (3.40) yields the desired result. QED.

A comparable property for $\chi_{uu}^{(1)}(\tau,\phi)$ was derived by Siebert [18]:

$$\text{If } U(\omega) \Longrightarrow \chi_{uu}^{(1)}(\tau,\phi)$$

$$\text{then } U(\omega)\exp(jd\omega^2) \Longrightarrow \chi_{uu}^{(1)}(\tau - 2d\phi,\phi) . \tag{3.100}$$

Similar effects are achieved by a linear phase shift of $U(\omega)$, i.e., a time delay in $u(t)$, for the wideband function and a quadratic phase shift of $U(\omega)$ for the narrowband function.

Theorem: If $u(t) \Longrightarrow \hat{\chi}_{uu}^{(2)}(\tau,\beta)$

then $a^{1/2}u(at) \Longrightarrow \hat{\chi}_{uu}^{(2)}(a\tau,\beta)$, $a > 0$. (3.101)

Proof:

$$a^{1/2}u(at) \Longrightarrow \frac{(1-\beta^2)^{1/2}}{2}\int \frac{U\left[\frac{\omega}{a}(1+\beta)\right]}{a^{1/2}} \frac{U\left[\frac{\omega}{a}(1-\beta)\right]}{a^{1/2}} e^{-j\omega(1+\beta)\tau} d\omega . \tag{3.102}$$

Changing variables gives the result. QED.

Siebert's property for the narrowband function [18] is:

$$\text{If } u(t) \Longrightarrow \chi_{uu}^{(1)}(\tau,\phi)$$

$$\text{then } a^{1/2}u(at) \Longrightarrow \chi_{uu}^{(1)}(a\tau,\phi/a). \tag{3.103}$$

When $u(t)$ is compressed, the $\chi_{uu}^{(1)}$-function compensates for compression along the τ-axis by expansion along the ϕ-axis. The wideband function does not have this compensation feature. This helps to explain the volume result (3.80), i.e., the wideband function loses volume as the signal is compressed in time.

Corollary: If $u(t) \Longrightarrow \hat{\chi}_{uu}^{(2)}(\tau,\beta)$

$$\text{then } a^{1/2}u(at+d) \Longrightarrow \hat{\chi}_{uu}^{(2)}\left(a\tau - \frac{2d\beta}{1+\beta}, \beta\right). \tag{3.104}$$

The comparable result for narrowband:

$$\text{If } U(\omega) \Longrightarrow \chi_{uu}^{(1)}(\tau,\phi)$$

$$\text{then } a^{-1/2}U(\omega/a)e^{jd(\omega/a)^2} \Longrightarrow \chi_{uu}^{(1)}(a\tau-2d\phi/a,\phi a). \tag{3.105}$$

<u>Theorem</u>:

$$\text{If } u(t) \Longrightarrow \hat{\chi}_{uu}^{(2)}(\tau,\beta)$$

$$\text{then } u^{(n)}(t) \Longrightarrow (-1)^n\left(\frac{1-\beta}{1+\beta}\right)^n \frac{\partial^{2n}}{\partial\tau^{2n}}\left[\hat{\chi}_{uu}^{(2)}(\tau,\beta)\right], \tag{3.106}$$

$$\text{where } u^{(n)}(t) = d^n/dt^n[u(t)] .$$

<u>Proof</u>:

$$u^{(n)}(t) \longleftrightarrow (j\omega)^n U(\omega) . \tag{3.107}$$

Therefore,

$$\hat{\chi}_{u^{(n)}u^{(n)}}^{(2)}(\tau,\beta) \tag{3.108}$$

$$= \frac{(1-\beta^2)^{1/2}}{2\pi}\int [j\omega(1+\beta)]^n U[\omega(1+\beta)][-j\omega(1-\beta)]^n U^*[\omega(1-\beta)]e^{-j\omega(1+\beta)\tau}\,d\omega .$$

But

$$[j\omega(1+\beta)]^n[-j\omega(1-\beta)]^n = \omega^{2n}(1-\beta^2)^n .$$

Therefore,

$$\hat{\chi}_{u^{(n)}u^{(n)}}^{(2)}(\tau,\beta)$$

$$= \frac{(1-\beta^2)^{1/2}}{2\pi}(1-\beta^2)^n\int U[\omega(1+\beta)]U^*[\omega(1-\beta)]\omega^{2n}e^{-j\omega(1+\beta)\tau}\,d\omega . \tag{3.109}$$

$$\frac{d^{2n}}{d\tau^{2n}}e^{-j\omega(1+\beta)\tau} = [-j\omega(1+\beta)]^{2n}e^{-j\omega(1+\beta)\tau}$$

$$= (-1)^n\omega^{2n}(1+\beta)^{2n}e^{-j\omega(1+\beta)\tau} , \tag{3.110}$$

so that,

$$\hat{\chi}^{(2)}_{u(n)_u(n)}(\tau,\beta)$$

$$= (-1)^n \frac{(1-\beta^2)^n}{(1+\beta)^{2n}} \frac{(1-\beta^2)^{1/2}}{2\pi} \frac{\partial^{2n}}{\partial\tau^{2n}} \int U[\omega(1+\beta)]U^*[\omega(1-\beta)]e^{-j\omega(1+\beta)\tau} d\omega$$

$$= (-1)^n \left(\frac{1-\beta}{1+\beta}\right)^n \frac{\partial^{2n}}{\partial\tau^{2n}} [\chi^{(2)}_{uu}(\tau,\beta)]. \quad \text{QED.}$$

The time differentiation property is similar to the corresponding property of the ordinary autocorrelation function,

$$R_u(\tau) = (1/2\pi) \int |U(\omega)|^2 e^{j\omega\tau} d\omega . \tag{3.111}$$

However, there seems to be no such simple result for the narrowband ambiguity function with $\phi \neq 0$.

Theorem: If $u(t) \Longrightarrow \hat{\chi}^{(2)}_{uu}(\tau,\beta)$

$$\text{then} \underbrace{\int\int\cdots\int}_{n} u(t)d\underline{t} \Longrightarrow (-1)^n \left(\frac{1+\beta}{1-\beta}\right)^n \underbrace{\int\cdots\int}_{2n} \hat{\chi}^{(2)}_{uu}(\tau,\beta)d\underline{\tau} \tag{3.112}$$

Proof: The proof follows directly from the proof of (3.106) by substituting -n for n throughout. QED.

Again, the $\chi^{(1)}_{uu}$ function exhibits no such simple behavior for integrated u(t).

Theorem: If $u(t) \Longrightarrow \hat{\chi}_{uu}^{(2)}(\tau,\beta)$

$$\text{then } u_1 * u_2 \Longrightarrow \frac{1+\beta}{(1-\beta^2)^{1/2}} \hat{\chi}_{u_1u_1}^{(2)}(\tau,\beta) \overset{\tau}{*} \hat{\chi}_{u_2u_2}^{(2)}(\tau,\beta) \tag{3.113}$$

$$\text{where } u_1 * u_2 \equiv \int u_1(x)u_2^*(t-x)dx \ , \tag{3.114}$$

so that

$$\hat{\chi}_{u_1*u_2,u_1*u_2}^{(2)}(\tau,\beta) = \frac{(1+\beta)}{(1-\beta^2)^{1/2}} \int \hat{\chi}_{u_1u_1}^{(2)}(x,\beta)\hat{\chi}_{u_2u_2}^{(2)}(\tau-x,\beta)dx. \tag{3.115}$$

Proof: $$u_1(t) * u_2(t) \longleftrightarrow U_1(\omega)U_2(\omega) \tag{3.116}$$

so that

$$\hat{\chi}_{u_1*u_2,u_1*u_2}^{(2)}(\tau,\beta) = \frac{(1-\beta^2)^{1/2}}{2\pi} \int U_1[\omega(1+\beta)]U_2[\omega(1+\beta)]$$

$$\cdot U_1^*[\omega(1-\beta)]U_2^*[\omega(1-\beta)]e^{-j\omega(1+\beta)\tau}\, d\omega \tag{3.117}$$

$$\int \hat{\chi}_{u_1u_1}^{(2)}(x,\beta)\hat{\chi}_{u_2u_2}^{(2)}(\tau-x,\beta)dx$$

$$= \frac{1-\beta^2}{(2\pi)^2} \iiint U_1[\omega_1(1+\beta)]U_1^*[\omega_1(1-\beta)]e^{-j\omega_1(1+\beta)x}$$

$$\cdot U_2[\omega_2(1+\beta)]U_2^*[\omega_2(1-\beta)]e^{-j\omega_2(1+\beta)(\tau-x)}\, d\omega_1 d\omega_2 dx. \tag{3.118}$$

Using (3.72) and integrating with respect to x and ω_2:

$$\int \hat{\chi}^{(2)}_{u_1 u_1}(x,\beta)\hat{\chi}^{(2)}_{u_2 u_2}(\tau-x,\beta)dx$$

$$= \frac{(1-\beta^2)}{2\pi(1+\beta)}\int U_1[\omega_1(1+\beta)]U_2[\omega_1(1+\beta)]U_1^*[\omega_1(1-\beta)]U_2^*[\omega_1(1-\beta)]$$

$$\cdot e^{-j\omega_1(1+\beta)\tau} d\omega_1$$

$$= \frac{(1-\beta^2)^{1/2}}{1+\beta}\ \hat{\chi}^{(2)}_{u_1^* u_2, u_1^* u_2}(\tau,\beta)\ . \qquad \text{QED.}$$

The narrowband version of the above theorem was derived by Siebert, and can be found in the doctoral dissertation of E. L. Titlebaum [19]:

$$\chi^{(1)}_{u*v,u*v}(\tau,\phi) = \chi^{(1)}_{uu}(\tau,\phi) \overset{\tau}{*} \chi^{(1)}_{vv}(\tau,\phi)\ . \qquad (3.119)$$

The following two theorems use the type of transformation suggested by J. Speiser [20]. Speiser's theory is summarized in section 3.7.

Theorem: If $U(\omega) \Longrightarrow \hat{\chi}^{(2)}_{uu}(0,\beta)$

then for $\beta \ll 1$, $U(\log\omega)/\omega^{1/2} \Longrightarrow \chi^{(1)}_{uu}(0,-2\beta)$. (3.120a)

provided u(t) is Analytic. In other words, if $U(\omega) = 0$ for $\omega < 0$ and $\beta \ll 1$,

$$\hat{\chi}^{(2)}_{U(\log\omega)/\omega^{1/2}}(0,\beta) \approx \chi^{(1)}_{U(\omega)}(0,-2\beta), \qquad (3.120b)$$

Proof:

$$\frac{U(\log\omega)}{\omega^{1/2}} \Longrightarrow \frac{(1-\beta^2)^{1/2}}{2\pi}\int_0^\infty \frac{U[\log\omega+\log(1+\beta)]U^*[\log\omega+\log(1-\beta)]}{\omega(1-\beta^2)^{1/2}}d\omega$$

for $\tau = 0$. Letting $\omega' = \log\omega$:

$$\frac{U(\log\omega)}{\omega^{1/2}} \Longrightarrow \frac{1}{2\pi}\int U[\omega'+\log(1+\beta)]U^*[\omega'+\log(1-\beta)]d\omega'. \qquad (3.122)$$

For $\beta \ll 1$, $\log(1+\beta) \approx \beta$ and $\log(1-\beta) \approx -\beta$, so that

$$\frac{U(\log\omega)}{\omega^{1/2}} \Longrightarrow \frac{1}{2\pi}\int U(\omega+\tfrac{2\beta}{2})U^*(\omega-\tfrac{2\beta}{2})d\omega = \chi^{(1)}_{uu}(0,-2\beta) \text{ QED.}$$

Theorem: If $u(t) \Longrightarrow \hat{\chi}^{(2)}_{uu}(0,\beta)$, then for $\beta \ll 1$ and $u(t)$ causal,

$$u(\log t)/t^{1/2} \Longrightarrow \chi^{(1)}_{uu}(2\beta,0), \qquad (3.123)$$

i.e., $$\hat{\chi}^{(2)}_{\frac{u(\log t)}{\sqrt{t}}}(0,\beta) \approx \chi^{(1)}_{uu}(2\beta,0).$$

Proof: Using equation (3.39),

$$\hat{\chi}^{(2)}_{\frac{u(\log t)}{\sqrt{t}}}(0,\beta) \approx \int_0^\infty u[\log t-\log(1+\beta)]u^*[\log t-\log(1-\beta)]\frac{dt}{t}$$

$$\approx \int_{-\infty}^{\infty} u(t-\beta)u^*(t+\beta)dt = \int_{-\infty}^{\infty} u(t)u(t+2\beta)dt$$

$$= \chi^{(1)}_{uu}(2\beta,0). \quad \text{QED.}$$

Theorem: If $U(\omega) \Longrightarrow |\chi_{uu}^{(2)}(\tau,s)|^2$

$$\text{then } U(\omega)\exp(jk \log \omega) \Longrightarrow |\chi_{uu}^{(2)}(\tau,s)|^2. \qquad (3.124)$$

That is, the added phase factor $\exp(jk \log \omega)$ has no effect at all on the magnitude-squared wideband ambiguity function.

Proof: If $U(\omega) \rightarrow U(\omega)\exp(jk \log \omega)$, then

$$\chi_{uu}^{(2)}(\tau,s) \longrightarrow \frac{1}{2\pi}\int U(\omega)\, \frac{U^*(\omega/s)}{\sqrt{s}}\, e^{-j\omega\tau}\cdot e^{jk[\log \omega - \log(\omega/s)]}\, d\omega \qquad (3.125)$$

But $\log \omega - \log(\omega/s) = \log s$. Therefore,

$$\chi_{uu}^{(2)}(\tau,s) \longrightarrow e^{jk \log s}\, \chi_{uu}^{(2)}(\tau,s) \qquad (3.126)$$

so that $|\chi_{uu}^{(2)}(\tau,s)|^2 \longrightarrow |\chi_{uu}^{(2)}(\tau,s)|^2$. QED.

As one would suspect from (3.120), the narrowband equivalent is:

$$\text{If } U(\omega) \Longrightarrow |\chi_{uu}^{(1)}(\tau,s)|^2$$

$$\text{then } U(\omega)\exp(jk\omega) \Longrightarrow |\chi_{uu}^{(1)}(\tau,s)|^2. \qquad (3.127)$$

Unfortunately, the time version is a bit more restrictive for the wideband case:

Theorem: If $u(t) \Longrightarrow |\chi_{uu}^{(2)}(0,s)|^2$

$$\text{then } u(t)\exp(jk\log t) \Longrightarrow |\chi_{uu}^{(2)}(0,s)|^2. \qquad (3.128)$$

The proof is basically the same as for (3.124). The function $\log t - \log[s(t+\tau)]$ is not a function of t only if $\tau = 0$; this is the source of the restriction to the s-axis.

The narrowband case is as general as before, since the form of $\chi_{uu}^{(1)}$ is symmetrical in time and frequency (compare 2.2 and 3.35):

$$\text{If } u(t) \Longrightarrow |\chi_{uu}^{(1)}(\tau,s)|^2$$

$$\text{then } u(t)\exp(jkt) \Longrightarrow |\chi_{uu}^{(1)}(\tau,s)|^2. \qquad (3.129)$$

3.7 J. Speiser's Properties

The following properties were originally derived by J. Speiser [20] for the $\chi_{uu}^{(3)}(\tau,s)$ function. They appear here adapted to the $\chi_{uu}^{(2)}(\tau,s)$ function for the special case that u(t) is causal ($u(t) \equiv 0$, $t < 0$).

The results derived below will show that, along certain curves in the (τ,s) plane, the wideband ambiguity function may be written as an autocorrelation function. The major implication of Speiser's work is that, since much is known about autocorrelation functions, this knowledge can now be applied to the synthesis of

ambiguity functions. For example, certain pulse train modulations (such as Huffman codes or Barker codes [4]) have been devised to give a large autocorrelation peak with minimal sidelobe levels. These waveforms can now be applied to the wideband function in order to achieve good doppler resolution properties.

$$\text{If} \quad s = e^{z} \ , \tag{3.130}$$

then for causal signals

$$\chi_{uu}^{(2)}(0,z) \equiv e^{z/2} \int_{0}^{\infty} u(t)\, u^{*}(e^{z}t)dt \ . \tag{3.131}$$

Letting $t = e^{t'}$,

$$\begin{aligned}
\chi_{uu}^{(2)}(0,z) &= e^{z/2} \int_{-\infty}^{\infty} u(e^{t'})u^{*}(e^{t'+z})e^{t'}dt' \\
&= \int_{-\infty}^{\infty} [e^{t'/2}\, u(e^{t'})][e^{(t'+z)/2}\, u^{*}(e^{t'+z})]dt' \\
&= \int_{-\infty}^{\infty} h(t')h^{*}(t'+z)dt' \qquad (3.132)
\end{aligned}$$

where $h(t) = e^{t/2}u(e^{t})$ (3.133)

or $u(t) = (1/t^{1/2})h(\log t)$. (3.134)

Hence, the $\tau = 0$ profile of the wideband ambiguity function may be written as the autocorrelation function of $h(t)$.

The transformations (3.133-4) are energy-preserving (unitary) since

$$\int_0^\infty |h(t)|^2 dt = \int_0^\infty e^t |u(e^t)|^2 dt = \int_{-\infty}^\infty |u(t')|^2 dt'. \tag{3.135}$$

A similar transformation turns $\chi_{uu}^{(2)}$ evaluated along other curves on the τ,s plane into autocorrelation functions. In particular, consider those curves through the point $\tau = 0$, $s = 1$, having the equation:

$$\tau(s) = c(1 - 1/s). \tag{3.136}$$

Then $$\chi_{uu}^{(2)}(c,z) = e^{z/2} \int_0^\infty u(t)u^*[e^z(t+c) - c]dt. \tag{3.137}$$

Letting $t + c = e^{t'}$:

$$\chi_{uu}^{(2)}(c,z) = e^{z/2} \int_{\log c}^\infty u(e^{t'} - c)u^*(e^{z+t'} - c)e^{t'}dt'$$

$$= \int_{\log c}^\infty [e^{t'/2} u(e^{t'} - c)][e^{(z+t')/2} u^*(e^{z+t'} - c)]dt' \tag{3.138}$$

$$= \int_{\log c}^\infty h_c(t')h_c(t' + z)dt', \tag{3.139}$$

where $h_c(t) = e^{t/2}u(e^t - c)$ (3.140)

or $$u(t) = h_c[\log(t + c)]/(t + c)^{1/2} \ . \qquad (3.141)$$

Since $u(t) \equiv 0$ for $t < 0$, $h_c(t) \equiv 0$ for $t < \log c$. Thus (3.139) can be written as a true autocorrelation function:

$$\chi_{uu}^{(2)}(c,s) = \int_{-\infty}^{\infty} h_c(t)h_c^*(t+z)dt \ . \qquad (3.142)$$

As before,

$$\int_{\log c}^{\infty} |h_c(t)|^2 dt = \int_0^{\infty} |u(t)|^2 dt \ . \qquad (3.143)$$

It should be mentioned that the $\chi_{uu}^{(3)}(\tau,s)$ function, with which Speiser originally worked, has (3.139) true for $\tau(s) = c(s-1)$, i.e., straight lines through the origin ($\tau = 0$, $s = 1$). On the τ,β plane, however, $c(s-1) = c[2\beta/(1-\beta)]$, while $c(1-1/s) = c[2\beta/(1+\beta)]$, indicating the basic similarity of the curves so far as velocity is concerned.

It is interesting to note that, if $h(t)$ in (3.133) is equal to the non-L^2 function $\cos(kt)$, then $u(t)$ in (3.134) equals $(1/t)^{1/2}\cos(k \log t)$, a waveform which will reappear in chapter IV.

3.8 D. Hageman's Counter-example

As the reader has undoubtedly noticed, the major emphasis in this chapter has been on the $\chi_{uu}^{(2)}$ (Kelly-Wishner) version of the

wideband ambiguity function. In addition to the argument in section 2.2, the following example should demonstrate the advantage of $\chi_{uu}^{(2)}$ over $\chi_{uu}^{(3)}$. The example was devised by D. Hageman of the Naval Undersea Research and Development Center.

Suppose the signal is sufficiently narrow in time to be represented as a delta function, $\delta(t)$. For a target with doppler factor s and delay parameter $\tau = 2R/\tilde{v}$, where R is the radial distance to the target at the instant of reflection, the various echos are:

For $\chi_{uu}^{(2)}$: $r(t) = \delta[s(t - \tau)] = (1/s)\delta(t - \tau)$ (3.144a)

For $\chi_{uu}^{(3)}$: $r(t) = \delta(st - \tau) = (1/s)\delta(t - \tau/s)$. (3.144b)

It clearly makes sense to write the time of arrival of the echo as $t = \tau$. The Kelly-Wishner return is the only model for which this result holds if $s \neq 1$.

3.9 Skew Symmetry Relations

It follows from (3.40) and (3.41) that

$$\hat{\chi}_{iu}^{(2)}(\tau, \beta) = \hat{\chi}_{uu}^{(3)*}(-\tau, -\beta) \ . \qquad (3.145)$$

Equation (3.145) explains the similarity of the curves along which the $\chi_{uu}^{(2)}$ and $\chi_{uu}^{(3)}$ functions may be written as autocorrelations

(Section 3.7); it also explains the identical first order origin properties of $|\chi_{uu}^{(2)}|^2$ and $|\chi_{uu}^{(3)}|^2$ (Section 3.2.2).

It also follows from (3.40) that

$$\hat{\chi}_{uu}^{(2)}\left(-\frac{1+\beta}{1-\beta}\,\tau,\ -\beta\right) = \hat{\chi}_{uu}^{(2)*}(\tau,\beta)$$

so that

$$\chi_{uu}^{(2)}(-s\tau,\ 1/s) = \chi_{uu}^{(2)*}(\tau,s)\ . \tag{3.146a}$$

The well-known narrowband version of (3.146a) is skew symmetry in range and velocity, and follows directly from (3.37):

$$\chi_{uu}^{(1)}(-\tau,-\phi) = \chi_{uu}^{(1)*}(\tau,\phi) \tag{3.146b}$$

3.10 Separation Properties

Theorem (J. Speiser [21]):

If $F_{u_1u_2}(\tau,s) = \chi_{u_1u_2}^{(3)}(\tau,s)$, that is, if F is a wideband cross-ambiguity function, then

$$\int e^{jB\tau} F_{u_1u_2}(\tau,A/B)\,d\tau = \sqrt{\frac{A}{B}}\, H_1(A)H_2^*(B) \qquad \text{for } B \neq 0 \tag{3.147}$$

and

$$\int F_{u_1 u_2}(\tau,s)d\tau = \sqrt{\frac{A}{B}}\, U_1(0)U_2^*(0) \text{ (for all s)}, \quad (3.148)$$

where

$$U_k(\omega) \longleftrightarrow u_k(t) .$$

Proof: The equivalent of (3.148) has already been proven in connection with (3.87) (distribution of volume). By substituting $\chi^{(3)}_{u_1 u_2}(\tau,s)$ into (3.147):

$$\int e^{jB\tau}\left[\frac{1}{2\pi\sqrt{A/B}}\int U_1(\omega)U_2^*(\frac{\omega B}{A})e^{-j\omega(B/A)\tau}d\omega\right]d\tau$$

$$= \frac{\sqrt{B/A}}{2\pi}\int U_1(\omega)U_2^*(\frac{\omega B}{A})\left[\int e^{-jB\tau[(\omega/A)-1]}d\tau\right]d\omega$$

$$= \sqrt{B/A}\int \frac{1}{B/A}\delta(\omega-A)U_1(\omega)U_2^*(\frac{\omega B}{A})d\omega$$

$$= (A/B)^{1/2}\, U_1(A)U_2^*(B) \qquad \text{QED} \qquad (3.149)$$

Corollary 1: Equation (3.87) holds for cross-ambiguity functions as well as auto-ambiguity functions, provided one of the signals has zero d.c. component.

Corollary 2: (Speiser): If $\chi^{(3)}_{u_1 u_1}(\tau,s) = \chi^{(3)}_{u_2 u_2}(\tau,s)$, then $u_1(t) = e^{jk}u_2(t)$, where k is an arbitrary constant.

Corollary 3 (Speiser): If (3.147) holds for some function $F_{u_1u_1}$, then $F_{u_1u_1}$ is a $\chi^{(3)}_{uu}$-type ambiguity function. That is, condition (3.147) is both a necessary and sufficient requirement for some function of two variables to be an ambiguity function of type $\chi^{(3)}_{uu}$.

Corollary 4: $$\int e^{jA\tau} F_{u_1u_2}(\tau, A/B)d\tau = (B/A)^{1/2} U_1(A)U_2^*(B) \qquad (3.150)$$

if and only if $F_{u_1u_2}(\tau,s) = \chi^{(2)}_{u_1u_2}(\tau,s)$.

3.11 Narrowbandedness and Narrowtimeness

The discussion leading to equation (3.69) was concerned with conditions under which the true echo approximates the Woodward echo model. It is also relevant to consider band limited signals for which the conditions (3.69) do not necessarily hold true. One does not expect such cases to be amenable to the Woodward approximation, but some simplified results may still be possible, along with added insight concerning wideband analysis.

Consider first a strictly band limited signal,

$$|U(\omega)| \neq 0 \text{ if and only if } \omega_{min} \leq \omega \leq \omega_{max} \qquad (3.151)$$

where $\omega_{min} > 0$. See Figure 3.2.

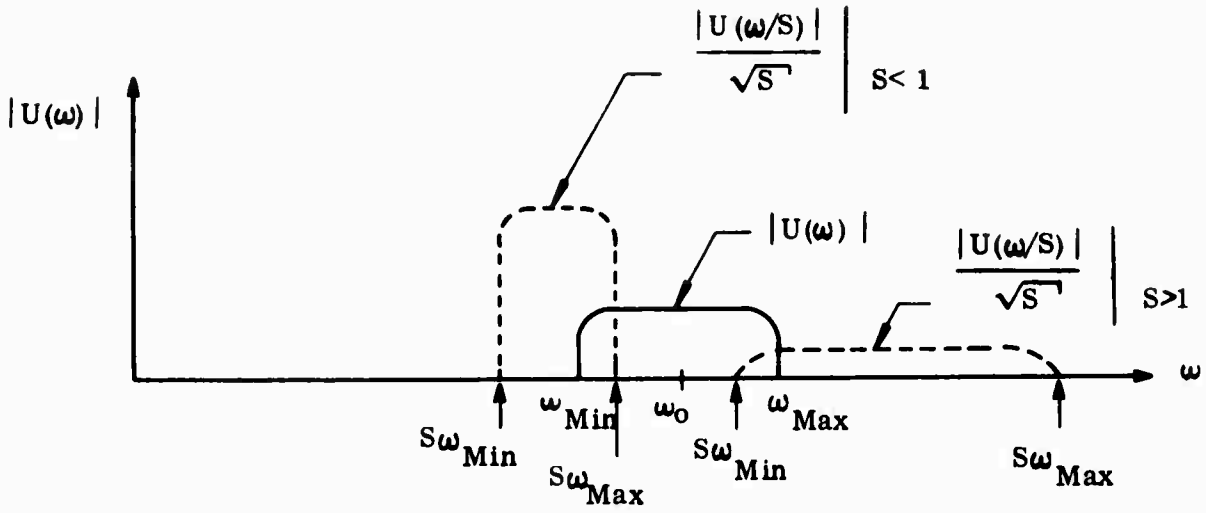

Figure 3.2. Doppler Scale Factors Applied to a Bandlimited Signal.

There will be no overlap between the band limited signal (3.151) and its scaled self if either

$$s\omega_{max} < \omega_{min}; \qquad s < \frac{\omega_{min}}{\omega_{max}} \tag{3.152}$$

or

$$s\omega_{min} > \omega_{max}; \qquad s > \frac{\omega_{max}}{\omega_{min}} \quad . \tag{3.153}$$

It follows from (3.152) and (3.153) that

$$\chi_{uu}^{(2)}(\tau,s) \equiv 0 \text{ if } \begin{cases} s > \dfrac{\omega_o + W/2}{\omega_o - W/2} \\ s < \dfrac{\omega_o - W/2}{\omega_o + W/2} \end{cases} \tag{3.154}$$

where

$$\omega_{min} = \omega_o - W/2$$

$$\omega_{max} = \omega_o + W/2 \qquad (3.155)$$

$$0 < W/2 < \omega_o \ .$$

The greatest possible support for the ambiguity function in the s-direction is then the interval

$$\frac{\omega_o + W/2}{\omega_o - W/2} - \frac{\omega_o - W/2}{\omega_o + W/2} = \frac{2W/\omega_o}{1 - (W/2\omega_o)^2} \approx 2\frac{W}{\omega_o}\Big|_{\omega_o >> W/2} \qquad (3.156)$$

Equation (3.156) suggests that one way (but not necessarily the only way) to achieve high resolution in velocity is to make the signal comparatively narrowbanded. If, on the other hand, an insensitivity to velocity is desired (i.e., good doppler tolerance), it is necessary that the signal be made comparatively widebanded.

Now consider a time function u(t) such that

$$u(t) \equiv 0 \text{ if and only if } t_o - T/2 \leq t \leq t_o + T/2. \qquad (3.157)$$

By an argument similar to that given above, one sees immediately that the greatest possible support for the $\chi_{uu}^{(2)}(0,s)$ function is confined to the interval

$$\frac{2T/t_o}{1 - (T/2t_o)^2} \approx 2\frac{T}{t_o}\Big|_{t_o >> T/2} \qquad (3.158)$$

where $0 < T/2 < t_o$.

Equation (3.158) is a rather strange result. It implies that $\chi_{uu}^{(2)}(0,s)$ is dependent upon the time origin of a time limited signal. Mathematically, it is a result analogous to the narrowband solution (3.156) arising from the identical operations in time and frequency of stretching-followed-by-correlation. Physically, it would seem to indicate a trade-off between duration of observation time and accuracy of velocity measure, somewhat similar to the time-energy uncertainty principle of quantum mechanics.

3.12 Utilization of Ambiguity Function Properties Derived in this Chapter.

The foregoing results are so varied that comparatively few will be utilized in the remainder of this dissertation. Those properties that will be used or referenced in the sequel are as follows:

1. The second derivatives of $|\chi_{uu}^{(2)}(\tau,s)|^2$ at $(\tau,s) = (0,1)$ (equations 3.18) and the average curvature concept (3.31).

2. The upper bound for ambiguity volume over any strip drawn parallel to the τ-axis (3.83-3.85), and its dependence upon D_t^2.

3. The fact that the time scaling $a^{1/2}u(at)$ results in a τ-scaled wideband ambiguity function with no change of scale along the velocity axis (3.101).

4. The ambiguity function of two convolved signals is a τ-convolution of two auto-ambiguity functions (3.113).

5. $\chi_{uu}^{(2)}(\tau,s)$ is the only ambiguity function whose echo model has a straightforward physical interpretation for $u(t) = \delta(t)$. (3.144)

6. The more narrowbanded a function becomes, the smaller is its support along the s-axis (3.156).

Although many of the ambiguity properties of this chapter are not necessarily germane to the remainder of the dissertation, they have nevertheless been catalogued as possible aids to future analysis.

CHAPTER IV

DOPPLER TOLERANCE

The following discussion is still concerned with the special case of constant velocity point targets. The basic task of this chapter is to illustrate the ways in which some of the ideas developed in Chapters II and III can be used to derive a wideband signal possessing a specific desired property. The particular property which will be required of the signal is chosen to be doppler tolerance [6].

Doppler tolerance can be defined in several equivalent ways. Basically, the property implies that a doppler compressed (or stretched) signal will still be recognized (by a single correlation process) as a reflected version of the transmitted waveform, regardless of the reflector's velocity. If one makes hypotheses about target velocity as discussed in Section 3.1, the maximum correlator output will be relatively insensitive to the velocity hypothesis if the signal is doppler tolerant. Such a waveform will make $\max_{-\infty<\tau<\infty} |\chi_{uu}^{(2)}(\tau, s)|^2$ relatively insensitive to changes in s.

If one envisions a target whose parts move relative to one another, the doppler tolerant waveform can be a means of obtaining maximum correlator response if the signal is reflected from such a target. This sort of advantage tends to be obscured by an energy normalization, but it is obviously of practical importance if such targets exist. Two examples:

1. A missile or meteor whose ionized "chaff" or tail is constantly created and left behind, resulting in a composite target with a wide range of velocities.
2. An insect (e.g., a moth) whose wings add greatly to its acoustic cross section, provided their reflections add to correlator output in spite of the wings' velocities relative to the thorax.

The above comments concerning targets whose parts move relative to each other are subject to some qualification. It is true in both narrowband [4] and wideband [22] analysis that the ambiguity function can have a long, narrow constant amplitude ellipse near the origin, like that shown in Figure 4.1.

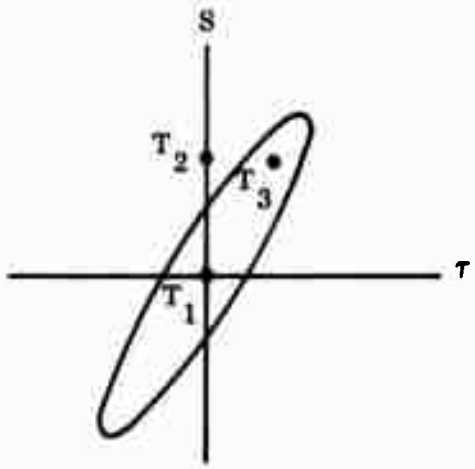

Figure 4.1. Illustration of Point Target Resolution Capability.

If the target is characterized by points T_1 and T_2 in Figure 4.1 (two points at exactly the same range but with differing velocities), the correlator will not react strongly to the response from both targets. If, however, the target consists of T_1 and T_3, then a greater correlator response will occur.

Both the meteor and the insect will probably have some target points outside the ellipse and others within it. To the extent that echo points lie within the ellipse, one can think of correlator output power as being embellished, enhancing initial detectability. In this sense, doppler tolerance may be conceived as antithetical to unambiguous target resolution . If one seeks to separate a missile from its chaff (perhaps with the intent of distinguishing it from a meteor), a "thumbtack" ambiguity function is desirable. Such a resolving waveform separates the target into its component parts; the tolerant waveform seeks to lump the parts (or, at least, some of the parts) together.

4.1 Trajectory Diagram Approach.

4.1.1 Trajectories to Reduplicate a Given Signal.

If the correlation between two signals (or the inner product of two signal vectors in the space of square-integrable functions) is really a measure of their similarity, then a doppler tolerant signal is one which reduplicates itself under a whole group of possible energy invariant time scalings. Consider, then, an arbitrary waveform that is reduplicated by reflection from a moving target (Figure 4.2).

Figure 4.2 indicates a group of possible trajectories that result in reduplication (more or less) of the arbitrary waveform. These trajectories are constructed by connecting the intersections (or reflection points) of the 45^{o} construction lines [6]. The trajectories with more reflection points will yield better reduplications. The best such trajectory is seen to be the horizontal one, i.e., a motionless point target. This corresponds well with the definition of a point target as one which, when held motionless, returns an undistorted version of the transmitted signal.

As demonstrated by the above argument (paraphrased from Rihaczek [6]) it is a straightforward process to obtain acceptance trajectories (i.e., trajectories which result in a reduplicated waveform and therefore "acceptance" of the returned echo as a reflected version of the signal) if the signal is given. But the reverse process, i.e., finding the signal-matched filter pair when the target trajectory is given, is not explicitly discussed by Rihaczek. It is simple to find an unmatched filter to accept a given trajectory for a given signal; an important example is the compressed version of the

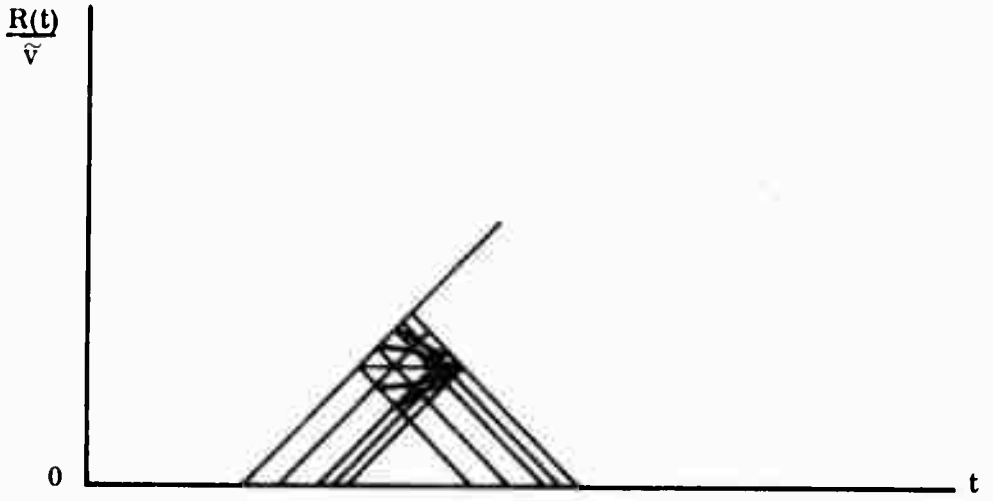

Figure 4.2. Trajectories Which Result in Approximate Reduplication of a Given Waveform.

signal used for velocity hypothesis testing and illustrated in Figure 2.4. In fact, it is also possible to find a matched signal-filter pair when an arbitrary trajectory is given. A graphical method for doing this will now be introduced.

4.1.2 A Method of Deriving Signals That Reduplicate Themselves When Reflected From a Point Target With Given Trajectory.

Careful study of Figure 4.2 reveals the following properties of trajectory diagrams.

1. The horizontal line always produces a reflection that duplicates the incident signal (a property that has already been discussed).
2. The other trajectories which (more or less) reduplicate the incident waveform must pass through the intersections of the 45° construction lines. Certain points on the trajectory are thus apexes of 45° right triangles with bases on a horizontal line (a fact that was used in Chapter II).
3. Because of the geometry of the diagram, if a trajectory reduplicates a given signal, then its reflection about the horizontal trajectory also reduplicates the signal. For constant-velocity (linear) trajectories, this means that a signal-matched filter pair accepting a trajectory with slope β will also accept the one with slope $-\beta$.

The above three properties suggest a straightforward graphical method to find the signal that reduplicates itself when reflected from a point target with a particular trajectory (linear or nonlinear).

1. Given the trajectory, construct its mirror image about a horizontal line.
2. Inscribe diamond-shaped figures with 45^{o} sides between the two curves (trajectory and image) as shown in Figure 4.3.
3. The matched signal's zero crossings, maxima and minima, etc., are found from the abscissa intercepts of the lines delineating the inscribed diamonds.

This method will be called "the inscribed diamond construction technique."

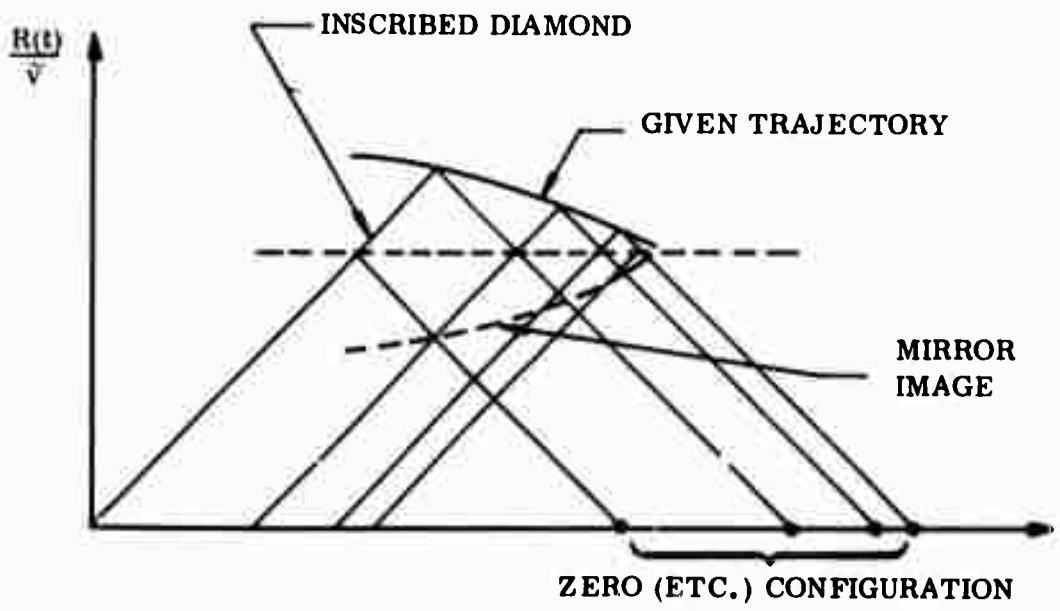

Figure 4.3. The Inscribed Diamond Construction Technique.

4.1.3 Application of the Inscribed Diamond Method to Linear Trajectories.

Given a linear trajectory with slope β , one wishes to design a signal-matched filter pair that will accept this trajectory. In other words, one wishes to find a signal which will very nearly reduplicate itself upon reflection from a point target with given constant velocity.

The inscribed diamond technique, when applied to a linear trajectory such as that shown in Figure 2.2, results in a diagram like the one shown in Figure 2.3. The only difference is that now there are many (instead of only two) triangles inscribed side-by-side within the two rays. Just as the ratio of t_1 to t_2 (Figure 2.3) was shown to be s, this is the ratio of t_2 to t_3 (t_3 being the base of the next triangle, corresponding to the diagonal of the next inscribed diamond).

If the construction lines are taken to symbolize real zero locations, and if one is working with an analytic signal:

$$u(t) = u_R(t) + j\hat{u}_R(t) = \alpha(t)\, e^{j\theta(t)} \tag{4.1}$$

$$u_R(t) = \alpha(t) \cos \theta(t) \tag{4.2}$$

where

$\hat{u}(t)$ = the Hilbert transform of u(t),

then if $\alpha(t)$ is slow-varying or non-oscillatory, $u_R(t)$ will have zeros at times z_n such that

$$\theta(z_n) = (2n+1)\, \pi/2 \quad . \tag{4.3}$$

If the first zero occurs at t = 0, then it is evident from the inscribed diamond technique that

$$t_2 = t_1/s;\ t_3 = t_2/s = t_1/s^2;\ t_n = t_1/s^{n-1} \quad . \tag{4.4}$$

If z_o occurs at t = 0, then z_1 occurs at $t = t_1$, z_2 occurs at $t = t_1 + t_2$, z_n at time $t = t_1 + t_2 + \ldots + t_n$. That is, if $t_1 = 1$:

$$z_1 = t_1 = 1 \tag{4.5a}$$

$$z_2 = t_1 + t_2 = (1 + 1/s)\, t_1 = (1 + 1/s) \tag{4.5b}$$

$$z_n = t_1 = t_2 + \ldots + t_n = (1 + 1/s + \ldots + 1/s^{n-1}) \ . \tag{4.5c}$$

It is clear from (4.4) and Figure 2.3 that $1/s < 1$. Therefore (4.5c) may be written in closed form as

$$z_n = \frac{1 - (1/s)^n}{1 - (1/s)} \quad . \tag{4.6}$$

Thus the desired phase function $\theta(t)$ is such that

$$\theta \left\{ [1 - (1/s)^n] / [1 - (1/s)] \right\} = 2n\,\pi/2 + \pi/2 \ . \tag{4.7}$$

$\theta(t)$ must be capable of converting n as exponent to n as multiplier. This immediately suggests a logarithmic variation with n. One can therefore attempt to write $\theta(t)$ in a general form such as:

$$\theta(t) = f(s) \log [h(s) + g(s)\, t] \tag{4.8}$$

and determine whether there exist three functions (or constants) f, h, and g such that (4.7) holds true:

$$f(\zeta) \log \left[h(\zeta) + g(\zeta) \left(\frac{1 - \zeta^n}{1 - \zeta} \right) \right] = (2n + 1)\, \pi/2 \qquad (4.9)$$

where

$$\zeta = 1/s.$$

Letting

$$g(\zeta) = (1 - \zeta)\, g_1(\zeta)\, e^{\pi/2f(\zeta)}$$

$$h(\zeta) = h_1(\zeta)\, e^{\pi/2f(\zeta)} ,$$

(4.9) gives

$$h_1(\zeta) + (1 - \zeta^n)\, g_1(\zeta) = e^{n\pi/f(\zeta)} .$$

Letting $h_1 = 1$ and $g_1 = -1$ gives

$$\zeta = e^{\pi/f(\zeta)}$$

so that

$$f(\zeta) = \pi/\log \zeta .$$

(4.8) thus becomes

$$\theta(t) = (\pi/\log \zeta) \log \left[e^{1/2 \log \zeta} - t(1 - \zeta)\, e^{1/2 \log \zeta} \right]$$

$$= \pi/2 + (\pi/\log(1/s)) \log \left[1 - t(1 - 1/s) \right] . \qquad (4.10)$$

The reader can verify that (4.10) satisfies (4.7). For a given value of s, one can rewrite (4.10) as:

$$\theta(t) = \pi/2 + k_1 \log (1 - k_2 t) . \qquad (4.11)$$

Then

$$\text{Cos } \theta(z_n) = -\text{Sin } [k_1 \log(1 - k_2 t)\ ]$$

$$= -\text{Sin}(n\pi) = 0. \qquad (4.12)$$

Using a more heuristic approach, Rihaczek [6] derived a phase function:

$$\theta_R(t) = k_3 \log(1 - k_2 t) \quad . \qquad (4.13)$$

If $k_3 = k_1/2$, then Cos $\theta_R(z_n)$ = Cos$(n\pi/2) = 0$ for odd values of n. The Rihaczek phase function is seen to match a slightly different linear trajectory than that of (4.10-11); aside from this, the two solutions are equivalent.

The horizontal construction line in Figure 4.3 could just as easily have been drawn above the given trajectory as below it. As shown in Figure 4.4, this is equivalent to reflecting all the inscribed diamonds about a vertical line passing through the intersection of trajectory and horizontal construction line (point A).

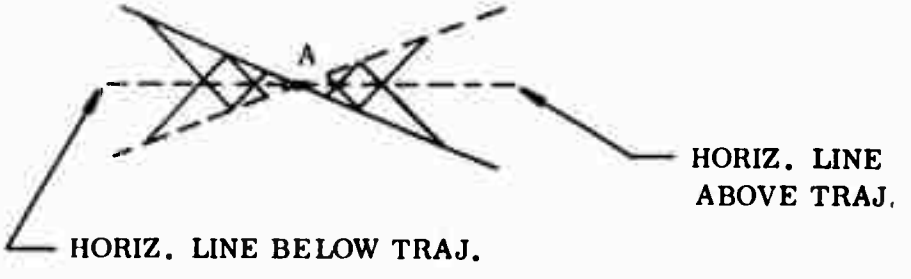

Figure 4.4. Two Possible Inscribed Diamond Solutions for a Given Trajectory.

In terms of the solution $\theta(t) = k_3 \log(1 - k_2 t)$, the construction shows that an equally valid solution is obtained by letting $t' = -t + 1/k_2$;

$$\theta(t') = k_3 \log(1 + k_2 t - 1) = k_3 \log(k_2 t) \quad . \tag{4.14}$$

It has thus been demonstrated via trajectory diagrams that a doppler accepting phase has the form (4.11), (4.13), or (4.14). In the process of the demonstration, a new construction technique has been derived. This technique should prove especially useful for cases involving non-linear trajectories.

4.1.4 Doppler Tolerant Pulse Trains.

Suppose that each of the 45° lines in Figure 2.2 represents the position of a pulse within a signal composed of a sequence of pulses. A doppler tolerant pulse train would then have interpulse spacings as described by Equation (4.4):

$$t_n = (1/s)\, t_{n-1} = (1/s)^2 t_{n-2} = (1/s)^k t_{n-k}$$

or

$$t_n = \left(\frac{1-\beta}{1+\beta}\right)^k t_{n-k} \approx (1 - 2\beta)^k t_{n-k} \quad . \tag{4.15}$$

Rihaczek has derived a similar expression without reference to trajectory diagrams ([6], Equation (12.30)) .

4.2 Compression Diagram Interpretation.

For the special case of constant velocity point targets, there is another diagrammatic way to view the doppler time-scaling effect. One can draw the signal as if it were projected onto a movie screen. Compressed or

stretched images are then obtained by moving the screen closer to or further from the projector. The pictorial representation of this process will be called a "compression diagram." See Figure 4.5.

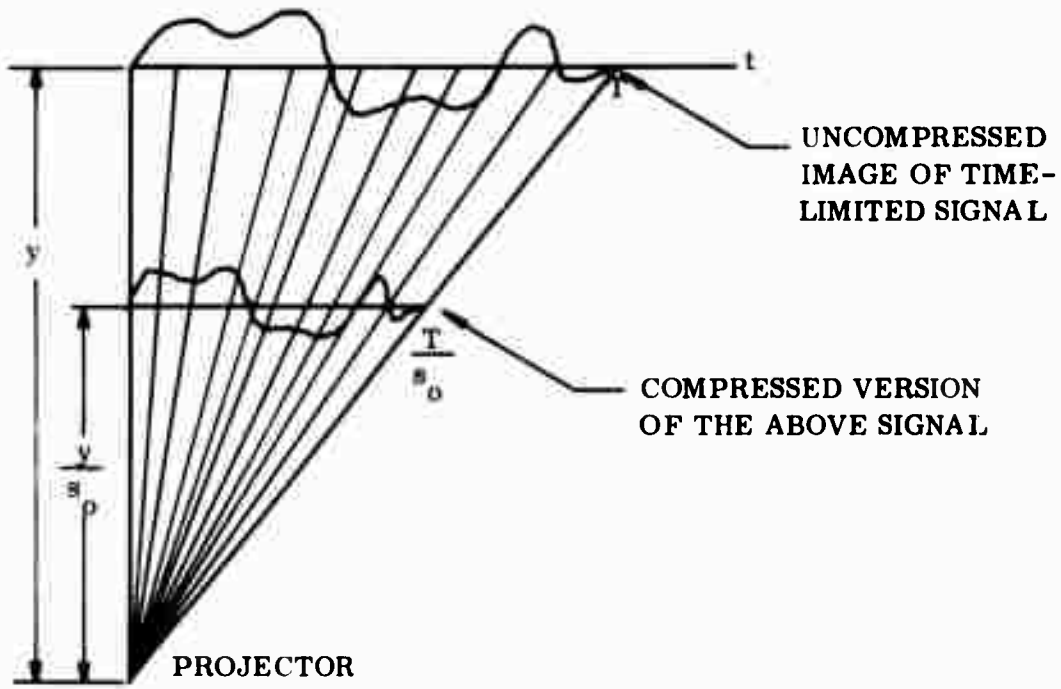

Figure 4.5. Compression Diagram.

The problem is to determine the zero distribution (and/or distribution of maxima and minima, etc.) that will give rise to a compressed waveform which correlates closely with the original waveform. If the compression factor is $s_o(>1)$, then the new movie screen would be inserted as shown in Figure 4.5.

In order to have a large correlation between signals when they are phased as in Figure 4.5 (i.e., when their starting times are identical), the zero at T/s_o should correspond to a zero of the original signal. Line A-A' (Figure 4.6) is therefore constructed; the original signal should have a zero

at point A ' . But the new zero at A ' causes a zero at point B in the compressed signal, where B is on the line A ' - P. For a large correlation, B should have its counterpart B ' in the original signal. B ' , in turn, causes a zero in the compressed waveform. Continuation of this process leads to the diagram in Figure 4.6.

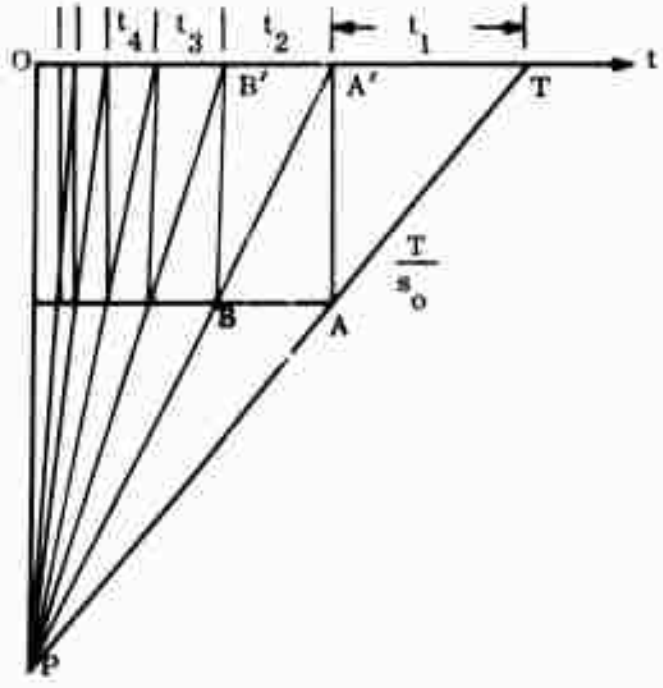

Figure 4.6. Compression Diagram Derivation of a Doppler-Tolerant Signal.

It is clear from the construction process that

$$t_2 = t_1/s_o;\ t_3 = t_2/s_o = t_1/s_o^2;\ \cdots \quad . \tag{4.16}$$

Since (4.16) is identical to (4.4), the same method as before will yield the phase expression (4.14). If the compression triangle POT were flipped over about its vertical side PO, the resulting phase would be that of Equation (4.13).

4.3 Global Optimization Approach.

Doppler tolerant phase functions can, in fact, be derived by more conventional methods, i.e., by using the ambiguity function.

Definition: Given an acceptance threshold η_a and a specific value of $s = s_o$, a real unit energy signal u(t) is doppler accepting for s_o if

$$\max_{-\infty < \tau < \infty} \chi^{(2)}_{uu}(s_o, \tau) \geq \eta_a \quad . \tag{4.17}$$

Furthermore, the signal $u_o(t)$ is defined to be maximally doppler accepting if

$$\max_{-\infty < \tau < \infty} \chi^{(2)}_{u_o u_o}(s_o, \tau) \geq \max_{-\infty < \tau < \infty} \chi^{(2)}_{uu}(s_o, \tau) \quad , \tag{4.18}$$

where u(t) is any other admissible signal.

Defining the point in τ at which $\chi^{(2)}_{uu}(\tau, s_o)$ is largest by the expression $\tau_m(s_o)$, the definition says that one should maximize the functional

$$s_o^{1/2} \int_{-\infty}^{\infty} u_o(t)\, u_o\left[s_o(t + \tau_m(s_o))\right] dt - \lambda_E \int_{-\infty}^{\infty} u_o^2(t)\, dt \tag{4.19}$$

where $u_o(t)$ is assumed to be real and λ is Lagrange multiplier for an energy constraint.

Letting $u_o(t) \longrightarrow u_o(t) + \epsilon\, \eta(t)$, differentiating the functional with respect to ϵ and setting the result equal to zero for $\epsilon = 0$ (first variation = 0):

$$s_o^{1/2} \int \eta(t)\, u_o\left[s_o(t + \tau_m(s_o))\right] dt + s_o^{1/2} \int \eta\left[s_o(t + \tau_m(s_o))\right] u_o(t) dt$$

$$- 2\lambda_E \int \eta(t)\, u_o(t) dt = 0 \tag{4.20}$$

Changing variables in the first and third integrals, let

$$t = s_o(t' + \tau_m(s_o)) \; ; \; t' = t/s_o - \tau_m(s_o) \; . \tag{4.21}$$

Then

$$s_o^{\frac{3}{2}} \int \eta\left[s_o(t' + \tau_m(s_o))\right] u_o\left[s_o^2 t' + s_o^2 \tau_m(s_o) + s_o \tau_m(s_o)\right] dt'$$

$$+ s_o^{\frac{1}{2}} \int \eta\left[s_o(t + \tau_m(s_o))\right] u_o(t) dt$$

$$- 2\lambda_E s_o \int \eta\left[s_o(t' + \tau_m(s_o))\right] u_o\left[s_o(t' + \tau_m(s_o))\right] dt'$$

$$= 0 \; . \tag{4.22}$$

This equation is satisfied for all $\eta(t)$ if

$$s_o u_o\left[s_o^2 t + s_o^2 \tau_m(s_o) + s_o \tau_m(s_o)\right] + u_o(t)$$

$$- 2\lambda_E s_o^{\frac{1}{2}} u_o\left[s_o(t + \tau_m(s_o))\right] = 0 \; . \tag{4.23}$$

By the Schwarz inequality,

$$\tau_m(1) = 0 \; . \tag{4.24}$$

Applying condition (4.24) to (4.23):

$$u_o(t) + u_o(t) - 2\lambda_E u_o(t) = 0 \; , \text{ or } \lambda_E = 1 \; . \tag{4.25}$$

Therefore, (4.23) becomes, for the special case $\tau_m(s_o) = 0$:

$$s_o u_o(s_o^2 t) + u_o(t) = 2s_o^{\frac{1}{2}} u(s_o t) \ . \tag{4.26}$$

Now suppose that

$$u_o(t) = t^{-\frac{1}{2}} \cos\left[(2\pi/\log s_o) \log t\right] \ . \tag{4.27}$$

Then

$$s_o^{\frac{1}{2}} u_o(s_o t) = s_o u_o(s_o^2 t) = u_o(t) \ , \tag{4.28}$$

and (4.26) becomes an identity. Notice that $u_o(t)$ is not really square-integrable, so that other constraints should (and will) be applied to the problem. The phase function, however, is a perfect match with (4.14).

Having derived phase function (4.14) by ambiguity function analysis, one may again ask whether the Rihaczek function (4.13) is an equivalent solution for maximal doppler acceptance. As far as the ambiguity function is concerned, the initial definition (4.17-18) shows that two different signals $u_o(t)$ and $u_1(t)$ will have the same doppler acceptance property at $s = s_o$ if

$$\max_{-\infty<\tau<\infty} \chi^{(2)}_{u_o u_o}(\tau, s_o) = \max_{-\infty<\tau<\infty} \chi^{(2)}_{u_1 u_1}(\tau, s_o) \ . \tag{4.29}$$

If appropriate amplitudes are used, the signal u_o with phase function (4.14) can be related to the signal u_1 with phase function (4.13) by the transformation that has already been discussed, viz:

$$u_1(t) = u_o(1/k_2 - t) \ . \tag{4.30}$$

The complex wideband ambiguity function corresponding to $u_o(t)$ is

$$\chi^{(2)}_{u_o u_o}(\tau, s) = s^{\frac{1}{2}} \int_o^\infty u_o(t) u_o^* \left[s(t + \tau) \right] dt \tag{4.31}$$

where it has been assumed that u(t) is causal.

Letting $t = 1/k_2 - t'$:

$$\chi^{(2)}_{u_o u_o} = s^{\frac{1}{2}} \int_{-\infty}^{1/k_2} u_o(1/k_2 - t') u_o^* \left[1/k_2 - s(t' - \tau + \frac{1-s}{sk_2}) \right] dt' \tag{4.32}$$

The causality of $u_o(t)$ means that

$$u_o(t) = 0 \text{ for } t < 0 \ , \text{ or}$$
$$u_1(t) = 0 \text{ for } t > 1/k_2 \ . \tag{4.33}$$

Then by (4.33), (4.32), and (4.30),

$$\chi^{(2)}_{u_o u_o}(\tau, s) = \chi^{(2)}_{u_1 u_1}(-\tau + \frac{1-s}{sk_2}, s) \ . \tag{4.34}$$

It follows that for any given value s_o of s:

$$\max_{-\infty<\tau<\infty} \chi^{(2)}_{u_o u_o}(\tau, s_o) = \max_{-\infty<\tau<\infty} \chi^{(2)}_{u_1 u_1}(-\tau + \frac{1-s_o}{s_o k_2}, s_o)$$

$$= \max_{-\infty<\tau<\infty} \chi^{(2)}_{u_1 u_1}(\tau, s_o) \tag{4.35}$$

so that the property (4.29) holds true; the phase functions (4.14) and (4.13) correspond to signals that are equally doppler accepting.

The two log phase functions have thus been derived by a method that is independent of trajectory diagram ideas, by considering the ambiguity function from a global viewpoint. In the next section a slightly different approach will be used. The properties of the ambiguity function near the origin ($\tau = 0$, $s = 1$) will be utilized to attack the problem of doppler tolerance. Consideration of global properties will then appear as a constraint to keep ambiguity volume large. The advantage of such an approach lies in the emergence of certain moments of the waveform as important parameters for wideband signal design.

4.4 An Application of Ambiguity Function Properties.

The doppler tolerance problem provides an opportunity to apply some of the wideband ambiguity properties derived in Chapter III. Properties near the origin and a volume upper bound will be particularly helpful.

Section 3.2 investigated ambiguity function properties in the neighborhood of a correct hypothesis about the target parameters τ and s. For doppler tolerance purposes, the primary concern is with the behavior along the line $\tau_m(s)$ discussed in Section 4.3. Recall that $\tau_m(s_o)$ was defined as the point at which $\chi_{uu}^{(2)}(\tau, s_o)$ is largest, so that $\tau_m(s)$ must define the locus of such maxima and must pass through the origin, as expressed by equation (4.24).

E. L. Titlebaum (the author's thesis advisor) has derived an explicit expression for the behavior of $|\chi_{uu}^{(2)}|^2$ along $\tau_m(s)$ in the neighborhood of the origin. His argument is as follows.

By definition,

$$\frac{\partial}{\partial \tau} |\chi_{uu}^{(2)}(\tau, s)|^2 \Big|_{\tau = \tau_m(s)} = 0 . \qquad (4.36)$$

In the neighborhood of $(\tau, s) = (0, 1)$, the ambiguity function is approximately given by (3.9) and (3.12), i.e.,

$$|\chi_{uu}^{(2)}(\tau,s)|^2 \approx 1 - [\lambda^2\tau^2 + 2\gamma\tau(s-1) + \eta^2(s-1)^2] , \qquad (4.37)$$

where λ^2, η^2, and γ are given in (3.18).

Applying (4.36) to (4.37) gives

$$\tau_m(s) \approx -\gamma(s-1)/\lambda^2 . \qquad (4.38)$$

Substituting (4.38) back into (4.37) then gives an approximate expression for the behavior of the ambiguity function along the ridge line (near the origin):

$$|\chi_{uu}^{(2)}(\tau_m,s)|^2 \approx 1 - [\eta^2 - \gamma^2/\lambda^2](s-1)^2 . \qquad (4.39)$$

A doppler tolerant signal will give a large correlator output regardless of target velocity. That is,

$$\max_{-\infty<\tau<\infty} |\chi_{uu}^{(2)}(\tau,s)|^2 = |\chi_{uu}^{(2)}(\tau_m,s)|^2$$

should be as large as possible for any s if the signal is to be doppler tolerant. By (4.39), this implies that the expression

$$\eta^2 - \gamma^2/\lambda^2$$

should be minimized.

It was shown in Section 3.2.2 that

$$\eta^2\lambda^2 \geq \gamma^2 \quad \text{so that} \quad \eta^2 \geq \frac{\gamma^2}{\lambda^2} \ . \tag{4.40}$$

Thus if η^2 is made small, it follows from (4.40) that the whole quantity $\eta^2 - \gamma^2/\lambda^2$ will be made small. A simplified problem is then to minimize η^2.

Since, by (3.18) and (3.19)

$$\eta^2 = \int t^2 |u'(t)|^2 dt - \left| \int tu(t)u^{*\prime}(t)dt \right|^2 \geq 0 \ ,$$

the problem could be simplified further by seeking to minimize the moment

$$\int t^2 |u'(t)|^2 dt \equiv \alpha_u^{(1)} . \tag{4.41}$$

The problem solved here, however, will involve η^2 as a whole rather than the $\alpha_u^{(1)}$ - moment. A generalized α - moment is discussed in Appendix C.

One therefore seeks to minimize η^2, which can be written as the sum of two functionals:

$$\eta^2 = J_1(a) + J_2(a,\theta) \tag{4.42a}$$

where

$$J_1(a) = \int t^2 \dot{a}^2 dt - \frac{1}{4} \tag{4.42b}$$

$$J_2(a,\theta) = \int t^2 a^2 \dot{\theta}^2 dt - \left(\int ta^2 \dot{\theta} dt \right)^2 \tag{4.42c}$$

and $u(t) = a(t) \exp j\theta(t)$, as before.

Both $J_1(a)$ and $J_2(a, \theta)$ are positive or zero. This may be demonstrated by using the Schwarz inequality as shown:

$$\int a^2(t)dt \int t^2 \dot{a}^2(t)dt \geq \left| \int ta\dot{a}dt \right|^2$$

where

$$\int_{-\infty}^{\infty} a^2(t)dt = 1 \quad \text{for unit energy.}$$

$$\int_{-\infty}^{\infty} ta\dot{a}dt = ta^2 \Big|_{-\infty}^{\infty} - \int_{-\infty}^{\infty} a[t\dot{a}+a]dt$$

$$= ta^2 \Big|_{-\infty}^{\infty} - \int_{-\infty}^{\infty} ta\dot{a}dt - 1$$

or

$$\int_{-\infty}^{\infty} ta\dot{a}dt = \frac{1}{2}[ta^2 \Big|_{-\infty}^{\infty} - 1] .$$

Assuming that $ta^2 \Big|_{-\infty}^{\infty} = 0$,

$$\int_{-\infty}^{\infty} t^2\dot{a}^2dt \geq \frac{1}{4} ; \quad J_1(a) \geq 0 \tag{4.43}$$

with equality only if $t\dot{a} = k_1 a$ or $a(t) = k_2 t^{k_1}$, where k_1 and k_2 are constants. Also,

$$\left| \int_{-\infty}^{\infty} ta^2\dot{\theta}\,dt \right|^2 \leq \int_{-\infty}^{\infty} t^2a^2\dot{\theta}^2\,dt \cdot \int_{-\infty}^{\infty} a^2\,dt$$

or

$$J_2(a,\theta) \geq 0 \tag{4.44}$$

with equality only if $ta\dot{\theta} = k_3 a$, $\frac{d\theta}{dt} = \frac{k_3}{t}$, or

$$\theta(t) = k_3 \log t + k_4 \tag{4.45}$$

where k_3 and k_4 are constants.

η^2 is therefore minimized with respect to all admissible phase functions if $\theta(t) = k_3 \log t + k_4$, regardless of what amplitude $a(t)$ is used ($J_2(a,\theta) = 0$ for all $a(t)$). It will henceforth be assumed that $\theta(t) = k_3 \log t + k_4$ for an optimally doppler tolerant waveform. Then

$$\eta^2 = J_1(a) = \int_{-\infty}^{\infty} t^2\dot{a}^2\,dt - \frac{1}{4}. \tag{4.46}$$

Given the optimal phase $\theta(t) = k_3 \log t + k_4$, one seeks the optimal amplitude to minimize (4.46).

For a physical radar system, the energy E and absolute signal time duration T should be constrained. One should also include a constraint to ensure that $|\chi_{uu}^{(2)}(\tau_m, s)|^2$ is large away from the origin. Both (3.85 and (3.88) imply that if D_t^2 is allowed to become small, the height of $|\chi_{uu}^{(2)}|^2$

away from the origin will decrease rapidly. The mean square time duration is thus constrained to be large, helping to produce the desired global properties of the ambiguity function.

The problem is now to find the a(t) that minimizes the functional

$$\int_0^T F(t,a,\dot{a})dt = \int_0^T [t^2\dot{a}^2 + (\lambda_E - \tfrac{1}{4})a^2 + \lambda_t t^2 a^2]dt \ . \qquad (4.47)$$

The Euler-Lagrange equation [23,24] provides a necessary condition for the function a(t) to be an extremaloid of the functional (4.47):

$$\frac{\partial F}{\partial a} - \frac{d}{dt}\left[\frac{\partial F}{\partial \dot{a}}\right] = 0 \ . \qquad (4.48)$$

The Legendre necessary condition requires that

$$\frac{\partial^2 F}{\partial \dot{a}^2} \geq 0 \qquad (4.49)$$

in order that the extremaloid be such that the functional is minimized.

In the case (4.47):

$$\frac{\partial F}{\partial \dot{a}} = 2t^2\dot{a} \qquad (4.50)$$

$$\frac{\partial^2 F}{\partial \dot{a}^2} = 2t^2 \geq 0 \qquad (4.51)$$

$$\frac{d}{dt}\left(\frac{\partial F}{\partial \dot{a}}\right) = 4t\dot{a} + 2t^2\ddot{a} \qquad (4.52)$$

$$\frac{\partial F}{\partial a} = 2(\lambda_E - \frac{1}{4})a + 2\lambda_t t^2 a \ . \tag{4.53}$$

The Legendre condition is satisfied by (4.51). The Euler-Lagrange equation is

$$(\lambda_E - \frac{1}{4})a + \lambda_t t^2 a - 2t\dot{a} - t^2\ddot{a} = 0, \text{ or}$$

$$\ddot{a} + \frac{2}{t}\dot{a} + \left(\frac{1/4 - \lambda_E}{t^2} - \lambda_t\right) a = 0 \ . \tag{4.54}$$

This is a form of Bessel's differential equation [25]:

$$\ddot{a} + \frac{1 - 2\alpha}{t}\dot{a} + \left(\frac{\alpha^2 - p^2}{t^2} + \beta^2\right) a = 0 \ . \tag{4.55}$$

Equations (4.54) and (4.55) are identical if

$$\lambda_t = -\beta^2 \tag{4.56a}$$

$$\alpha = -\frac{1}{2} \tag{4.56b}$$

$$\lambda_E = p^2 \tag{4.56c}$$

A solution to (4.55) is

$$a(t) = t^{\alpha} J_p(\beta t) \tag{4.57}$$

so that a solution to (4.54) is

$$a(t) = k_5 t^{-1/2} J_p(\beta t) \tag{4.58}$$

where p and β are related to the Lagrange multipliers λ_E and λ_t by (4.56). The constant k_5 is chosen to yield the correct energy.

In order that a(t) be finite at t = 0, one must have $p \geq 1/2$, since [25]

$$\lim_{t \to 0} t^{-1/2} J_p(\beta t) = \frac{(\beta t)^{p-1/2}}{p!\, 2^p} \tag{4.59}$$

In order that a(t) be finite at t = T, it is necessary that

$$J_p(\beta T) = 0 . \tag{4.60}$$

That is, for a given value of p, β should be such that βT corresponds to one of the zeros of the function $J_p(\beta T)$.

In order to minimize the moment $\int_0^T t^2 \dot{a}^2 dt$, one can choose among the available functions (4.58) on the basis of which one(s) yields the lowest value(s) of this moment. Using various identities [25] and integral properties [26] of Bessel functions, it can be shown that for a(t) as given in (4.58) and (4.60):

$$\int_0^T t^2 \dot{a}^2 dt = k_5^2 \left\{ (p - 1/2)^2 + \frac{(\beta T)^2}{2} J_{p+1}^2(\beta T) - 2\,(p-1/2) \sum_{n=0}^{\infty} \left[J_{p+n+1}(\beta T) \right]^2 \right\} \tag{4.61}$$

where

$$E = \int_0^T \frac{J_p^2(\beta T)}{t} \, dt$$

Investigation of Bessel function zero properties [25] shows that there exist no Bessel functions such that $J_p(\beta T) = 0$ and $J_{p+1}(\beta T) = 0$ also. Given that condition (4.60) must be satisfied, it follows that the term $[(\beta T)^2/2]J_{p+1}^2(\beta T)$ will always be greater than zero. So to minimize (4.61) for a given value of p, it follows that βT should be as small as possible. This means that βT should correspond to the first zero of $J_p(t)$ for $t > 0$.

The waveform described by equations (4.45) and (4.58) bears a striking resemblance to the cruising pulse used by the little brown bat, Myotis lucifugus, for the initial detection of prey [27]. D. A. Cahlander's experimental picture of the Myotis cruising pulse is shown in Figure 4.7. (The bat's exact amplitude function a(t) may not be precisely as shown [54].) If a(t) is sufficiently non-oscillatory, the instantaneous frequency can be defined as the time derivative of the phase:

$$f(t) = 1/T(t) = \dot{\theta}(t) \, . \tag{4.62}$$

If $\theta(t) = k_3 \log t + k_4$, then $\dot{\theta}(t) = k_3/t$, and the instantaneous period T(t) is

$$T(t) = (1/k_3)t \tag{4.63}$$

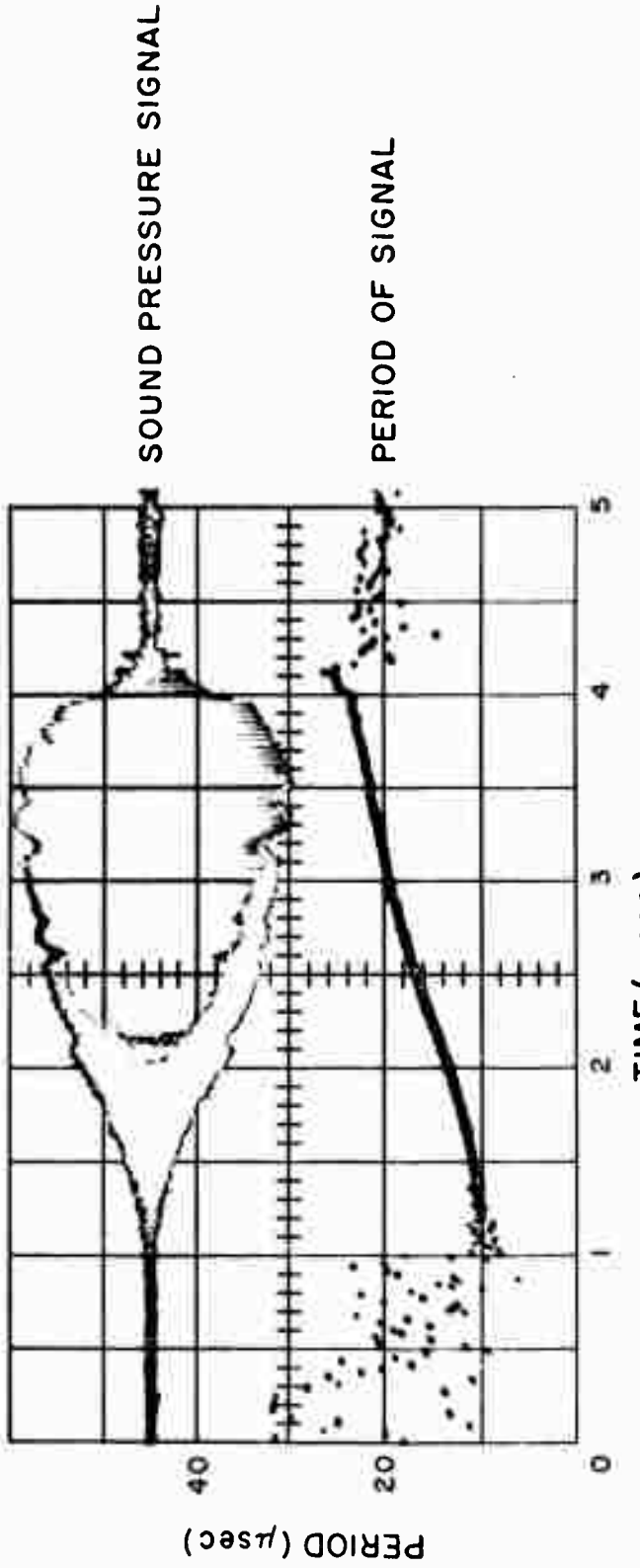

Figure 4.7. Measured Cruising Pulse of Myotis Lucifugus (Courtesy of J.J.G. McCue, M.I.T. Lincoln Laboratory)

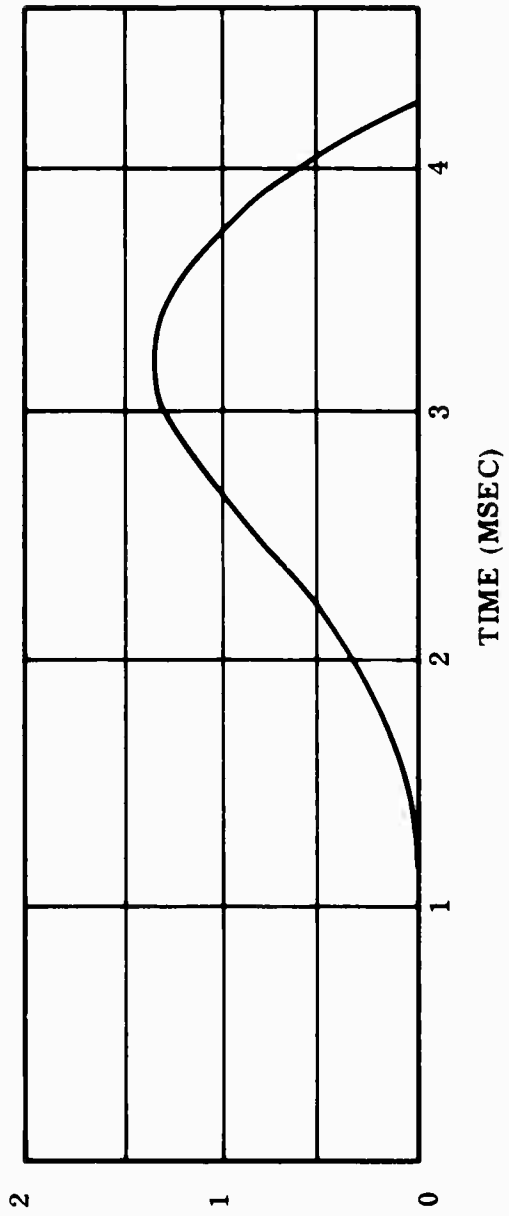

Figure 4.8. Theoretical Amplitude of a Doppler-Tolerant Waveform.

The expression (4.63) agrees with Cahlander's experimental measurement of instantaneous period versus time.

Figure 4.8 shows a sample function of the form (4.58) with $p = 7$ and $\beta = 2581$. This function is seen to correspond in its general shape to the amplitude of the cruising pulse shown in Figure 4.7.

Another bat signal is closely approximated by the solution to the above problem with one more constraint. Rewriting η^2 for convenience:

$$\eta^2 = \int_0^T t^2 |u'|^2 dt - \left[\int_0^T t\dot{\theta} a^2 dt\right]^2 - \frac{1}{4} . \tag{4.64}$$

The first term ($\alpha_u^{(1)}$ - moment) on the right side of (4.64) has a lower bound derivable from the Schwarz inequality:

$$\int t^2 |u'|^2 dt \int t^2 |u|^2 dt \geq \left|\int t^2 uu'^* dt\right|^2 . \tag{4.65a}$$

$$\int t^2 |u'|^2 dt \geq \frac{\left|\int t^2 uu'^* dt\right|^2}{D_t^2} . \tag{4.65b}$$

D_t^2 has already been constrained to be large, so if the left side of (4.65b) is to be small, a further necessary constraint would require that

$$\left|\int t^2 uu'^* dt\right|^2 = \left[\int ta^2 dt\right]^2 + \left[\int t^2 \dot{\theta} a^2 dt\right]^2 \tag{4.66}$$

be kept small.* One can thus define a new functional

$$K(a,\dot{\theta},t) = J(a,\dot{\theta},t) + \lambda_m\left[\int_0^T ta^2dt\right]^2 + \lambda_m\left[\int_0^T t^2\dot{\theta}a^2dt\right]^2 . \tag{4.67}$$

Define

$$\int_0^T ta^2dt \equiv M_o \tag{4.68a}$$

$$\int_0^T t\dot{\theta}a^2dt \equiv M_1 \tag{4.68b}$$

$$\int_0^T t^2\dot{\theta}a^2dt \equiv M_2 \tag{4.68c}$$

Replacing $\dot{\theta}$ by $[\dot{\theta} + \epsilon\eta(t)]$ where η is an arbitrary piecewise smooth** function such that

$$\eta(0) = \eta(T) \equiv 0 \tag{4.69}$$

and letting

---

*The moment (4.66) is also a measure of acceleration sensitivity. It will be demonstrated in Chapter V that constraining (4.66) amounts to an acceleration tolerance requirement.

**$\eta(t)$ must have a continuous first derivative except at a finite number of points.

$$\left.\frac{\partial K}{\partial \epsilon}\right|_{\epsilon = 0} = 0 \qquad \text{(first variation = 0)} \ , \tag{4.70}$$

one finds that

$$\int_0^T 2t\eta a^2[t\dot{\theta} - M_1 + \lambda_m M_2 t]dt = 0 \ . \tag{4.71}$$

(4.71) holds true for all $\eta(t)$ if

$$t\dot{\theta} - M_1 + \lambda_m M_2 t = 0$$

or

$$\dot{\theta} = M_1/t - \lambda_m M_2 \ . \tag{4.72}$$

Replacing a(t) by $[a + \epsilon\eta]$, repeating the above procedure, and using the fact that

$$\int_0^T t^2 \dot{a}\dot{\eta}dt = -\int_0^T \eta[t^2\ddot{a} + 2t\dot{a}]dt \ , \tag{4.73}$$

gives

$$-t^2\ddot{a} - 2t\dot{a} + t^2\dot{\theta}^2 a - 2M_1 t\dot{\theta} a + (\lambda_E - \tfrac{1}{4})a + \lambda_t t^2 a$$

$$+ 2\lambda_m M_2 t^2 \dot{\theta} a + 2\lambda_m M_o t a = 0 \ . \tag{4.74}$$

Substituting (4.72) into (4.74) and dividing through by $-t^2$:

$$\ddot{a} + 2\dot{a}/t + [(\lambda_m^2 M_2^2 - \lambda_t) - 2\lambda_m(M_1 M_2 + M_o)/t$$

$$+ (M_1^2 + \tfrac{1}{4} - \lambda_E)/t^2]a = 0 \ . \tag{4.75}$$

λ_m and λ_t may be chosen such that

$$\lambda_m^2 M_2^2 - \lambda_t = 0 \ . \tag{4.76}$$

The remaining part of (4.75) can be put into the form

$$\ddot{a} + \frac{1 - 2\alpha}{t}\ \dot{a} + \left[(\beta\gamma t^{\gamma-1})^2 + \frac{\alpha^2 - p^2\gamma^2}{t^2}\right] a = 0 \tag{4.77}$$

by letting

$$\alpha = -\frac{1}{2} \ , \tag{4.78}$$

$$\gamma = \frac{1}{2} \ , \tag{4.79}$$

$$\beta^2 = -8\lambda_m(M_1 M_2 + M_o) \ , \tag{4.80}$$

$$p^2 = 4(\lambda_E - M_1^2) \ . \tag{4.81}$$

The solution to (4.77) is [25]:

$$a(t) = kt^{\alpha} J_p(\beta t^{\gamma}) = kt^{-\frac{1}{2}} J_p(\beta t^{\frac{1}{2}}) \ . \tag{4.82}$$

It is evident that superfluous oscillations of a(t) will unnecessarily increase the moment $\int_0^T t^2 a^2 dt$. Therefore one requires that the first zero of (4.82) for $t > 0$ occur at $t = T$. In order that a(t) be bounded at $t = 0$, a further requirement is that $p \geq 1$.

Notice that (4.80) will be consistent with (4.68) and (4.72) if $\lambda_m < 0$. One can then write

$$\dot{\theta}(t) = k_1/t + k_2 \tag{4.83}$$

where k_1 and k_2 are both positive constants. The instantaneous period associated with (4.82) is then

$$T(t) = 1/\dot{\theta}(t) = t/(k_1 + k_2 t) . \tag{4.84}$$

The amplitude function (4.82) is drawn in Figure 4.9 for $p = 7$, $\beta = 105.7$. Also shown is the theoretical instantaneous period (4.84) with $k_1 = 26.7$, $k_2 = 33.3 \times 10^3$. Figure 4.9 compares favorably with Figure 4.10, which shows the experimentally observed cruising pulse of Lasiurus borealis, the red bat [27]. The time origin for the observed pulse should be made about 1 msec earlier for easy comparison with theory. (Again, the actual a(t) used by the bat may not be precisely as shown in Figure 4.10 [54].)

The reader may find it disturbing that the functional $K(t, a, \dot{\theta}, \dot{a})$ was minimized first with a(t) given (by setting the first variation of $\dot{\theta}$ equal to zero) and then with $\dot{\theta}(t)$ given (by taking the variation of a). Following the discussion of G. A. Bliss [55], p. 11, the procedure is justified by defining

$$I(\epsilon) = K(t, a_o + \epsilon\eta, \dot{\theta}_o + \epsilon\zeta, \dot{a}_o + \epsilon\dot{\eta}) \tag{4.85}$$

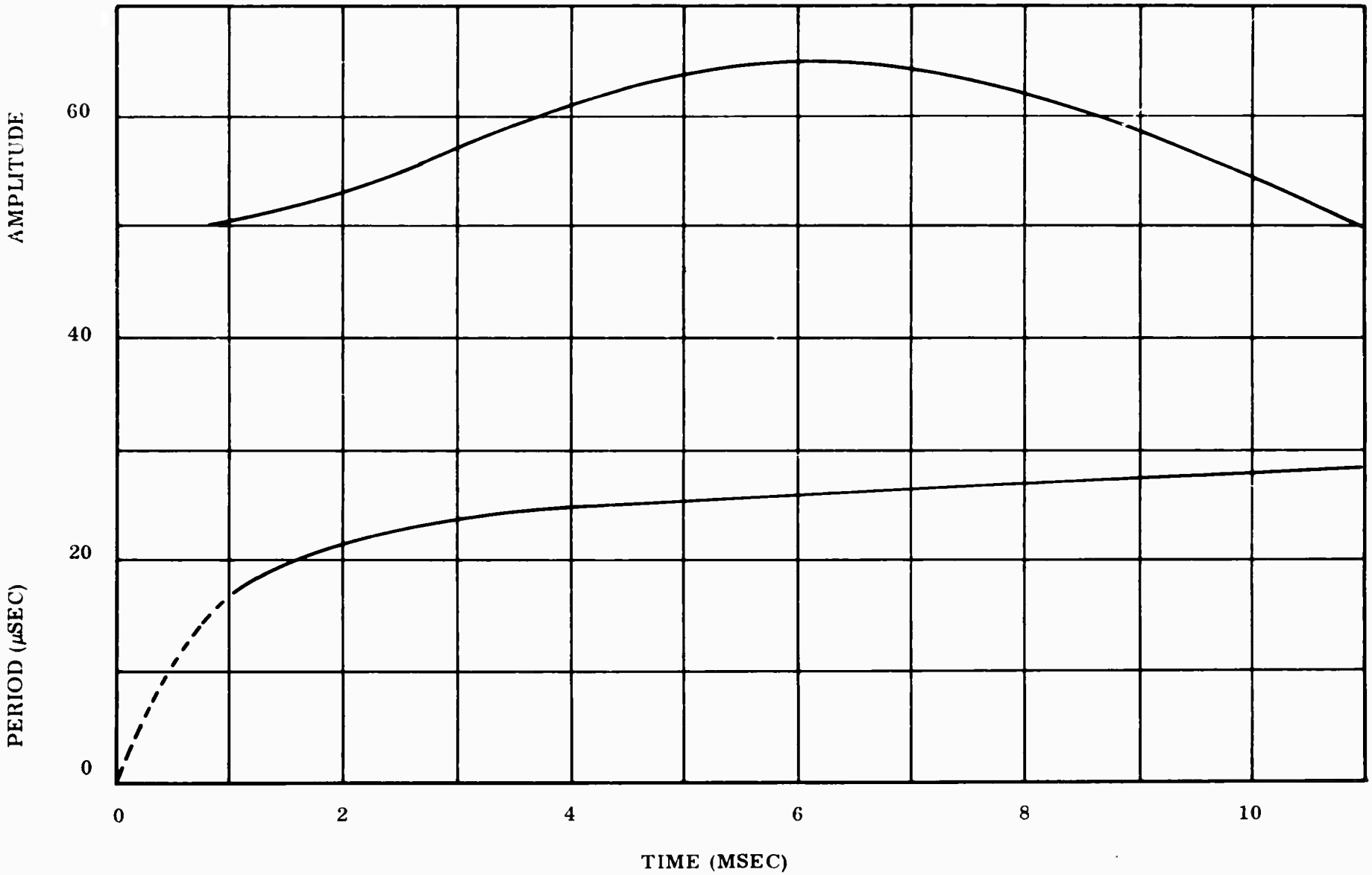

Figure 4.9. Theoretical Amplitude and Instantaneous Period of a Constrained Doppler-Tolerant Waveform.

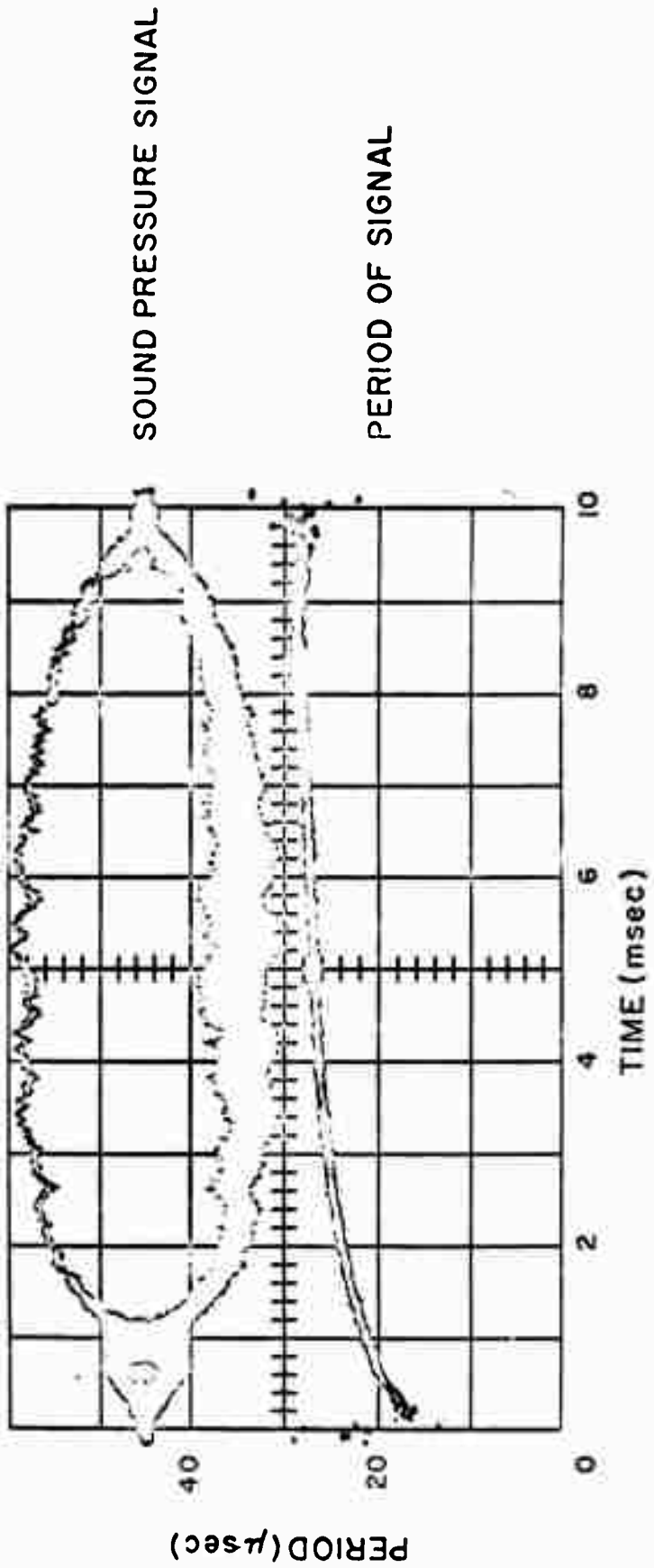

Figure 4.10. Measured Cruising Pulse of Lasiurus Borealis (Courtesy of J.J.G. McCue, M.I.T. Lincoln Laboratory).

where $a_o(t)$, $\dot{\theta}_o(t)$ are functions which minimize the functional K and where $\zeta(t)$, like $\eta(t)$, is an arbitrary piecewise smooth function such that $\zeta(0) = \zeta(T) = 0$. If $a_o(t)$ and $\dot{\theta}_o(t)$ are indeed functions which minimize the functional $K(t, a, \dot{\theta}, \dot{a})$, then the function $I(\epsilon)$ must have a minimum at $\epsilon = 0$, that is,

$$I'(0) \equiv I_1(\eta, \zeta) = 0 . \tag{4.86}$$

For the particular case $\zeta(t) = 0$, it must still be true that

$$I_1(\eta, 0) = 0 \text{ for all admissible } \eta(t). \tag{4.87}$$

Similarly, if $\eta(t) = 0$,

$$I_1(0, \zeta) = 0 \text{ for all admissible } \zeta(t). \tag{4.88}$$

It is assumed, of course, that for $\zeta(t) = 0$, $\dot{\theta}(t)$ is not only held fixed; it is equal to its optimum function $\dot{\theta}_o(t)$. For this reason, one must verify that any proposed solutions do not produce inconsistencies when they are substituted into the equations $I_1(\eta, 0) = I_1(0, \zeta) = 0$.

In Chapter VI, the same method will lead to a pair of nonlinear simultaneous integral equations. Whereas the above solutions for $a_o(t)$ and $\dot{\theta}_o(t)$ can be made consistent with each other by simple manipulation of some constants and Lagrange multipliers, a consistent solution in Chapter VI will usually be obtainable only with an iteration technique.

The many approaches to the doppler tolerance problem have undoubtedly been tiresome for the reader seeking only answers. The main purpose of this chapter, however, has been not so much to obtain results but rather to demonstrate the usefulness of the various analytical methods and properties of Chapters II and III.

CHAPTER V

IMPORTANT GENERALIZATIONS: ACCELERATING POINT TARGETS AND DISTRIBUTED TARGETS

Two generalized models for target echoes will be introduced in this chapter. The first model takes account of acceleration, so that the point target response is characterized by three parameters instead of two. It is pointed out that a system which is implemented with constant velocity targets in mind may well fail to detect a rapidly accelerating (or declerating) target. The consideration of acceleration is thus more than just pedantic hairsplitting.

The second echo model assumes that the target is no longer a flat, perfect reflector of undistorted waveforms. It will be shown that the more widebanded a signal becomes, the less likely that the echo is an exact (doppler compressed) replica of the incident waveform. It is postulated that an object's echo can be derived from a convolution of signal and impulse response, just as in linear system theory. A distributed target would then be characterized by its impulse response or by its reflectivity as a function of frequency (i.e., its transfer function, the Fourier transform of the impulse response).

Assuming that echoes can indeed be written as convolutions of signals with target impulse response, one can find signal functions which give

maximum power in the reflected waveform or maximum energy return, provided the target impulse response is known. It is pointed out that some practical situations exist for which the impulse response would be known a priori. It is also possible to estimate the target's impulse response by a sequence of hypotheses.

A class of distribution tolerant signals is then discussed. By analogy with doppler tolerance, a distribution tolerant signal is defined as one which nearly reduplicates itself upon reflection from any target, regardless of the target's shape.

By regarding the signal as a channel through which information about the target is conveyed, it is possible to define the target description capability of a signal in terms of channel capacity (information carrying ability).

Finally, two groups of associated waveform characteristics are described. In one group are very narrowband, doppler resolvent, distribution tolerant signals; in the other are wideband, doppler tolerant, high-capacity, range resolvent signals. It is postulated that bats use waveforms from both groups, depending upon what information they wish to extract from their environment.

5.1 Accelerating Point Targets.

5.1.1 An Ambiguity Function for Accelerating Targets.

Consider once more the argument in Section 2.2. As target motion is no longer restricted to constant velocities, acceleration is included in the expansions (2.4):

$$\tau(t) = t_o + \zeta(t-t_o) + \alpha(t-t_o)^2 + \ldots \tag{5.1a}$$

$$R(t) = R(t_o/2) - v(t-t_o/2) - (a/2)\,(t-t_o/2)^2 - \ldots \tag{5.1b}$$

As before,

$$\tilde{v}\,\tau(t)/2 = R(t-\tau(t)/2) \quad . \tag{5.2}$$

Differentiating (5.2) twice:

$$\tilde{v}\,\dot{\tau}(t)/2 = (1-\dot{\tau}(t)/2)\,\dot{R}(t-\tau(t)/2) \tag{5.3}$$

$$\tilde{v}\,\ddot{\tau}(t)/2 = (1-\dot{\tau}(t)/2)^2\,\ddot{R}(t-\tau(t)/2) - (\ddot{\tau}(t)/2)\,\dot{R}(t-\tau(t)/2) \quad . \tag{5.4}$$

At $t = t_o$, expressions (5.1) through (5.4) yield:

$$\tau(t_o) = t_o;\ \dot{\tau}(t_o) = \zeta;\ \ddot{\tau}(t_o) = 2\alpha \tag{5.5}$$

$$\dot{R}(t_o/2) = -v;\ \ddot{R}(t_o/2) = -a \tag{5.6}$$

$$\tilde{v}\, t_o/2 = R(t_o/2);\ \tilde{v}\, \zeta/2 = (1-\zeta/2)\,(-v);\ \alpha\, \tilde{v} = -(1-\zeta/2)^2\, a + \alpha\, v \tag{5.7}$$

Solving (5.7) for ζ and α:

$$\zeta = -2v/(\tilde{v}-v);\ \alpha = \tilde{v}^2\, a/(\tilde{v}-v)^3 \quad . \tag{5.8}$$

Here it is understood that $v = v\left[\frac{t_o}{2}\right]$, $a = a\left[\frac{t_o}{2}\right]$; one is concerned with velocity and acceleration at the time of reflection.

From (5.1),

$$t - \tau(t) = t - t_o - \zeta(t-t_o) - \alpha(t-t_o)^2 - \ldots$$

$$= (1-\zeta)\,(t-t_o) - \alpha(t-t_o)^2 - \ldots \tag{5.9}$$

so that

$$r(t) = u[t-\tau(t)] = u[(1-\zeta)\,(t-t_o) - \alpha(t-t_o)^2 - \ldots]$$

$$= u\left[\frac{\tilde{v}+v}{\tilde{v}-v}(t-t_o) - \frac{\tilde{v}^2 a}{(\tilde{v}-v)^3}(t-t_o)^2 - \ldots\right] \tag{5.10}$$

This is the generalized result originally derived by E. J. Kelly and R. P. Wishner [5].

If $\beta \equiv v(t_o/2)/\tilde{v}$ and $\epsilon \equiv a(t_o/2)/\tilde{v}$, then the ambiguity function corresponding to r(t) is approximated by

$$\chi_{uu}^{(5)}(\tau, \beta, \epsilon) \approx \int \left[\left(\frac{1+\beta}{1-\beta}\right) - \frac{2\epsilon(t+\tau)}{(1-\beta)^3}\right]^{1/2} u(t)u^*\left[\frac{1+\beta}{1-\beta}(t+\tau) - \frac{\epsilon}{(1-\beta)^3}(t+\tau)^2\right] dt \qquad (5.11)$$

where the approximation is caused by truncation of the time series. The first term after the integral sign normalizes the echo energy.

By Taylor's theorem [28], it is always possible to pick a time t_1 in the interval $[t_o/2, t]$ such that

$$R(t) = R(t_o/2) - v(t_1)(t-t_o/2) \ . \qquad (5.12)$$

Therefore, for a time limited signal it is still possible to write the ambiguity function in the form $\hat{\chi}_{uu}^{(2)}[\tau(t_o/2), \beta(t_1)]$, but it must be understood that the velocity which maximizes this function is not necessarily that at the reference time $t_o/2$; β can be the target velocity at any time during reflection. Also, if there is indeed acceleration, the maximum value of the ambiguity function

$\hat{\chi}_{uu}^{(2)}[\tau(t_o/2), \beta(t_1)]$ will always be less than one when u(t) and r(t) have unit energy.

If maximum signal power is restricted in a high attenuation, high noise level environment, one must use long-time-duration signals in order to make signal-to-noise ratio at the correlator output $(2E/N_o)$ greater than one. Such lengthy transmissions are particularly vulnerable to acceleration distortion from targets with highly nonlinear trajectories. Thus, even if τ and β are zero (corresponding to perfect velocity and time hypotheses) in (5.11), the ϵ-term may be large enough to make $\chi_{uu}^{(5)}(0,0,\epsilon) << \chi_{uu}^{(5)}(0,0,0)$.

If a system is designed expressly for the detection of constant velocity targets, then it is explicitly assumed that $\epsilon = 0$ and implicitly assumed that, should accelerating targets actually be encountered, $\chi_{uu}^{(5)}(0,0,\epsilon) \tilde{=} \chi_{uu}^{(5)}(0,0,0) = \chi_{uu}^{(2)}(0,1)$ for all possible ϵ. But if the implicit assumption proves untrue, then an accelerating target may not be detected at all, even at close range!

5.1.2 Acceleration Tolerance.

For receivers of limited complexity, the mismatch caused by acceleration should be minimized in order to insure the applicability of a linear trajectory assumption. That is, a class of acceleration tolerant waveforms should be found. A successful approach to such a problem has been to use

the origin properties of the ambiguity function. The same method will now be used to simultaneously optimize doppler and acceleration tolerance.

For combined doppler and acceleration tolerance, one seeks a signal such that acceleration sensitivity, as indicated by the quantity

$$\frac{\partial}{\partial \epsilon} \chi_{uu}^{(5)}(0,0,\epsilon)\Big|_{\epsilon=0} = -\int t|u(t)|^2 dt - \int t^2 u(t)\, u^{*\prime}(t)\, dt$$

is minimized. Constraints include η^2 (3.18b), D_t^2, and energy, where the η^2 and D_t^2 constraints insure doppler tolerance.

If

$$\left|\frac{\partial}{\partial \epsilon} \chi_{uu}^{(5)}(0,0,\epsilon)\Big|_{\epsilon=0}\right|^2 = \left[\int t|u|^2 dt\right]^2 + \left|\int t^2 uu^{*\prime} dt\right|^2 + 2\left[\int t|u|^2 dt\right] \mathrm{Re}\left\{\int t^2 uu^{*\prime} dt\right\}$$

$$= 4\left[\int t a^2 dt\right]^2 + \left[\int t^2 \theta' a^2 dt\right]^2$$

is used as a measure of acceleration sensitivity, then the following functional must be minimized:

$$J(t, a, \dot{\theta}, \dot{a}) = 4\left[\int_o^T ta^2\, dt\right]^2 + \left[\int_o^T t^2\, \dot{\theta} a^2\, dt\right]^2$$

$$+ \lambda_\eta \left\{ \int_o^T t^2\, \dot{a}^2\, dt + \int_o^T t^2\, \dot{\theta}^2 a^2\, dt - \left[\int_o^T ta^2\, \dot{\theta}\, dt\right]^2 \right\}$$

$$+ [\lambda_E - \lambda_\eta/4] \int_o^T a^2\, dt + \lambda_t \int_o^T t^2\, a^2\, dt \quad .$$

The above functional is essentially the same as the functional (4.67), except that Lagrange multipliers are used for different quantities. The answer is thus the same as that obtained in (4.82) and (4.83), i.e.,

$$a(t) = kt^{-1/2} J_p(\beta t^{1/2})$$

$$\dot{\theta}(t) = (k_1/t) + k_2$$

This development shows that the extra constraint (4.66) used to derive the cruising pulse of Lasiurus borealis is, in effect, a condition for acceleration tolerance. It is apparent that Lasiurus must be careful about acceleration effects; Figures 4.10 and 4.7 show the Lasiurus signal to be more than twice as long as the corresponding Myotis pulse. As already mentioned, long-time-duration signals are vulnerable to acceleration distortion.

The discussions associated with Figure 4.4 and Equations (4.29-4.35) demonstrate that two phase functions with equivalent doppler tolerance properties are

$$\theta_1(t) = k_1 \log (k_2 t) \quad \text{or} \quad \theta_2(t) = k_1 \log (1-k_2 t)$$

with associated instantaneous frequencies

$$\dot{\theta}_1(t) = k_1/t \quad \text{or} \quad \dot{\theta}_2(t) = (-k_1 k_2)/(1-k_2 t) \quad .$$

By Equation (4.66), it is evident that for a given amplitude the first solution (θ_1) is more acceleration tolerant than the second (because of the t^2 weighting factor of $\dot{\theta} a^2$ over the interval [0, T]). Although the derivation of the Myotis signal did not constrain acceleration tolerance per se, the signal chosen by the bat is thus the more acceleration tolerant of two equally doppler tolerant waveforms.

5.2 Distributed Targets.

5.2.1 Narrowbandedness and the Point Target Assumption.

Distributed targets are objects which cannot be treated as planar reflectors of undistorted waveforms. Before considering these generalized

targets, however, it is important to illustrate the need for such a consideration. After all, many workable narrowband radar systems, all based on a point target assumption, have been successfully implemented.

It would seem that the assumptions of narrowband signals and point targets are actually complementary ideas. In other words, the narrowband assumption itself assures that most objects will behave as planar reflectors. The connection between the two suppositions can be understood by considering the frequency dependence of target cross section for distributed targets. The basic frequency response behavior can be inferred from the frequency dependence of backscatter from a sphere. The cross section is determined by Rayleigh's law at low frequencies and by specular reflection at high frequencies, where the radar cross section approaches the geometrical cross section (πr^2) of the object [37]. A rough approximation to the frequency dependence of radar cross section for a sphere (based on Figure 3.1, p. 65, [37]) is shown in Figure 5.1.

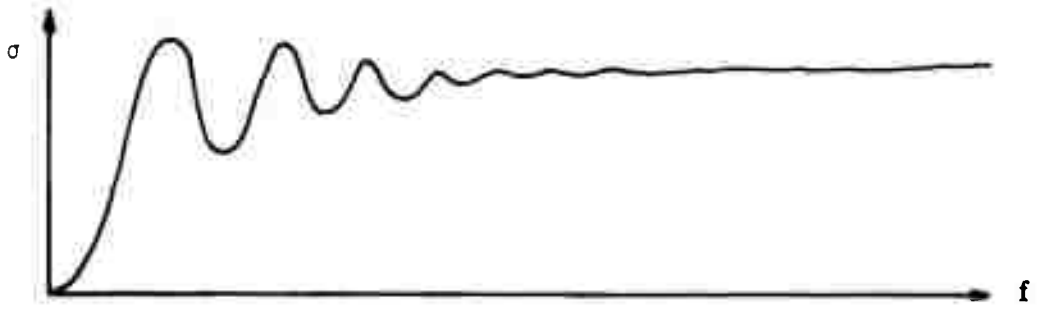

Figure 5.1. Approximate Frequency Dependence of Backscatter from a Sphere.

It is reasonable to assume that most other shapes have the property of asymptotically constant cross sections for large frequencies ($\sigma \approx$ geometrical cross section). Consider, then, a narrowband signal (with high carrier frequency) superposed on such a curve, as shown in Figure 5.2:

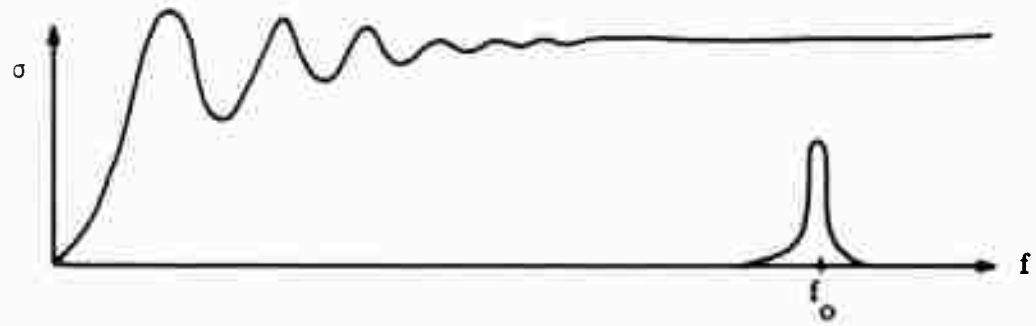

Figure 5.2. A Narrowband Signal Superimposed on the Backscatter Graph of Figure 5.1.

From Figure 5.2 it is evident that the target response is nearly flat over the frequency range of the narrowband signal. Over the frequency interval of interest, a delta-function impulse response (frequency response = constant) approximates the true target response. In the limit as bandwidth approaches zero, the distributed target behaves exactly as a point target, as will be shown in Section 5.5. But as the signal becomes more widebanded and/or the carrier frequency decreases, the applicability of the point target assumption becomes progressively more questionable.

5.2.2 Echo Model for Distributed Targets.

Consider now those targets whose cross sections vary with range in such a way that the targets no longer act as perfect mirrors. As in linear system theory, one can begin by considering the impulse response of such an object. That is, the signal is visualized as a very thin pulse that impinges upon the target and gives rise to a characteristic response. This response must be described in terms of some reference time $t_r = R_o/\tilde{v}$. R_o is taken to be the range of the point of first reflection, i.e., the part of the stationary distributed target closest to the transmitter. The situation described above is illustrated in Figure 5.3.

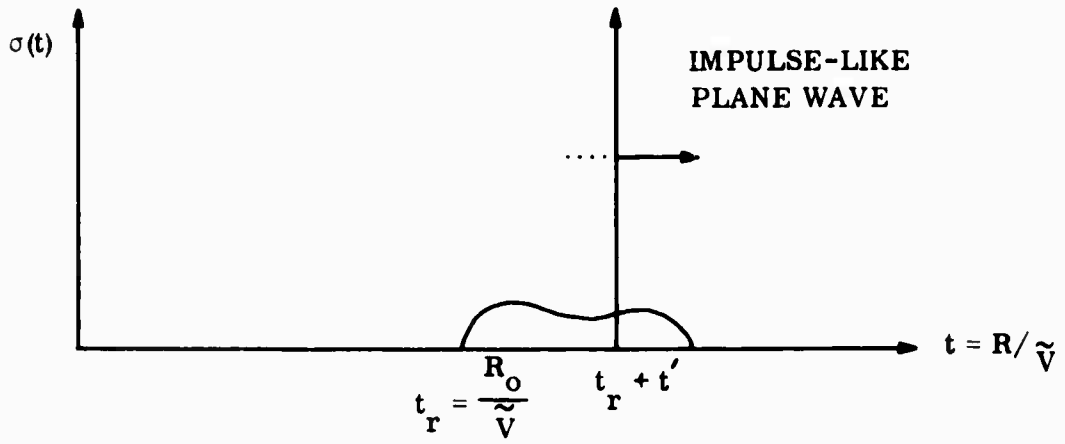

Figure 5.3. Reflectivity vs. Time.

The impulse-like signal is illustrated in Figure 5.3 as a vertical line which sweeps across the target from left to right, generating reflections as it goes. The impulse's reflection from the object at some time $t_r + t'$ will take t' seconds to reach the reference plane t_r. This reflection is therefore delayed, relative to the reflection at t_r, by $2t'$ seconds. This delay, which occurs for all t', will make the time duration of the impulse response twice as long as (length of target)/$\tilde{v}$. Thus if the target's impulse reflectivity as a function of distance is $\sigma(R)$, then the impulse response $c(t)$ may be written:

$$c(t) = \sigma(R/2\tilde{v}) \quad . \tag{5.13}$$

To reiterate, the impulse response $c(t)$ may be viewed as target reflectivity stretched (time-scaled) by a factor of two, the stretching caused by the round trip to each reflection point and back to the reference plane.

Assuming that the responses of a sequence of weighted pulses can be superposed, the resulting echo has the form:

$$u(t) = \sum_i a_i \, \delta(t-\tau_i) \Longrightarrow r(t) = \sum_i a_i \, c(t-\tau_i) \tag{5.14}$$

The continuous version of this relation is the well-known convolution equation of linear system theory:

$$r(t) = \int u(\tau)\, c(t-\tau)\, d\tau \quad . \tag{5.15}$$

Since a point target is assumed to reduplicate the incident signal, its impulse response would be

$$c(t) = \delta(t); \quad r(t) \equiv u(t) \quad . \tag{5.16}$$

A constant velocity point target would then be characterized by the kernel $s^{1/2}\,\delta(st-\tau)$:

$$r(t) = \int u(\tau)\, [\, s^{1/2}\, \delta\,(st-\tau)]\, d\tau = s^{1/2} u\,(st) \quad . \tag{5.17}$$

The analogous return from a moving distributed target would then be

$$r(t) = \int u(\tau)\, [\, s^{1/2}\, c(st-\tau)]\, d\tau$$

$$= \int [\, s^{1/2} u\,(st-\tau)]\, c(\tau)\, d\tau \quad . \tag{5.18}$$

All the echoes described above are referenced to time t_r (Figure 5.3). The function $r(t-2t_r)$ describes the echo as seen by the receiver (assuming that the signal was transmitted at time $t = 0$).

5.2.3 Target Impulse Response.

5.2.3.1 A Priori Knowledge of Impulse Response.

There are some detection problems for which one knows (with a high degree of certainty) the shape of the distributed target as seen by the radar/sonar. For incoming torpedoes, missiles, or mortar shells the shapes are all basically "conical sections nose-on" [34]. Sometimes the general shape of an oil-bearing geological formation is known. If one were designing a passive sonar navigation buoy, cylindrical or spherical symmetry would assure an aspect-invariant, known impulse response.

The advantage of a priori knowledge about a target's impulse response will become evident in Sections 5.3 and 5.4; the design of optimal signals for maximum reflected power and energy depends upon knowledge of the target.

5.2.3.2 Estimation of an Unknown Impulse Response.

In order to estimate a target's impulse response, one can visualize a processor that correlates the echo with synthesized echoes from hypothetical targets. The output of such a correlator would have the form:

$$\chi_{uu}^{(6)}(\tau, \tau_h; s, s_h; c, c_h)$$

$$= (ss_h)^{1/2}\int\left\{\int u(x)\, c_h\,[s_h(t-\tau_h)-x]\, dx\right\}\left\{\int u(y)\, c[s(t-\tau)-y]\, dy\right\}^{*} dt$$

$$= [(ss_h)^{-1/2}/2\pi]\int |U(\omega)|^2\, C_h(\omega/s_h)\, C^*(\omega/s)\, e^{-j\omega(\tau_h-\tau)}\, d\omega \qquad (5.19)$$

where c_h, s_h, and τ_h are hypothetical quantities and $C(\omega)$ is the Fourier transform of $c(t)$.

If one were using a conventional processor (point target model) to detect the return from a distributed target, c_h would be an impulse and the correlator output would be

$$\chi_{uu}^{(6)}(\tau, \tau_h; s, s_h; c, \delta(t)) = \frac{(ss_h)^{-1/2}}{2\pi}\int |U(\omega)|^2\, C^*(\omega/s)\, e^{-j\omega(\tau_h-\tau)}\, d\omega. \qquad (5.20)$$

As in the case of accelerating point targets, a processor designed to receive only time compressed versions of the transmitted signal may not detect a target whose transfer function $C(\omega)$ deviates significantly from a constant over the signal's passband (even though $\tau_h = \tau$, $s_h = s$). Equation (5.20) thus provides a mathematical basis for the discussion in Section 5.2.1 (connecting narrowbandedness with the point target assumption).

If one insists upon using a conventional receiver (i.e., a bank of filters matched to doppler compressed versions of the transmitted waveform) with a distributed target, then it will be of interest to find a signal which maximizes the function

$$|\chi_{uu}^{(6)}(\tau, \tau; s, s; c, \delta(t))|^2 = \left| \int u(t) \left[\int u(x)\, c(t-x)\, dx \right]^* dt \right|^2 . \tag{5.21}$$

Expression (5.21) is the magnitude-squared output of a correlator that has correctly hypothesized range and velocity, but which hypothesizes a point target when in fact the target is distributed. By the Schwarz inequality, (5.21) is maximized (for unit energy signal and echo) if

$$\lambda u(t) = \int_{-\infty}^{\infty} u(x)\, c(t-x)\, dx . \tag{5.22}$$

For time limited signals, (5.22) is a homogeneous Fredholm equation. The equation will be further investigated in Section 5.5.

5.3 Signals for Maximum Echo Power.

In order to receive a waveform r(t) with maximum instantaneous power P_r, the quantity

$$\max_t P_r = \max_t |r(t)|^2 = \max_t \left| \int u(\tau)\, c(t-\tau)\, d\tau \right|^2 \qquad (5.23)$$

should be maximized. But

$$\left| \int u(\tau)\, c(t-\tau)\, d\tau \right|^2 \le \int |u(\tau)|^2\, d\tau \int |c(t-\tau)|^2\, d\tau \qquad (5.24)$$

by the Schwarz inequality, with equality only if

$$u(t) = kc(\tau-t);\ u(t+\tau) = kc(-t) \quad . \qquad (5.25)$$

Assuming unit energy normalizations for both $u(t)$ and $c(t)$, the left side of (5.24) attains its maximum value of unity when (5.25) is satisfied. The translation τ in (5.25) has no effect upon the shape of the waveform, so that, without loss of generality, the condition (5.25) for maximum instantaneous echo power becomes:

$$u(t) = kc(-t) \quad . \qquad (5.26)$$

As an example, consider the phenomenon of constructive interference between two pulses. The target of Figure 5.3 is in this case taken to be two planar discontinuities, each with the same reflectivity (Figure 5.4).

If the signal is matched to the target in the sense that

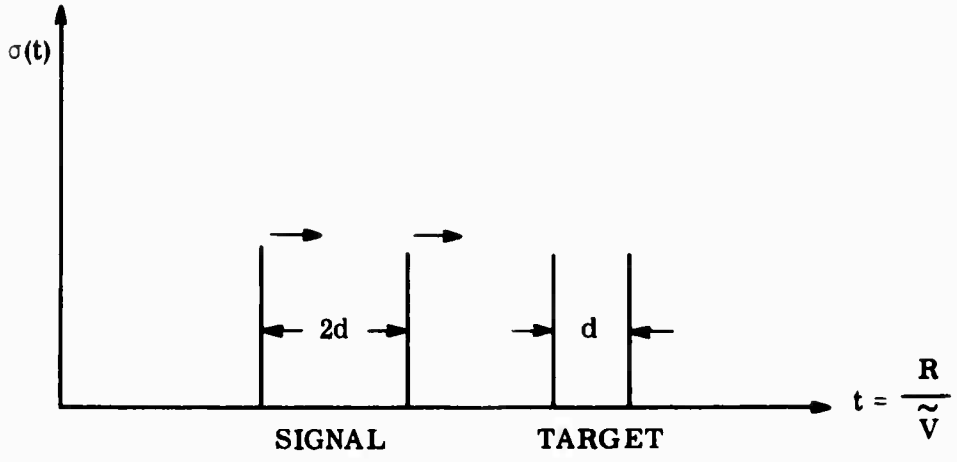

Figure 5.4. Maximization of Reflected Power from a Target with Two Planar Discontinuities.

$$u(t) = kc(-t) = k\sigma(-R/2\tilde{v}) \tag{5.27}$$

then it is evident that the signal will be as shown in Figure 5.4. The reflection (disregarding multiple echoes caused by reverberation between the two discontinuities) will consist of three pulses, with the second being twice as large as the other two because of constructive interference. Such a response clearly has the maximum possible power relative to any two-pulse signal that impinges upon the target of Figure 5.4.

It is also possible to illustrate constructive interference by means of Altar's trajectory diagram. A motionless target consisting of two discontinuities would appear on the trajectory diagram as two parallel horizontal lines (Figure 5.5).

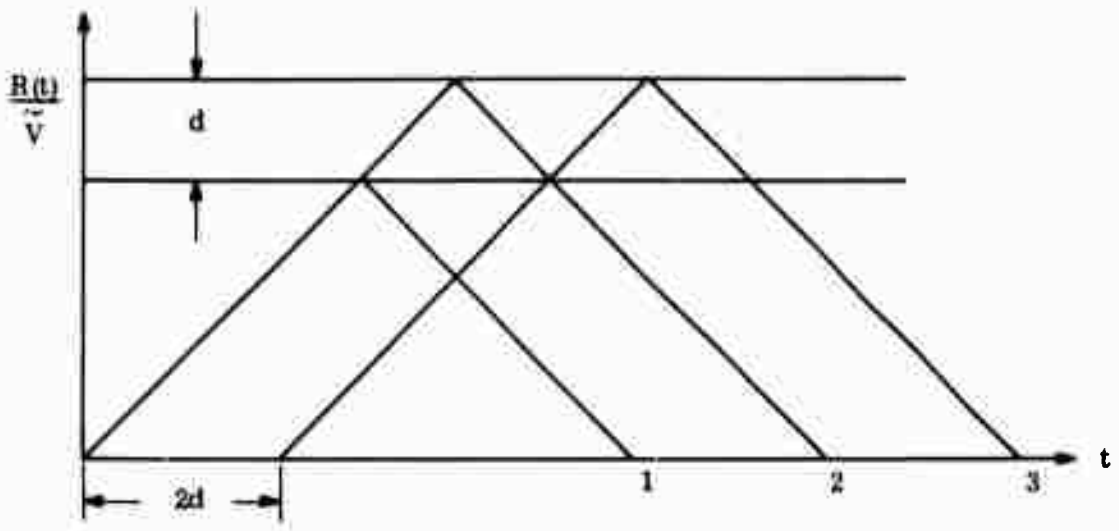

Figure 5.5. Trajectory Diagram Interpretation of Figure 5.4

If the time between trajectories is again d , then the signal pulses are again separated by 2d , so that the second received pulse (#2 in Figure 5.5) is the superposition of two reflections.

To achieve maximum instantaneous reflected power, one sees that the signal must be matched to the target. This matching requires a priori knowledge of target impulse response, and suggests the need for an adaptive system that changes its transmitted signal as better estimates of target response are obtained.

5.4 Signals for Maximum Echo Energy.

For a point target, the expected maximum signal power to noise power ratio at the output of a matched filter is $2E/N_o$, where E is signal energy and N_o is average noise energy. It is therefore important to receive a high energy echo from the target for conventional matched filter processing.

For maximum returned energy [29, 30] one must maximize $\int |\, r(t)\, |^2 dt$. But since convolution in the time domain is the same as multiplication in the frequency domain, (5.15) gives

$$r(t) \longleftrightarrow U(\omega)\, C(\omega) \tag{5.28}$$

where " $\longleftrightarrow$ " denotes a Fourier transform pair, so that, by Parseval's theorem,

$$\begin{aligned}
\int |\, r(t)\, |^2 dt &= (1/2\pi) \int |\, U(\omega)\, C(\omega)\, |^2 d\omega \\
&= (1/2\pi) \int \left[\int u(x)\, e^{-j\omega x} dx \right] \left[\int u^*(y)\, e^{j\omega y} dy \right] |\, C(\omega)\, |^2 d\omega \\
&= \int\int u(x)\, u^*(y) \left[(1/2\pi) \int |\, C(\omega)\, |^2 e^{j\omega(y-x)} d\omega \right] dx\, dy \\
&= \int\int u(x)\, u^*(y)\, R_c(y-x)\, dx\, dy \quad , \qquad (5.29)
\end{aligned}$$

where $R_c(\tau)$ is the autocorrelation function of the target impulse response.

Letting

$$f(y) = \int u(x)\, R_c(y-x)\, dx \tag{5.30}$$

one has

$$\int |\, r(t)\, |^2\, dt = \int u^*(y)\, f(y)\, dy \tag{5.31}$$

which is maximized (by the Schwarz inequality) if

$$f(y) = k\, u(y) \tag{5.32}$$

or

$$k\, u(y) = \int_{-\infty}^{\infty} u(x)\, R_c(y-x)\, dx \quad . \tag{5.33}$$

If $u(t)$ is assumed to be time limited to $[0, T]$, then Equation (5.33) becomes a homogeneous Fredholm integral equation whose solutions are the eigenfunctions of R_c. For a point target,

$$R_c(y-x) = \delta(y-x) \tag{5.34}$$

and (5.24) is identically satisfied for all admissible signals. Thus a point target does not favor one signal over another as far as returned energy is concerned (as one would intuitively expect). A distributed target's shape,

however, determines both energy and maximum power of the echo for a given transmitted waveform.

Theorem: The signal that maximizes the energy of a given target's echo is also the signal that results in an absolute maximum of $\chi_{uu}^{(6)}(\tau, s, c)$, the distributed target ambiguity function (5.19). This signal satisfies the integral Equation (5.33).

Proof: By the Schwarz inequality, $\chi_{uu}^{(6)}$ as given by (5.19) will be maximized if $s = s_h$, $\tau = \tau_h$. Then

$$\chi_{uu}^{(6)}(0, 1, c) = (1/2\pi) \int |U(\omega)\, C(\omega)|^2 \, d\omega \qquad (5.35)$$

But (5.35) is identical to the right hand side of (5.29), so that the signal which maximizes the maximum value of the distributed target ambiguity function $\chi_{uu}^{(6)}(\tau, s, c)$ is (not surprisingly) the same signal that maximizes the energy of the echo. QED.

There exists a special case for which (5.33) and (5.22) are satisfied by the same (non-causal) function:

Theorem: If there exists a function u(t) such that:

(1) $u(t) = u(-t)$ and

$$(2) \qquad \lambda\, u(t) = \int u(x)\, c(t-x)\, dx \quad ,$$

then this function also satisfies the relation

$$\lambda^2\, u(t) = \int u(x)\, R_c(t-x)\, dx \quad .$$

Proof: $\int u(x)\, R_c(t-x)\, dx = \int u(x) \left[\int c(y)\, c(y+t-x)\, dy \right] dx$

$$= \int c(y) \left[\int u(x)\, c(y+t-x)\, dx \right] dy$$

$$= \lambda \int c(y)\, u(y+t)\, dy \qquad \text{by (2)}$$

$$= \lambda \int c(y)\, u(-y-t)\, dy \qquad \text{by (1)}$$

$$= \lambda^2\, u(-t) \qquad \text{by (2)}$$

$$= \lambda^2\, u(t) \qquad \text{by (1). QED}$$

The above theorem is in fact a special case of a general result for iterated kernels, provided that $c(t-x) = c(x-t)$, i.e., c is a real, Hermitian kernel.* The iterate of such a kernel is

*The condition $u(t) = u(-t)$ implies that $\int u(x)\, c(t-x)\, dx = \int u(x)\, c(x-t)\, dx$. From this it follows that $c(t-x) = c(x-t) + f(x,t)$ where $\int u(x)\, f(x,t)\, dx = 0$.

$$c^2(t-x) \equiv \int c(t-y)\, c(y-x)\, dy = \int c(y-t)\, c(y-x)\, dy$$

$$= \int c(y)\, c(y+t-x)\, dy = R_c(t-x) \quad .$$

It is a well known result [32] that if x_n is an eigenfunction of K with eigenvalue λ_n, then x_n is also an eigenfunction of K^2 with eigenvalue λ_n^2, provided K is a Hermitian kernel.

It may be possible, then, to find a single waveform which maximizes correlator output when either distributed targets or point targets are hypothesized. It would appear from (5.22), however, that this signal is dependent upon c(t), so that one must hypothesize c(t) in any case, in order to generate the waveform. Only if a (distribution tolerant) signal exists such that (5.22) holds for <u>any</u> c(t) will no distribution hypothesis be necessary.

5.5 Distribution Tolerant Signals.

The eigenvalue equation (5.22):

$$\lambda\, u(t) = \int_{-\infty}^{\infty} u(x)\, c(t-x)\, dx \qquad (5.22)$$

is in fact a partial definition of distribution tolerance, since it defines a waveform that reproduces itself upon reflection from the target c(t). If (5.22) were true for <u>any</u> c(t) , then u(t) would indeed be distribution tolerant.

Van Trees [2] has demonstrated that any complex exponential function $\exp(j\omega_i t)$ will satisfy (5.22). That is,

$$\lambda e^{j\omega_i t} = \int_{-\infty}^{\infty} e^{j\omega_i x} c(t-x)\, dx \quad ,$$

or

$$\lambda = \int_{-\infty}^{\infty} e^{-j\omega_i (t-x)} c(t-x)\, dx = C(\omega_i) \quad . \tag{5.36}$$

The value of λ corresponding to the solution with frequency ω_i is the Fourier transform $C(\omega)$ evaluated at $\omega = \omega_i$.

Equation (5.22) does not take account of the fact that both c(t) and u(t) are generally time limited functions. Accordingly, the limits on the integral in (5.22) are not really infinite, so that the change of variables in (5.36) no longer produces a constant on the right hand side when time limited functions are used.

There are several ways [2, 23, 31] to solve the equation

$$\lambda\, u(t) = \int_{o}^{T_o} u(x)\, c(t-x)\, dx \quad , \tag{5.37}$$

the simplest (given access to a computer) probably being the method that will be used in Chapter VI of this dissertation, i.e., the utilization of a set of orthonormal components whose coefficients must satisfy a matrix characteristic equation.

An eigenfunction for a specific value of $c(t)$, however, is not what is needed for distribution tolerance. What is really required is a solution which at least approximately satisfies (5.37) for all $c(t)$, just as $\exp(j\omega_i t)$ satisfies (5.22) for all $c(t)$.

Many distributed targets can be described as arrays of point targets. The impulse response of such objects may then be written as

$$c(t) = \sum_{n=1}^{N} c_n\, \delta(t-t_n) \quad . \tag{5.38}$$

Perhaps an approximate solution to (5.37) can be found for the important special case (5.38).

The trajectory diagram and inscribed diamond construction technique were helpful aids to the derivation of doppler tolerant waveforms. The same methods will also prove helpful for the distribution tolerance problem. Indeed, the relevance of these diagrams to distributed targets has already been demonstrated in connection with constructive interference (Figure 5.5).

For diagrammatic simplicity, let N = 3 in Equation (5.38). The trajectory diagram representation of the target (5.38) is shown in Figure 5.6. The inscribed diamond construction technique then leads to a network of construction lines as illustrated.

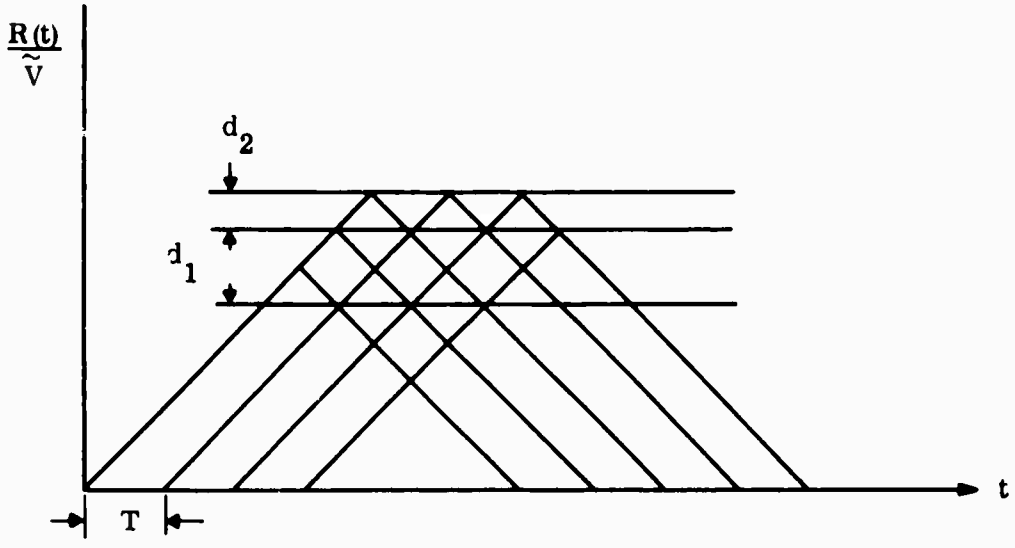

Figure 5.6. Approximate Waveform Reduplication for an Array of Stationary Point Targets.

The distribution accepting signal is in this case a periodic signal with $T = 2d_2$. The target in Figure 5.6 is obviously contrived; $d_1 = 2d_2$. But for an arbitrary number of reflectors at various distances $d_1, d_2, d_3, \ldots, d_n$ from each other, one would simply have $T = 2d_o$, where d_o is a number such that each of the $\{d_1, d_2, \ldots, d_n\}$ is an integer multiple of $2\,d_o$. A signal whose basic form is unaltered by the distributed target (5.38) has thus been graphically derived.

If the signal must be time-limited to $[0, T_o]$ then the derivation suggests that the simplest signal to use would be a sinusoid with zeroes at $t = 0$ and $t = T_o$. Furthermore, if the spacings $d_1, d_2, \ldots, d_n$ are unknown a priori, then the number d_o should be made as small as possible to increase the likelihood that each of the $d_1, d_2, \ldots, d_n$ is an integer multiple of $2\,d_o$. That is, the period $T = 2d_o$ should be made as small as possible; the signal should be a time-limited sinusoid with as high a frequency as is practicable. In other words, the distribution tolerant signal is a quasi-monochromatic sinusoid with period T much less than time duration T_o. As T_o is allowed to become large and/or T is made very small, the signal spectrum becomes increasingly narrowbanded, approaching the solution $\exp(j\omega_i t)$ as a limiting case.

In terms of the convolution Equation (5.15), one sees that if a periodic function u(t) is convolved with a "comb" of impulse functions, u(t) will indeed retain its basic shape provided each tooth of the comb is separated by an integral number of periods. If u(t) is time limited, distortion will occur near the endpoints of the reflected waveform; this distortion will appear as discontinuous changes in amplitude. These sudden amplitude changes will take place at the zeroes of the waveform, so that the reflected signal will still be a continuous function of time.

If the limits in Equation (5.37) were written as $[-T_o/2, T_o/2]$, then a reasonable solution to the above problem would be a time-limited cosine, so that $u(t) = u(-t)$. This waveform would then (approximately) satisfy the two conditions of the iterated kernel theorem in Section 5.4, implying that the waveform is not only distribution tolerant, but also that it provides for maximum energy return.

5.6 Target Description Capability.

Equation (5.15) can be written in terms of Fourier transforms as in (5.28):

$$r(t) \longleftrightarrow C(\omega)\, U(\omega) \tag{5.39}$$

where $C(\omega) \longleftrightarrow c(t)$ and $U(\omega) \longleftrightarrow u(t)$, the " $\longleftrightarrow$ " denoting a Fourier transform pair.

It is immediately obvious from (5.39) that if the signal transform $U(\omega)$ is zero (or indetectably small) over some frequency interval, then the echo $C(\omega)\, U(\omega)$ will provide no information about $C(\omega)$ over that interval. This observation is related to the concept of a signal's information-carrying capacity. The relation is easily recognized when one interprets the function $U(\omega)$ as a channel through which the function $C(\omega)$ is being transmitted. For a given time duration, the capacity of this channel varies directly as its bandwidth [49]. If the signal-channel $U(\omega)$ is to have large capacity to carry information about the target function $C(\omega)$, then $U(\omega)$ must be widebanded.

The power spectrum $|\, U(\omega)\, |^2$ is the transform of the signal's autocorrelation function $\chi_{uu}^{(2)}(\tau, 1)$. This again implies that widebanded signals are suitable for target characterization.

It was shown in Chapter III that signal bandwidth is indicative of range resolving ability. Range resolution, in turn, is intimately related to the problem of distributed target characterization. Range resolution describes the ability of a signal to distinguish between two point targets at the same velocity but with slightly different ranges. It follows that range resolving

capability would also be useful to describe a target that is distributed in range, especially if such an object were represented as an array of point targets. By the origin properties in Chapter III and the uncertainty relation (Appendix C) one sees that range resolvent signals are necessarily widebanded.

The above arguments demonstrate the need for wideband signals if one seeks an accurate description of target impulse response. An ideal signal for this purpose is, of course, the impulse itself ($U(\omega) = 1$). Unfortunately, peak power limitations often forbid the transmission of any actual signal that approximates a unit-energy impulse. The alternative is to achieve widebandedness by drastic, sudden changes in the amplitude and/or instantaneous frequency of u(t).

5.7 Relations Between Doppler and Distribution Tolerance, Resolution, and Target Description Capability.

In Section 5.6 it was shown that range resolution and target description capability are related concepts which exact similar requirements of the radar-sonar signal. Similar relations exist between these and other waveform design concepts. In fact, it would seem that many radar system requirements (and their associated demands upon waveform characteristics) can be categorized under one of two signal types: very narrowband or very wideband.

The very narrowband (quasi-monochromatic) signal has appeared in several contexts. In Section 3.11 it was shown that such a waveform is sufficient (but perhaps not necessary) for good velocity resolution. (The same result will reappear in the next chapter as an idealized solution of a system optimization algorithm.) It was demonstrated in Section 5.5 that a quasi-monochromatic signal is also distribution tolerant. On the other hand, the target description capability (a concept antithetical to distribution tolerance) is very poor, as is range resolving capability and doppler tolerance.

The very wideband signal, on the other hand, has been found to possess good range resolving ability and target description capability. Furthermore, those wideband signals that are doppler tolerant should also be useful for target characterization when correlation processing is used. The connection between doppler tolerance and target description capability is clarified by the identity (3.113), which may be rewritten in terms of $\chi_{uu}^{(2)}(\tau, s)$:

$$\chi_{u*c_h, u*c}^{(2)}(\tau, s) = s^{1/2} \chi_{uu}^{(2)}(\tau, s) \overset{\tau}{*} \chi_{c_h c}^{(2)}(\tau, s) \quad . \qquad (5.40)$$

By Equation (5.19),

$$\chi_{u*c_h, u*c}^{(2)}(\tau, s) = \chi_{uu}^{(6)}(\tau, s, c, c_h) \qquad (5.41)$$

so that

$$\chi_{uu}^{(6)}(\tau, s, c, c_h) = s^{1/2} \int \chi_{uu}^{(2)}(x, s)\, \chi_{c_h c}^{(2)}(\tau - x, s)\, dx \quad (5.42)$$

If the radar-sonar system forms the function $|\chi_{uu}^{(6)}|^2$, then it will gain little information about $\chi_{c_h c}^{(2)}(\tau, s)$ over an interval of s where $|\chi_{uu}^{(2)}(\tau, s)|^2$ is small. That is, if $|\chi_{uu}^{(2)}(\tau, s)|^2$ is indetectably small (below noise level) over a given s-interval, then τ-convolution of $\chi_{uu}^{(2)}$ with an arbitrary function $\chi_{c_h c}^{(2)}(\tau, s)$ will generally result in another function that is small over the same s-interval* (assuming that max $\{\chi_{c_h c}^{(2)}\} = 1$). Since doppler tolerant signals maintain a large amplitude of $|\chi_{uu}^{(2)}(\tau, s)|^2$ over an extended domain in s, one expects such signals to be comparatively effective in conveying target descriptions to the receiver.

For comparison, consider again the quasi-monochromatic, distribution tolerant, doppler resolvent waveform. Distribution tolerance implies that the signal reproduces itself no matter what the target from which it is reflected. Such a signal does not gain any information about target distribution; it merely tells the radar that a target is present and presents some

---

*The problem is, in a sense, the converse of the usual SIR clutter rejection problem to be defined in Chapter VI. For a distributed target, important information may be contained in the "clutter"; this information should not be destroyed by the correlation process.

indication of target range and velocity. Such behavior (i.e., good doppler resolution associated with poor ability to describe the target's impulse response) can be interpreted as a simple manifestation of Equation (5.42). That is, if $\chi_{uu}^{(2)}(\tau, s_o) \approx 0$ for $s_o \neq 1$, then $\chi_{uu}^{(6)}(\tau, s_o, c, c_h) \approx 0$ for $s_o \neq 1$, and little information can be gained about the behavior of $\chi_{c_h c}^{(2)}(\tau, s)$ for $s \neq 1$.

It has already been established that range resolution is another helpful property for the description of distributed targets. In terms of Equation (5.42), the τ-integration will destroy the fine-structure of $\chi_{c_h c}^{(2)}(\tau, s)$ unless $\chi_{uu}^{(2)}(\tau, s)$ is very narrow in range at each value of s. That is, a razor-blade-shaped signal ambiguity function should result in an accurate target description. Such a razor-blade function is associated with large bandwidth, good doppler tolerance, and good range resolution.*

*An extreme (and impossible) example of a razor-blade function would be $\chi_{uu}^{(2)}(\tau, s) = \delta(\tau)$. Then by (5.42), $s^{-1/2}\chi_{uu}^{(6)}(\tau, s, c, c_h) = \chi_{c_h c}^{(2)}(\tau, s)$, the original target auto-ambiguity function. A signal whose ambiguity function approaches the razor blade is $u(t) = \lim_{T \to 0} K \sin(\pi t/T)/(\pi t/T) = \lim_{T \to 0} K(\pi t/T)^{-1/2} J_{1/2}(\pi t/T)$. This is one of the doppler tolerant waveforms derived in Chapter IV. (If $C(\omega)$ is band limited, it is unnecessary to take the limit of $T \to 0$.)

Although a range resolvent, doppler tolerant (razor blade) signal ambiguity function gives more information about $\chi_{c_h c}(\tau, s)$ than a range and doppler resolvent ("thumbtack") ambiguity function, the relevance of this information is not immediately obvious. A thumbtack signal function will make $\chi_{uu}^{(6)}$ equal to the cross correlation function $\chi_{c_h c}^{(2)}(\tau, 1)$. For $c_h(t) = \delta(t)$, $\chi_{c_h c}^{(2)}(\tau, 1)$ equals $c^*(\tau)$, the conjugate of target impulse response.

For a distributed target whose parts all move at the same radial velocity, $c(\tau)$ is indeed all the information one needs. But because of radar-sonar beam spreading, almost any moving rigid target with large range-extent will possess parts with differing radial velocities.* This fact is used to enhance the resolution of side-looking radars [56]. In addition, targets with moving parts (discussed in the introduction to Chapter IV) will often have a characteristic "signature" when viewed as functions of both range and velocity. For many practical situations, then, a two dimensional representation of the target ambiguity function is a helpful description of the object.

---

*This phenomenon occurs for translational motion with a non-radial component. A rotating rigid target would, of course, also give rise to velocity differences.

It seems evident that the extent to which a signal can become simultaneously range resolving and doppler tolerant determines the accuracy with which the correlation processor can describe a target. By Equation (3.101), Section 3.6, a given doppler tolerant signal can be made more range resolvent (without sacrificing doppler tolerance) by simply compressing the waveform in time.

For a given peak power, noise level, and target cross section, the extent to which the doppler tolerant signal can be compressed depends upon how much the signal energy can be reduced. This, in turn, depends upon target range. For a peak power constraint, the extent to which the doppler tolerant waveform can be compressed depends upon the range of a specific object; the closer the target, the more compression is allowed (at a sacrifice of signal energy).

The associations established in this section are exhibited in Table 5.1.

The Horseshoe bats (e.g., Rhinolophus ferrum-equinum and Rhinolophus euryale) provide an interesting commentary on the above arguments. The pulses of Rhinolophus, as measured by H. U. Schnitzler [50], consist of a

Table 5.1. Two Types of Signals with their Associated Properties

Signal:	Quasi-Monochromatic	Time-Compressed Doppler Tolerant
$\frac{\text{(Centralized BW)}}{\text{(Carrier Freq.)}}$:	small (narrowband)	large (wideband)
Range Resolution:	poor	good
Velocity Resolution:	good	range dependent*
Doppler Tolerance:	poor	good
Distribution Tolerance:	good	poor
Target Description Capability:	poor	good

*See the discussion associated with Figure 4.1.

long, constant frequency (CW) signal followed by a rapid decrease of frequency (FM) at the very end of the pulse. When the bats are at rest or cruising (free flight), the FM part of the pulse has low intensity compared with the CW part. But when the bats are landing or flying through an obstacle course, the intensity of the FM part is increased. *

The interpretation of this behavior in terms of target characterization is straightforward. For resting and cruising situations, one is interested in initial detection of a target, regardless of its distribution. Hence, a distribution tolerant signal is permissible. But when landing, avoiding obstacles, or closing in on prey, target shape should be investigated in some detail. For these cases, a signal with large information-carrying capacity should be accentuated.

---

*The use of FM versus CW as described here seems to be typical of all species: "As with all other bats yet studied, difficult maneuvers and demanding situations elicit shortened pulses of the "chirp" or frequency modulated pattern. But when flying at moderate altitudes in relatively straight lines, longer pulses often show considerable periods with a nearly constant, or slowly changing frequency. Is different information being extracted from the environment by these different types of orientation sounds?" - from D. R. Griffin [33] (underlining added).

For correlation processing, the target-describing signal should be a time-compressed, doppler tolerant waveform. Such waveforms are indeed observed for bats of another species, Myotis lucifugus, which seem to transmit time-compressed versions of Figure 4.7 as they pursue their prey [27]. These waveforms become progressively more compressed as the bat nears his target, a phenomenon that has been justified by assuming a peak power constraint.

CHAPTER VI.

OPTIMUM SYSTEMS FOR A CLUTTERED ENVIRONMENT

This chapter considers wideband radar-sonar operation in a cluttered or reverberation-prone environment. Such a consideration leads naturally to the concept of discrimination against spurious returns (as well as uncorrelated noise) while seeking to detect a target. This concept is expressed quantitatively in two ways: First, in terms of a constrained Schwarz inequality which seeks a signal whose target echo is easily distinguished from spurious echoes; second, in terms of a signal-filter pair to maximize signal-to-interference ratio (SIR). For point targets, these two concepts are equivalent. This will become apparent when the constrained Schwarz inequality is used as an alternate means of deriving the optimal signal-filter pair for maximum SIR.

The SIR problem has recently been considered in detail by three groups of authors: (1) L. J. Spafford and C. A. Stutt [38], [39], [40]; (2) W. D. Rummler [41]; and (3) D. F. Delong, Jr. and E. M. Hofstetter [42], [43]. All three groups have been concerned with narrowband signals. The major contribution of this chapter will therefore lie in the generalization of SIR optimization ideas to wideband analysis.

6.1 Applicability of Existing Methods.

6.1.1 Representation of Noise.

Both the Spafford-Stutt and Delong-Hofstetter approaches use a narrowband complex envelope representation of white Gaussian noise. This representation has been discussed by C. W. Helstrom [44]. The conceptual basis of the argument is that, for a narrowband signal, one can envision passing the signal through an ideal band pass filter without significantly affecting the waveform, provided the passband of the filter is wider than the signal's bandwidth. When this operation is performed on signal plus noise, the resulting noise power spectrum is made narrowbanded, i.e., it has support only in a relatively small band of frequencies surrounding a large carrier frequency.

For a wideband approach, the above reasoning is usually inapplicable. We shall therefore conceive of white noise in a more general sense. If it should become necessary to use energy-limited noise in wideband theory, the ideal noise-shaping filter would be low pass with cutoff above the highest significant signal frequency.

For real Gaussian noise n(t) with a constant power density spectrum height of $N_o/2$, the expected noise response power of a filter with unit energy impulse response v(-t) is:

$$E\left\{\left|\int v(-\tau)n(t-\tau)\,d\tau\right|^2\right\} = \iint v(x)E\{n(t+x)n^*(t+y)\}v^*(y)\,dx\,dy$$

$$= \iint v(x)[(N_o/2)\,\delta(x-y)]v^*(y)\,dx\,dy$$

$$= N_o/2\int |v(x)|^2 dx = N_o/2\,. \qquad (6.1)$$

6.1.2 An Invariance Property of the Ambiguity Function.

Both the Rummler and Delong-Hofstetter approaches use an invariance property of $|\chi_{uu}^{(1)}(\tau,\phi)|^2$. The algorithms of these two groups depend upon the assertion that

$$|\chi_{uv}^{(1)}(\tau,\phi)|^2 = |\chi_{\tilde{v}\tilde{u}}^{(1)}(\tau,\phi)|^2 \qquad (6.2)$$

where $\tilde{u}(t) = u(-t)$ and $\tilde{v}(t) = v(-t)$.

Relation (6.2) implies that the signal and filter may be interchanged without changing the SIR. For the wideband function,

$$\chi_{\tilde{v}\tilde{u}}^{(2)}(\tau,s) = s^{1/2}\int v(-t)u^*[s(-t-\tau)]dt$$

$$= s^{-1/2}\int u^*(t')v(t'/s+\tau)\,dt'$$

$$= \chi_{uv}^{(2)*}(s\tau,\,1/s)\,. \qquad (6.3)$$

Although the right-hand side of (6.3) resembles the left-hand side of (3.146A), the latter equation was formulated for auto-ambiguity functions. For cross-ambiguity functions:

$$\chi_{uv}^{(2)*}(s\tau,\ 1/s) = \chi_{vu}^{(2)*}(-\tau, s).$$

Thus (6.3) is <u>not</u> equivalent to (6.2).

The wideband equivalent of (6.2) is based on more subtle transformations than simple time reversal. If $\hat{v}(t) = s^{1/2}v(-st)$ and $\hat{u}(t) = s^{-1/2}u(-t/s)$, then*

$$\left|\chi_{\hat{v}\hat{u}}^{(2)}(\tau, s)\right|^2 = \left|\chi_{uv}^{(2)}(\tau, s)\right|^2 \quad . \tag{6.4}$$

The optimization algorithms of Rummler and Delong-Hofstetter can be applied to wideband systems by using the above transformations. The Spafford-Stutt algorithm is immediately made applicable to wideband problems by simply replacing $\chi_{uu}^{(1)}$ by $\chi_{uu}^{(2)}$. The Stutt-Spafford approach will be used in this dissertation.

---

* This transformation was pointed out by an anonymous IEEE reviewer as criticism of a paper submitted to the Information Theory Transactions.

6.2 Detailed Expression for the SIR.

If the energy of the signal u(t) is unity, then the energy E_s of the signal Au(t) will be A^2. The power of the maximum filter response to such a signal is then

$$\left| \int Au(t)v^*(t)dt \right|^2 = A^2 \left| \chi_{uv}^{(2)}(0,1) \right|^2 = E_s \left| \chi_{vu}^{(2)}(0,1) \right|^2 . \qquad (6.5)$$

Having derived the signal and noise responses, it remains to find an expression for clutter response. There is some evidence [45,35] that in many situations the clutter can be treated as a distribution of point targets whose positions and velocities are uncorrelated. (One should note that such a model may be more attuned to mathematical convenience than reality. In order not to overly complicate the initial development, this reservation will be saved for future discussion. The present concern is with the conventional representation of clutter as developed by Delong and Hofstetter [42].)

The clutter return $r_c(t)$ is the superposition of returns from an array of point targets with various velocities and ranges:

$$r_c(t) = \sum_{i,k} a_{ik} s_k^{1/2} u[s_k(t - \tau_i)] . \qquad (6.6)$$

Here the delays τ_i and stretch factors s_k are measured relative to the point target. The a_{ik} are statistically independent complex random variables with uniformly distributed phases, so that [42]

$$E\{a_{ik}\} = 0 \tag{6.7a}$$

$$E\{a_{ik} a^*_{mn}\} = p_{ik} \delta_{im} \delta_{kn} . \tag{6.7b}$$

Here p_{ik} may be thought of as a quantity proportional to the radar cross section of the $(i,k)^{th}$ scatterer. The number of scatterers is assumed large enough so that the Central Limit Theorem may be invoked, thus making $r_c(t)$ a sample function of a Gaussian process. The expected value of $r_c(t)$ is zero by (6.7a). By (6.7b) and (6.6):

$$\begin{aligned} R_{r_c}(t,t') &= E\{r_c(t)\, r_c^*(t')\} \\ &= \sum_{i,k} p_{ik} s_k u[s_k(t-\tau_i)] u^*[s_k(t'-\tau_i)] . \end{aligned} \tag{6.8}$$

The development may be generalized to a continuum of scatterers by replacing $\sum_{i,k}$ by integrals over τ and s:

$$R_{r_c}(t,t') = \int_{-\infty}^{\infty}\int_{0}^{\infty} p(\tau,s)\, su[s(t-\tau)]u^*[s(t'-\tau)]\,ds\,d\tau \qquad (6.9)$$

where $p(\tau,s)$ is the clutter probability density function.

The expected clutter response may now be calculated in the same manner as the noise response in Equation (6.1):

$$\begin{aligned} E\left\{\left|\int v(-\eta)\, r_c(t-\tau)\,d\tau\right|^2\right\} &= \iint v(x)\, E\{r_c(t+x)\, r_c^*(t+y)\}\, v^*(y)\,dx\,dy \\ &= \iint v(x)\, R_{r_c}(y,x) v^*(y)\,dx\,dy \\ &= \int_{-\infty}^{\infty}\int_{0}^{\infty} p(\tau,s)\left[s^{1/2}\int_{-\infty}^{\infty} v(x)u^*[s(x-\tau)]dx\right] \\ &\quad \cdot\left[s^{1/2}\int_{-\infty}^{\infty} v^*(y)u[s(y-\tau)]dy\right]d\tau ds \\ &= \int_{-\infty}^{\infty}\int_{0}^{\infty} p(\tau,s)\left|\chi_{vu}^{(2)}(\tau,s)\right|^2 d\tau\, ds\ . \qquad (6.10) \end{aligned}$$

Combining (6.1), (6.5) and (6.10):

$$SIR = \frac{E_s\left|\chi_{vu}^{(2)}(0,1)\right|^2}{(N_o/2)\int|v(t)|^2 dt + E_c\iint p(\tau,s)\left|\chi_{vu}^{(2)}(\tau,s)\right|^2 d\tau ds} \qquad (6.11)$$

where E_s is signal energy, $N_o/2$ the amplitude of the noise power density spectrum, E_c is clutter energy, u(t) is the signal, v(-t) the filter impulse response, and $p(\tau,s)$ the clutter pdf.

When $E_c = 0$ and v(t) = u(t),

$$SIR = SNR = 2E_s/N_o \tag{6.12}$$

the well-known signal-to-noise ratio of matched filter theory.

6.3 Maximization of the SIR.

6.3.1 Time Domain Optimization.

Using a variational approach, one first seeks the optimum filter assuming that the signal is given. Letting $v(t) \rightarrow v(t) + \epsilon\eta(t)$, where $\eta(t)$ has piecewise continuous derivative, the signal-to-interference ratio becomes

$$SIR(\epsilon) = \frac{f(\epsilon)}{g(\epsilon) + h(\epsilon)} \tag{6.13}$$

where

$$f(\epsilon) = E_s \left| \int u(t)\left[v^*(t) + \epsilon\eta^*(t)\right]dt \right|^2 , \tag{6.14}$$

$$g(\epsilon) = (N_o/2) \int \left|v(t) + \epsilon\eta(t)\right|^2 dt, \tag{6.15}$$

$$h(\epsilon) = E_c \iiiint sp(\tau,s)u\left[s(y+\tau)\right]u^*\left[s(x+\tau)\right]\left[v(x) + \epsilon\eta(x)\right]$$
$$\left[v^*(y) + \epsilon\eta^*(y)\right] dx\,dy\,d\tau\,ds . \tag{6.16}$$

Setting the first variation equal to zero, i.e.,

$$\partial/\partial\epsilon\,[\mathrm{SIR}(\epsilon)]\,\Big|_{\epsilon=0} = 0 \tag{6.17}$$

gives

$$\{[g(\epsilon)+h(\epsilon)]f'(\epsilon) - f(\epsilon)[g'(\epsilon)+h'(\epsilon)]\}\Big|_{\epsilon=0} = 0$$

or

$$f'(\epsilon)\Big|_{\epsilon=0} = (\mathrm{SIR})\cdot[g'(\epsilon)+h'(\epsilon)]\Big|_{\epsilon=0} \tag{6.18}$$

where

$$f'(\epsilon)\Big|_{\epsilon=0} = 2E_s\,\mathrm{Re}\left\{\int u(t)\left[\int u^*(x)v(x)\,dx\right]\eta^*(t)\,dt\right\}, \tag{6.19}$$

$$g'(\epsilon)\Big|_{\epsilon=0} = N_o\,\mathrm{Re}\left\{\int[v(t)]\,\eta^*(t)\,dt\right\}, \tag{6.20}$$

$$h'(\epsilon)\Big|_{\epsilon=0} = 2E_c\,\mathrm{Re}\left\{\int\left[\iiint sp(\tau,s)\,u[s(t+\tau)]\,u^*[s(x+\tau)]\,v(x)\,dx\,ds\,d\tau\right]\eta^*(t)\,dt\right\}. \tag{6.21}$$

Substituting (6.19, (6.20), and (6.21) into (6.18):

$$E_s u(t) \int u^*(x)\, v(x)\, dx = [\,(N_o/2)v(t) + E_c \int H_u(t,x)\, v(x)\, dx\,]\,SIR \qquad (6.22)$$

where

$$H_u(t,x) \equiv \int_{-\infty}^{\infty} \int_{0}^{\infty} sp(\tau, s)\, u[s(t+\tau)]\, u^*[s(x+\tau)]\, ds\, d\tau \,. \qquad (6.23)$$

Defining

$$\mu \equiv \left[\frac{\int u^*(t)\, v(t)\, dt}{SIR}\right] [E_s/E_c]\,, \qquad (6.24a)$$

$$\lambda \equiv N_o/2E_c = [\,2E_c/N_o\,]^{-1} = \text{inverse clutter-to-noise ratio} \qquad (6.24b)$$

one has

$$\mu u(t) = \lambda v(t) + \int H_u(t,x)\, v(x)\, dx \quad . \qquad (6.25)$$

The solution of (6.25) for a given signal u(t) is a filter function v(t) which provides a local extremum of the SIR.

Having derived the best filter for a given signal, it is clear that one can also find the best signal when the filter is given. In order to do this easily, change variables in the expression for $\chi^{(2)}_{vu}(\tau,s)$:

$$\chi^{(2)}_{vu}(\tau,s) = s^{1/2}\int v(t)u^*\left[s(t+\tau)\right]dt = s^{-1/2}\int v\left[t'/s) - \tau\right]u^*(t')\,dt'. \tag{6.26}$$

Since $\int |v(t)|^2\,dt = \int |u(t)|^2\,dt = 1$, SIR($\epsilon$) in (6.13) may be rewritten with

$$f(\epsilon) = E_s\left|\int v(t)\left[u^*(t) + \epsilon\eta^*(t)\right]dt\right|^2, \tag{6.27}$$

$$g(\epsilon) = (N_o/2)\int |u(t) + \epsilon\eta(t)|^2\,dt, \tag{6.28}$$

$$h(\epsilon) = E_c\iiiint (1/s)p(\tau,s)v\left[(y/s) - \tau\right]v^*\left[(x/s) - \tau)\right]$$
$$\left[u(x) + \epsilon\eta(x)\right]\left[u^*(y) + \epsilon\eta^*(y)\right]dx\,dy\,d\tau\,ds. \tag{6.29}$$

It follows that

$$\mu v(t) = \lambda u(t) + \int G_v(t,x)u(x)\,dx \tag{6.30}$$

where

$$G_v(t,x) = \iint (1/s)p(\tau,s)v\left[(t/s) - \tau\right]v^*\left[(x/s) - \tau\right]ds\,d\tau. \tag{6.31}$$

Equations (6.25) and (6.30) are two simultaneous integral equations for the unknown optimal signal-filter pair. Unfortunately, it is extremely difficult to combine the two equations and thus obtain a straightforward solution for u(t) and v(t). But, if the equations are kept separate, it is possible to recursively solve for a locally optimum signal-filter pair given a particular starting signal (or filter).

6.3.2 Frequency Domain Optimization.

It will be of interest to obtain the frequency domain version of the above derivations. The procedure is the same as above, except that, by Parseval's theorem,

$$\chi_{vu}^{(2)}(\tau, s) = (s^{-1/2}/2\pi) \int V(\omega)\, U^*(\omega/s)\, e^{-j\omega\tau}\, d\omega \tag{6.32}$$

and

$$\int |v(t)|^2 dt = (1/2\pi) \int |V(\omega)|^2\, d\omega \ . \tag{6.33}$$

Equations (6.14 through 6.16) are then:

$$f(\epsilon) = E_s \left| (1/2\pi) \int U(\omega) [V^*(\omega) + \epsilon \eta^*(\omega)]\, d\omega \right|^2, \tag{6.34}$$

$$g(\epsilon) = (N_o/2)(1/2\pi) \int |V(\omega) + \epsilon \eta(\omega)|^2 d\omega \ , \tag{6.35}$$

$$h(\epsilon) = E_c(1/2\pi)^2 \iiint\!\!\iint (1/s)p(\tau,s)\,U(y/s)\,U^*(x/s)\,e^{-j(x-y)\tau}$$

$$[V(x) + \epsilon\eta(x)][V^*(y) + \epsilon\eta^*(y)]\,dx\,dy\,d\tau\,ds \qquad (6.36)$$

so that

$$\mu U(\omega) = 2\pi\lambda V(\omega) + \int H_U(\omega,x)\,V(x)\,dx \qquad (6.37)$$

where

$$H_U(\omega,x) = \int_{-\infty}^{\infty}\int_{0}^{\infty}(1/s)p(\tau,s)\,U(\omega/s)\,U^*(x/s)\,e^{-j(x-\omega)\tau}\,ds\,d\tau\,. \qquad (6.38)$$

Finally, one solves for $U(\omega)$ given $V(\omega)$ by writing

$$\chi_{vu}^{(2)*}(\tau,s) = (s^{1/2}/2\pi)\int U(\omega)\,V^*(s\omega)\,e^{js\omega\tau}\,d\omega \qquad (6.39)$$

so that

$$f(\epsilon) = E_s\left|(1/2\pi)\int V^*(\omega)\,[\,U(\omega) + \epsilon\eta(\omega)\,]\,d\omega\right|^2, \qquad (6.40)$$

$$g(\epsilon) = (N_o/2)(1/2\pi)\int\left|U(\omega) + \epsilon\eta(\omega)\right|^2 d\omega\ , \qquad (6.41)$$

$$h(\epsilon) = E_c/(2\pi)^2 \iiint\!\!\iint sp(\tau,s)\,V(sy)\,V^*(sx)\,e^{js(x-y)\tau}$$

$$\cdot[U(x) + \epsilon\eta(x)]\,[U^*(y) + \epsilon\eta^*(y)]\,dx\,dy\,d\tau\,ds \qquad (6.42)$$

and

$$\mu V(\omega) = 2\pi\lambda U(\omega) + \int G_V(\omega, x)\, U(x)\, dx \tag{6.43}$$

where

$$G_V(\omega, x) = \int_{-\infty}^{\infty} \int_{0}^{\infty} sp(\tau, s)\, V(s\omega)\, V^*(sx)\, e^{js(x-\omega)\tau} ds\, d\tau. \tag{6.44}$$

Equations (6.37) and (6.43) provide a means of recursively solving for the frequency domain versions of the optimal signal-filter pair.

6.3.3 Alternate Approach.

It has already been mentioned that, for point targets, a constrained Schwarz inequality yields a solution that maximizes the SIR. It is important that such an alternate derivation exists, as it is very difficult to ascertain the sign of the second variation of the SIR. Thus, without the alternate approach given below, one could never be certain whether the extrema found by the variational method were local maxima (rather than local minima). By obtaining the results with a Schwarz inequality, however, one is assured that he has indeed found necessary conditions for a local maximum.

Given the class of signals such that $\int |v(t)|^2 dt = 1$ and the clutter response $\int p(\tau, s) |\chi_{vu}^{(2)}(\tau, s)|^2 d\tau\, ds$, which is constrained to equal a small number (preferably zero), one seeks a function $v_o(t)$ in this class such that

the target response $\left|\int v(t)u^*(t)\,dt\right|^2$ is a maximum. Writing the clutter response as an inner product:

$$\int p(\tau,s)\left|\chi^{(2)}_{vu}(\tau,s)\right|^2 d\tau\,ds = \int v(t)\,f^*(t)\,dt$$

where $f^*(t) = \iiint sp(\tau,s)\,u[s(y+\tau)]\,u^*[s(t+\tau)]\,v^*(y)\,ds\,d\tau dy$. (6.45)

According to Papoulis [36], the solution is

$$v(t) = k\left[u(t) + \epsilon\iiint sp(\tau,s)\,u[s(t+\tau)]u^*[s(y+\tau)]\,v(y)\,ds\,d\tau dy\right]$$

$$= k[u(t) + \epsilon\int H_u(t,y)\,v(y)\,dy]. \qquad (6.46)$$

By proper choice of k and ϵ, (6.46) can be made identical to (6.25). The other solutions can be obtained in the same manner.

6.4 A General Method of Solution.

Again following Stutt [39] and Spafford [ ], the signal and filter functions are decomposed into a finite set of orthonormal basis functions:

$$u(t) = \sum_{m=1}^{N} a_m \varphi_m(t)$$

$$v(t) = \sum_{m=1}^{N} b_m \varphi_m(t) \quad . \qquad (6.47)$$

It is important to realize that (6.47) is written not as an approximation but as an equality. In other words, the solution is restricted to only those functions which can be expressed as a linear combination of the N chosen basis functions. The larger and more complete the basis, the bigger the class of functions that can qualify as solutions.

The two-dimensional function $H_u(t,x)$ in (6.23) can be written*:

$$H_u(t,x) \cong \sum_{m,n}^{N} c_{mn} \varphi_m(t) \varphi_n^*(x) \ . \tag{6.48}$$

Then (6.25) becomes

$$\mu \sum_m a_m \varphi_m(t) = \lambda \sum_m b_m \varphi_m(t) + \sum_{m,n,k} c_{mn} b_k \varphi_m(t) \int \varphi_n^*(x) \varphi_k(x)\, dx$$

$$\sum_m [\mu a_m] \varphi_m(t) = \sum_m [\lambda b_m + \sum_n c_{mn} b_n] \varphi_m(t)$$

$$\mu a_m = \lambda b_m + \sum_n c_{mn} b_n \ . \tag{6.49}$$

(6.49) describes each element of the column matrix A in terms of the elements of the column matrix b and a square matrix C. That is, (6.49) is equivalent to the matrix equation.

$$\mu A = \lambda B + CB = [C + \lambda I] B$$

or

$$B = \mu [C + \lambda I]^{-1} A \ . \tag{6.50}$$

*For a given basis set, the accuracy of this approximation depends upon the clutter distribution.

Similarly, if (6.31) is written

$$G_v(t,x) = \sum_{m,n} d_{mn}\, \varphi_m(t)\, \varphi_n^*(x) \ , \tag{6.51}$$

then (6.30) becomes:

$$A = \mu[D + \lambda I]^{-1} B \ . \tag{6.52}$$

The elements of C and D are obtained from (6.48), (6.23), (6.51) and (6.31):

$$\begin{aligned} c_{k\ell} &= \iint H_u(t,x)\, \varphi_k^*(t) \varphi_\ell(x)\, dt\, dx \\ &= \sum_{m,n} a_m a_n^* \int_{-\infty}^{\infty} \int_0^{\infty} sp(\tau,s)\, Y_{mk}(\tau,s)\, Y_{n\ell}^*(\tau,s)\, ds\, d\tau \ . \end{aligned} \tag{6.53}$$

$$\begin{aligned} d_{k\ell} &= \iint G_v(t,x)\, \varphi_k^*(t) \varphi_\ell(x)\, dt\, dx \\ &= \sum_{m,n} b_m b_n^* \int_{-\infty}^{\infty} \int_0^{\infty} (1/s) p(\tau,s)\, X_{mk}(\tau,s) X_{n\ell}^*(\tau,s)\, ds\, d\tau \end{aligned} \tag{6.54}$$

where

$$Y_{mk}(\tau,s) \equiv \int \varphi_m[s(t+\tau)]\, \varphi_k^*(t)\, dt \tag{6.55}$$

$$X_{mk}(\tau,s) \equiv \int \varphi_m[(t/s) - \tau]\, \varphi_k^*(t)\, dt \ . \tag{6.56}$$

A general method of solving for an optimum signal-filter pair would then be to start with some arbitrary unit energy signal vector and to solve for the C matrix elements using (6.53). Having found the components of an optimum filter via (6.50), the energy of this filter would be normalized to unity and the components used in (6.54) to find the D matrix. Using (6.52), another A vector would be determined. The process would be repeated until the improvement in the signal-to-interference ratio became negligible. *

The SIR may be written** [38]:

$$SIR = A^{*}\left[C + \lambda I\right]^{-1} A(E_s/E_c). \qquad (6.57)$$

Equation (6.57) provides a convenient way to calculate the value of SIR at each stage of the iteration process.

The signal-to-interference ratio is guaranteed to be larger or unchanged after each stage of the iteration. This is because each stage finds a locally optimum filter (signal) vector given a particular signal (filter)

---

* The resulting signal and filter vectors would then be consistent with each other in terms of Equations (4.85 through 4.88).

** An asterisk, when applied to a matrix quantity, indicates the conjugate transpose of the matrix. Equation (6.57) can be derived by solving (6.24a) for SIR and applying the condition (6.12).

vector. Since the SIR is nondecreasing for every iteration, and since it is bounded above by the signal-to-noise ratio, the iterations must converge to a local maximum.

6.5 Some Special Cases.

Most solutions to the pair of integral equations (6.25) and (6.30) are best obtained by the iterative method implemented with a computer. However, it is possible to solve a few special cases without resort to extensive computations. Since these solutions provide some insight into the workings and results of the general method, they will now be discussed.

6.5.1 Clutter Uniform in Range.

Suppose first that the clutter's probability density function is uniform in range: $p(\tau, s) = \lim_{T\to\infty} p(s)(1/2T)\mathrm{rect}(\tau/T)$, where

$$\mathrm{rect}(x) = \begin{cases} 1, & |x| < 1 \\ 0, & |x| > 1 \end{cases} .$$

Such a situation could occur when a whole region (encompassing the maximum range of the radar) is enveloped in a dense fog; Spafford has labelled this "weather clutter". For this particular case, one can use the frequency domain equations developed in Section 6.3.2. Specifically, Equation (6.38) becomes:

$$H_U(\omega,x) = \int_0^\infty (1/s)p(s)\,U(\omega/s)\,U^*(x/s)\,[\lim_{T\to\infty}(1/2T)\int_{-T}^{T} e^{-j(x-\omega)\tau}d\tau]ds$$

$$= 2\pi\int_0^\infty (1/s)p(s)U(\omega/s)\,U^*(x/s)\,ds\,\delta(x-\omega) \qquad (6.58)$$

and Equation (6.44) becomes

$$G_V(\omega,x) = 2\pi\int_0^\infty p(s)\,V(s\omega)\,V^*(sx)\,\delta(x-\omega)\,ds. \qquad (6.59)$$

From (6.37) and (6.43):

$$V(\omega) = \frac{(\mu/2\pi)\,U(\omega)}{\lambda + \int_0^\infty (1/s)p(s)\,|U(\omega/s)|^2\,ds} \qquad (6.60)$$

$$U(\omega) = \frac{(\mu/2\pi)\,V(\omega)}{\lambda + \int_0^\infty p(s)\,|V(s\omega)|^2\,ds}\,. \qquad (6.61)$$

Given $U(\omega)$ and $p(s)$ it is a simple matter to solve (6.60) for $V(\omega)$. Using this $V(\omega)$, a new and better $U(\omega)$ can be found from (6.61).

As a specific example, consider the case of a motionless target (in motionless fog):

$$p(s) = \delta(s-1) \quad . \tag{6.62}$$

Then

$$V(\omega) = \frac{(\mu/2\pi)\, U(\omega)}{\lambda + |U(\omega)|^2} \tag{6.63}$$

$$U(\omega) = \frac{(\mu/2\pi)\, V(\omega)}{\lambda + |V(\omega)|^2} \quad . \tag{6.64}$$

Substituting (6.63) into (6.64) gives the relation

$$[\lambda + |U(\omega)|^2]^2 = (\mu/2\pi)^2$$

or $$|U(\omega)|^2 = (\mu/2\pi) - \lambda = \text{constant}$$

so that, by (6.63),

$$V(\omega) = \frac{(\mu/2\pi)\, U(\omega)}{\lambda + [(\mu/2\pi) - \lambda]} = U(\omega) \ ,$$

or

$$|V(\omega)|^2 = |U(\omega)|^2 = (\mu/2\pi) - \lambda = \text{constant.} \tag{6.65}$$

This says that the best signal for detecting motionless point targets in weather clutter has a uniform power spectral density (corresponding to an impulse-like autocorrelation function for large system bandwidth).

6.5.2 Clutter Near the Target (Resolution Problem).

The following example illustrates the matrix computation and manipulation involved in the actual computer algorithm. The waveforms are constrained only in energy, with the result that extremely high frequencies are called for in the solution. The answer, in fact, is analogous to that found in singular detection problems [2], wherein an obvious (and generally unusable) solution is obtained for a problem that is unrealistically formulated.

Here one assumes that the time duration of the signal is much larger than the delay between target and clutter; it is also assumed that clutter velocity is very near the target velocity. If the clutter is concentrated at a single point on the (τ, s) plane, this becomes a classical radar resolution problem.

The upshot of the clutter-near-target assumption is that an approximation may be made concerning the limits of the integrals $Y_{km}(\tau, s)$ and $X_{km}(\tau, s)$ defined in Equations (6.55) and (6.56). Assume that the signal and filter functions are time limited to $[-T, T]$. Then

$$\varphi_m[s(t+\tau)] \not\equiv 0 \text{ only if } -T \le s(t+\tau) \le T$$

$$\text{or } (-T/s) - \tau \le t \le (T/s) - \tau, \qquad (6.66a)$$

and

$$\varphi_m[(t/s) - \tau] \neq 0 \text{ for } -T \leq [(t/s) - \tau] \leq T$$

$$\text{or } s(-T + \tau) \leq t \leq s(T + \tau). \tag{6.66b}$$

Equations (6.55) and (6.56) thus become

$$Y_{mk}(\tau, s) = \int_{a_y}^{b_y} \varphi_k^*(t)\, \varphi_m[s(t + \tau)]dt \tag{6.67}$$

where $a_y = \max\{-T, (-T/s) - \tau\}$ and $b_y = \min\{T, (T/s) - \tau\}$

and

$$X_{mk}(\tau, s) = \int_{a_x}^{b_x} \varphi_k^*(t)\, \varphi_m[(t/s) - \tau]\, dt \tag{6.68}$$

where $a_x = \max\{-T, s(-T + \tau)\}$ and $b_x = \min\{T, s(T + \tau)\}$.

By Equations (6.53) and (6.54) it is apparent that, if $p(\tau, s)$ is significantly different from zero only for $\tau << T, s \approx 1$, then little error will result by making the limits a_x, b_x and a_y, b_y equal to $-T, T$. This is especially true if the $\varphi_m(t)$ are relatively smooth functions that go to zero at the endpoints of the time interval.

Letting

$$\varphi_m(t) = (1/2T)^{1/2}\, e^{j2\pi mt/T},\ t\in[-T,T] \tag{6.69}$$

the clutter-near-target assumption allows an easy caiculation of the C and D matrices when clutter is from a limited number of separated point targets:

$$p(\tau,s) = \sum_{i,j} p_{ij}\,\delta(\tau-\tau_i)\,\delta(s-s_j)\ . \tag{6.70}$$

Using the limits $[-T,T]$ along with the basis functions (6.69) in the integrals (6.67) and (6.68):

$$X_{mk}(\tau,s) = e^{-j2\pi\, m\tau/T}\ \frac{\operatorname{Sin} 2\pi\,(m/s-k)}{2\pi(m/s-k)} \tag{6.71}$$

$$Y_{mk}(\tau,s) = e^{j2\pi ms\tau/T}\ \frac{\operatorname{Sin}\,[\,2\pi(ms-k)\,]}{2\pi(ms-k)}\ . \tag{6.72}$$

Using (6.70-72) and (6.53-54), the elements of C and D are:

$$c_{k\ell} = \sum_{i,j} p_{ij} s_j \sum_{m,n} a_m a_n^*\ e^{j2\pi s_j\tau_i(m-n)/T}$$

$$\cdot\ \frac{\operatorname{Sin}\,[2\pi(ms_j-k)]}{2\pi(ms_j-k)}\cdot\frac{\operatorname{Sin} 2\pi(ns_j-\ell)}{2\pi(ns_j-\ell)} \tag{6.73}$$

$$d_{k\ell} = \sum_{i,j} (p_{ij}/s_j) \sum_{m,n} b_m b_n^* e^{-j2\pi \tau_i (m-n)/T}$$

$$\cdot \frac{\mathrm{Sin}\,[2\pi(m/s_j - k)]}{2\pi(m/s_j - k)} \cdot \frac{\mathrm{Sin}\,2\pi(n/s_j - \ell)}{2\pi(n/s_j - \ell)} \quad . \tag{6.74}$$

Now suppose that

$$A^* = [0,0,\cdots,0,1,0,\cdots,0] \tag{6.75}$$

where the nonzero element is the M^{th} element. The integer M is chosen as follows:

Write the s_j as rational numbers. (This may be done with arbitrarily small error because "between any two distinct real numbers there is a rational and an irrational" [46]. Thus in a finite interval, no matter how small, around the true value of s_j there is at least one rational number.) Then

$$s_1 = \gamma_1/\gamma_2,\ s_2 = \gamma_3/\gamma_4,\cdots,\ s_N = \gamma_{2N-1}/\gamma_{2N} \tag{6.76}$$

where $\gamma_1,\gamma_2,\cdots,\gamma_{2N}$ are integers. Let M be defined as the product:

$$M \equiv \gamma_1\gamma_2\gamma_3\cdots\gamma_{2N} \quad . \tag{6.77}$$

With M so chosen, Ms_j is an integer (ν_j) for all s_j, j=1,···,N. Also, M/s_j is an integer (ρ_j) for all s_j. From this observation, with the vector A as defined in (6.75):

$$c_{k\ell} = \sum_{i,j} p_{ij} s_j \delta_{\nu_j k} \delta_{\nu_j \ell} \tag{6.78}$$

where the δ's are Kronecker delta functions. It is obviously impossible that $c_{k\ell} \neq 0$ unless $k = \ell$ (or, more precisely, $k = \ell = \nu_j$). The C matrix has therefore been diagonalized. As a result, $[C+\lambda I]^{-1}$ is also diagonalized, and the filter vector B, obtained from Equation (6.50) and normalized to unit energy, will have exactly the same form as A (matched filter case), i.e.,

$$B^* = [0,0,\cdots,0,1,0,\cdots,0] \tag{6.79}$$

where the nonzero element is again the M^{th} element. But with B so defined,

$$d_{k\ell} = \sum_{i,j} (p_{ij}/s_j) \delta_{\rho_j k} \delta_{\rho_j \ell} \tag{6.80}$$

so that D and $[D + \lambda I]^{-1}$ are also diagonalized. The result, using (6.52) and normalizing to unit energy, is just the original signal vector described

by (6.75). This is then an optimal signal for doppler resolution. In fact, if none of the s_j's are equal to one, then none of the ν_j's or ρ_j's are equal to M. It then follows that $c_{MM} = d_{MM} = 0$, so that

$$SIR = A^* [C + \lambda I]^{-1} A(E_s/E_c) = 2E_s/N_o, \tag{6.81}$$

which is the maximum possible SIR (i.e., the signal-to-noise ratio for a matched signal-filter pair whose ambiguity function is orthogonal to clutter). Assuming $E_s = E_c = 1$, the maximum SIR is $1/\lambda$. In other words, the signal-filter pair described by (6.75), (6.77), and (6.79) is a global optimum to the SIR maximization problem.

Although the above solution is the best possible one, it will now be shown that the solution is not unique. Consider the d.c. component of $\{\varphi_m(t)\}$ in Equation (6.69), i.e., the m = 0 component. If this component is included in the set of basis functions, then one can choose an initial signal vector:

$$A^* = [1,0,0,\cdots,0,0] \tag{6.82}$$

where the first component corresponds to m = 0. Such a choice makes

$$c_{k\ell} = \sum_{i,j} p_{ij} s_j \delta_{k,0} \delta_{\ell,0} \quad . \tag{6.83}$$

Once again, $[C + \lambda I]^{-1}$ is a diagonal matrix, so that B = A. Then

$$d_{k\ell} = \sum_{i,j} (p_{ij}/s_j) \delta_{k,0} \delta_{\ell,0} \tag{6.84}$$

so that $[D + \lambda I]^{-1}$ is diagonalized and A is regenerated. For this case (with $E_s = E_c = 1$):

$$SIR = A^* [C + \lambda I]^{-1} A = 1/(\lambda + \sum_{i,j} p_{ij} s_j) < 1/\lambda. \tag{6.85}$$

Thus a second solution to the problem exists, namely a rectangular pulse. This solution gives a local maximum of the SIR but not a global one.*

Because the first answer results in an absolute maximum of the SIR, it is evident that the signal-filter ambiguity function is orthogonal to the clutter pdf (and that the signal and filter functions are identical). That is, the algorithm demonstrates the way in which the zeroes of the signal auto-ambiguity function can be made coincident with clutter points. It would seem

---

* The two special results derived here, i.e., a narrowband signal and a rectangular pulse, should be compared with equation (3.166) and the corollary to (3.81), respectively.

that the frequency $f_M = M/T$ must be accurately implemented in order that the SIR actually assume its theoretical optimum. Notice also that for a given value of M, the frequency may be made smaller by using a larger time duration. Unfortunately, time duration is generally limited by the supposition that the echo not overlap the transmission. (The system should avoid simultaneous transmission and reception so that the strong outgoing signal does not "swamp out" the comparatively weak echo.) By the argument associated with (3.166), one sees that as f_M becomes arbitrarily large, the resulting quasi-monochromatic signal can attain any prespecified doppler resolution capability. This limiting solution is then less sensitive to an accurate frequency implementation, provided the frequency is so large that the ambiguity function has no support in s beyond a prespecified interval around $s = 1$. In this sense, the solution is analogous to the perfect performance attained for the singular detection problem, wherein the problem formulation is not sufficiently realistic. (Realism in this case would dictate a constraint on maximum signal frequency.)

The above example accentuates certain characteristics of the iteration process for SIR maximization:

1. The solution is dependent upon the basis functions from which it is constructed. For clutter points very near the target in velocity, the value of M could be exceedingly large. The M^{th} component might

then be omitted for practical reasons, thus forcing the procedure to find a less impressive but more tenable optimum signal-filter pair. Although M can be a large frequency, the frequencies required to realize the abrupt endpoint jumps for m=0 are even larger. To avoid such discontinuities (as well as a d.c. component) the d.c. term might also be left out of the basis, again forcing the procedure to a different result. From these remarks one sees that many physical system constraints can be included in the optimization procedure by restricting the available choice of basis components.

2. Solutions are not necessarily unique.

3. The procedure is not only prejudiced by the choice of basis, but also by the initial (starting) vector.

6.6 Computer Algorithm for General Solutions.

To formulate the problem for computer solutions, the first step is to superpose a grid onto the (τ, s) plane. Samples of the clutter probability density function will be taken at each intersection of grid lines (hereafter called grid points). The grid lines should be spaced at small enough intervals to allow a reasonably accurate reconstruction of both the clutter pdf and the ambiguity function from their sampled values at the grid points.

At each grid point (τ_i, s_j), the values of $X_{mk}(\tau_i, s_j)$ and $Y_{mk}(\tau_i, s_j)$ are determined. In reality only one of these quantities need be calculated, since by a change of variables

$$X_{mk}(\tau, s) = \int_{a_x}^{b_x} \varphi_k^*(t)\,\varphi_m(t/s - \tau)\,dt = s \int_{a_y}^{b_y} \varphi_k^*[s(t'+\tau)]\,\varphi_m(t')\,dt'$$

$$= sY_{km}^*(\tau, s)\,. \tag{6.86}$$

(The limits a_x, b_x, a_y, b_y are given in conjunction with Equations 6.67 and 6.68.)

Notice that $X_{mk}(\tau_i, s_j)$ and $Y_{mk}(\tau_i, s_j)$ are not functions of the clutter pdf but depend only upon the basis functions and grid that are used for the problem. The X_{km}'s or Y_{km}'s should then be computed and stored, since they can be used with a wide variety of specific clutter distributions to find optimal signal-filter pairs.

For a particular clutter pdf evaluated at the grid points as $p(\tau_i, s_j)$, and a given starting vector **A**, one can now form the elements of the C matrix from (6.53):

$$c_{k\ell} = \sum_{m,n} a_m a_n^* \left\{ \int_{-\infty}^{\infty} \int_{0}^{\infty} s_j p(\tau_i, s_j) Y_{mk}(\tau_i, s_j) Y_{n\ell}^*(\tau_i, s_j)\,d\tau_i ds_j \right\} \tag{6.87}$$

where the integrations are performed as summations over the grid points τ_i and s_j (e.g., by using Simpson's rule).

Notice that the integral in brackets in (6.87) is independent of A. This means that it need only be calculated once and stored:

$$F_{k\ell mn} = \int_{-\infty}^{\infty}\int_{0}^{\infty} s_j p(\tau_i, s_j)\, Y_{mk}(\tau_i, s_j) Y^*_{n\ell}(\tau_i, s_j)\, d\tau_i ds_j$$

$$= \int_{-\infty}^{\infty}\int_{0}^{\infty} (1/s_j) p(\tau_i, s_j) X^*_{km}(\tau_i, s_j) X_{\ell n}(\tau_i, s_j)\, d\tau_i ds_j \quad . \qquad (6.88)$$

Then

$$c_{k\ell} = \sum_{m,n} a_m a^*_n F_{k\ell mn} \, . \qquad (6.89)$$

Similarly, by (6.86):

$$\int_{-\infty}^{\infty}\int_{0}^{\infty} (1/s_j) p(\tau_i, s_j) X_{mk}(\tau_i, s_j) X^*_{n\ell}(\tau_i, s_j)\, d\tau_i ds_j$$

$$= \int_{-\infty}^{\infty}\int_{0}^{\infty} s_j p(\tau_i, s_j) Y^*_{km}(\tau_i, s_j) Y_{\ell n}(\tau_i, s_j)\, d\tau_i ds_j$$

$$= F^*_{mnk\ell}$$

$$= F_{nm\ell k} \qquad (6.90)$$

so that

$$d_{k\ell} = \sum_{m,n} b_m b_n^* F_{nm\ell k} \quad . \tag{6.91}$$

Having found C, one can use standard computer subroutines to form the inverse of $C+\lambda I$. Then the filter vector B is found from (6.50). After B is normalized to unit energy, D is calculated by using (6.91). Again, $[D+\lambda I]^{-1}$ is found and a new energy-normalized vector A is determined from (6.52). At this point one computes the SIR by using (6.57). The procedure is then repeated.

Succeeding values of the SIR are compared, and when the difference between them is less than a certain small number, then it is concluded that future iterations will result in very little further improvement; a locally optimum signal-filter pair has been found.

Finally, it is desirable to have a measure, other than the SIR itself, as to how well the cross-ambiguity function of the best signal-filter pair is avoiding high-clutter regions on the τ,s plane. To this end, one can easily generate and print out samples of the ambiguity function taken at the grid points:

$$\chi_{vu}^{(2)}(\tau_i, s_j) = s_j^{1/2} \int v(t) u^*[s_j(t+\tau_i)]dt$$

$$= \sum_{m,n} s_j^{1/2} b_m a_n^* \int \varphi_m(t) \varphi_n^*[s_j(t+\tau_i)]dt$$

$$= \sum_{m,n} b_m a_n^* s_j^{-1/2} \chi_{mn}(\tau_i, s_j). \qquad (6.92)$$

The flow charts corresponding to the above procedure are given in Appendix D. Some specific results are given below.

Note that all examples use the orthonormal components:

$$\varphi_n(t) = (2/T)^{1/2} \mathrm{Sin}(n\pi t/T), \; t \in [0, T] \; . \qquad (6.93)$$

Real functions were chosen because complex basis functions will generally yield complex waveforms. If these waveforms were modulating a high carrier frequency, one could justify an argument that the real parts of the waveforms are approximately the Hilbert transforms of the imaginary parts, and the real parts of the results would thus have meaning in terms of the Gabor complex representation. But for truly wide-band signals there is no guarantee that the optimal waveforms will be Analytic. There is then no justification for taking the real parts of the results and calling them the "answers". This pitfall is easily avoided by using real basis functions.

Sines (instead of cosines) were chosen so that there would be no discontinuities at the endpoints of the interval $[0,T]$. These components are also optimally smooth in the sense that they minimize mean square bandwidth under an energy constraint [25,56].

6.7 Significance of the SIR Algorithm.

The SIR algorithm may be considered an alternate approach to a classical problem of radar signal design. Once one becomes convinced that the ambiguity function describes the capabilities of a radar/sonar system, it is natural to simply specify the ambiguity function that best suits one's needs. But the designer is then faced with the questions: (1) Is this idealized function that he has specified really an ambiguity function, and if so, (2) To what signal-filter pair does it correspond? Much recent research effort has been directed towards finding an answer to these questions for the narrow-band case [46,47,48]. The first question has also been answered for the wide-band case (3.150).

The SIR optimization procedure attempts to solve the same problem without the necessity of answering the above questions. When the designer decides upon the ambiguity function he wants, he need only put a high clutter probability in those parts of the ambiguity plane where his ideal

function should be small.* As already pointed out, system constraints are conveniently included by a realistic choice of basis functions. Given the basis and the clutter, the algorithm systematically determines a locally optimum signal-filter pair. If the corresponding ambiguity function is still far different from the one he needs, the designer may consider a different set of basis functions and a different time (or frequency) duration. The properties of Chapter III should be of some help in making these choices.

The SIR optimization solution has implications for two-way communication links as well as for radar. Consider, for example, binary radio communication through (or reflected from) the ionosphere. If two sets of basis functions are established such that one set is orthogonal to the other, then two orthogonal signal-filter pairs can be found such that each is optimally designed for transmission through a given channel. The channel would be characterized by a certain probability density function of point reflectors in time and velocity; delays and velocity distortions would be measured relative to a predetermined transmission path. If it is decided that transmission should occur along a specific ray traced from transmitter to receiver, then all other possible rays connecting the terminals are to be considered as sources of unwanted information; their associated delays and

---

* Some examples of this procedure will be presented in Section 6.8.

doppler factors (relative to the desired transmission) would define the clutter distribution for the SIR algorithm.

6.8 Specific Results.

For a signal time limited to T = 0.1 second, five components of the form (6.93) were used. The 10 x 10 grid sampled the ambiguity function at equal intervals between $-0.025 < \tau \leq +0.025$ and $0.90 \leq s < 1.10$. The clutter distributions were as follows:

I. Uniform clutter on the tau axis to encourage range resolution.

II. Uniform clutter on the s axis to encourage velocity resolution.

III. Two-dimensional Gaussian clutter distribution with mean at the origin (0,1) to encourage volume clearance (ambiguity volume small near the origin).

IV. Uniform clutter on tau and s axes to encourage combined range-velocity resolution.

V. Uniform clutter in first and third quadrants to encourage a sharp ridge-shaped (razor blade) function near the origin.

The clutter distributions were designed to have almost all their volume within the grid area. Since the grid area was only a small part of the ambiguity plane, this led to very large clutter amplitudes and generally unimpressive values of SIR (on the order of 1 for a maximum possible value of 10). A notable exception occurred for clutter distribution V.

Three sets of components were tried for each of the five clutter distributions given above. In order to have reasonably small interpolation errors, the maximum value of n in Equation (6.93) was always less than 20:

a. $n = 1,5,9,13,17$

b. $n = 3,11,15,17,18$

c. $n = 13,14,15,16,17$

For T = 0.1 second, the corresponding frequencies (from 6.93) are $f(n) = 5n$; $f(1) = 5$ Hz, $f(18) = 90$ Hz. It should be remarked that the problem is invariant to a consistent time scaling. The same results would apply for T = 1 msec, $f(1) = 0.5$ kHz, $f(18) = 9$ kHz, and the 10 x 10 grid sampling over the area $-2.5 \times 10^{-4} < \tau \leq +2.5 \times 10^{-4}$, $0.90 \leq s < 1.10$. (The grid width in the s-direction is unchanged by virtue of Equation 3.101.) The grid still covers a range parameter interval equal to half the signal duration.

The component sets a and c both consist of uniformly spaced frequencies with the same maximum frequency. They were picked in order to test the effect of different bandwidths. The component set b has a logarithmic spacing $(2^3, 2^2, 2^1, 2^0)$ between succeeding values of n.

Results were found to be highly dependent upon the starting vector, as one would expect from the example in Section 6.5.2. Therefore at least two different starting vectors were tried for each combination of component set (a,b,c) and clutter distribution (I-V).

Table 6.1 shows the best three SIR's obtained for a given clutter distribution. As already remarked, these results were obtained by trying at least two different starting vectors for each orthonormal basis and clutter pdf. The results in the table then represent the three largest SIR's out of at least six local maxima. Also shown are some computed moments* of the Analytic signal associated with each optimum signal-filter pair. The

---

* All the quantities shown in Table 6.1 are defined in Chapter III or Appendix A except for Woodward's T function, T_W [1,p.117]:

$$T_W \equiv (1/2\pi)\int |U(\omega)|^4 d\omega = \int |R_u(\tau)|^2 d\tau.$$

The importance of this function is demonstrated by the proofs of the volume theorems in Chapter III.

Clutter pdf	Basis Set	Signal Compo-nents	Filter Compo-nents	ω_o (rad)	λ^2	η^2	γ	T_W	D_t^2	Avg Curva-ture	$\alpha_u^{(1)}$	$\alpha_u^{(2)}$	Wave-forms	$\lvert\chi_{uv}^{(2)}\rvert$
I	a.	.332	.237	352	38572	237	1847	.021	.0035	38809	541	117×10^4	Fig. 6.1	Fig. 6.2
		.408	.545											
SIR = 0.45		-.312	-.474											
		.494	.402											
		.618	.510											
I	a.	.287	.135	313	41115	235	1906	.020	.0037	41350	474	129×10^4	Fig.6.3	Fig. 6.4
		.430	.380											
SIR = 0.45		.475	.506											
		.497	.522											
		.511	.555											
I	b.	-.509	-.542	354	33346	214	1617	.019	.0033	33560	532	70.3×10^4	---	---
		.524	.572											
SIR = 0.44		.519	.357											
		-.073	.064											
		.438	.497											
II	b.	.172	.140	457	24704	380	1749	.027	.0047	25083	1144	351×10^4	Fig. 6.5	Fig. 6.6
		.408	.434											
SIR = 0.29		.544	.498											
		.608	.598											
		-.373	-.432											

Table 6.1. Computational Results for SIR Problems.

Clutter pdf	Basis	Signal Components	Filter Components	ω_o (rad)	λ^2	η^2	γ	T_W	D_t^2	Avg Curvature	$\alpha_u^{(1)}$	$\alpha_u^{(2)}$	Waveforms	$\lvert\chi_{uv}^{(2)}\rvert$
II	c.	.558 -.166	.366 -.014	465	18277	357	846	.031	.0047	18634	1054	297×10^4	---	---
SIR = 0.29		.390 -.030	.682 -.232											
		.713	.589											
II	c.	.483 .129	.492 -.314	462	17217	397	1068	.027	.0045	17614	1072	302×10^4	---	---
SIR = 0.29		.595 -.243	.367 .023											
		.581	.724											
III	b.	.360 .503	.389 .549	397	37061	371	2168	.023	.0042	37431	860	261×10^4	Fig. 6.7	Fig. 6.8
SIR = 0.60		.454 .613	.437 .546											
		-.189	-.242											
III	a.	.162 .379	.160 .342	353	37599	248	1734	.020	.0036	37847	551	149×10^4	Fig. 6.9	Fig. 6.10
SIR = 0.57		.481 .510	.490 .484											
		.582	.619											

Table 6.1 --- Continued

Clutter pdf	Basis	Signal Components	Filter Components	ω_o (rad)	λ^2	η^2	γ	T_W	D_t^2	Avg Curvature	$\alpha_u^{(1)}$	$\alpha_u^{(2)}$	Waveforms	$\lvert\chi_{uv}^{(2)}\rvert$
III	a.	-.258	-.440	365	31259	230	1479	.021	.0034	31490	556	126×10^4	---	---
		-.390	-.289											
SIR = 0.56		.393	.348											
		.508	.497											
		.607	.595											
IV	b.	.335	.354	401	35394	361	1877	.023	.0040	35755	812	243×10^4	Fig. 6.11	Fig. 6.12
		.494	.521											
SIR = 1.84		.520	.484											
		.601	.587											
		-.111	-.157											
IV	a.	.144	.161	358	35648	245	1640	.020	.0036	35894	557	149×10^4	Fig. 6.13	Fig. 6.14
		.350	.373											
SIR = 1.79		.469	.486											
		.551	.517											
		.577	.576											
IV	a.	-.353	-.338	353	35111	236	1667	.020	.0034	35347	541	122×10^4	---	---
		-.361	-.348											
SIR = 1.77		.314	.370											
		.552	.546											
		.584	.575											

Table 6.1 --- Continued.

Clutter pdf	Basis Set	Signal Components	Filter Components	ω_o (rad)	λ^2	η^2	γ	T_W	D_t^2	Avg Curvature	$\alpha_u^{(1)}$	$\alpha_u^{(2)}$	Waveforms	$\lvert\chi_{uv}^{(2)}$
V	a.	.285	.280	262	32803	181	1515	.022	.0037	32984	384	91×10^4	Fig. 6.15	Fig. 6.16
		.527	.528											
SIR = 9.72		.547	.542											
		.486	.482											
		.326	.341											
V	a.	.455	.450	243	24940	129	1245	.021	.0034	25068	275	27×10^4	---	---
		.532	.533											
SIR = 9.44		-.449	-.450											
		-.486	-.497											
		.269	.252											
V	b.	.487	.464	328	39099	295	1991	.023	.0038	39395	582	172×10^4	---	---
		.603	.490											
SIR = 5.15		.439	.440											
		.447	.565											
		-.076	-.178											

Table 6.1 --- Continued.

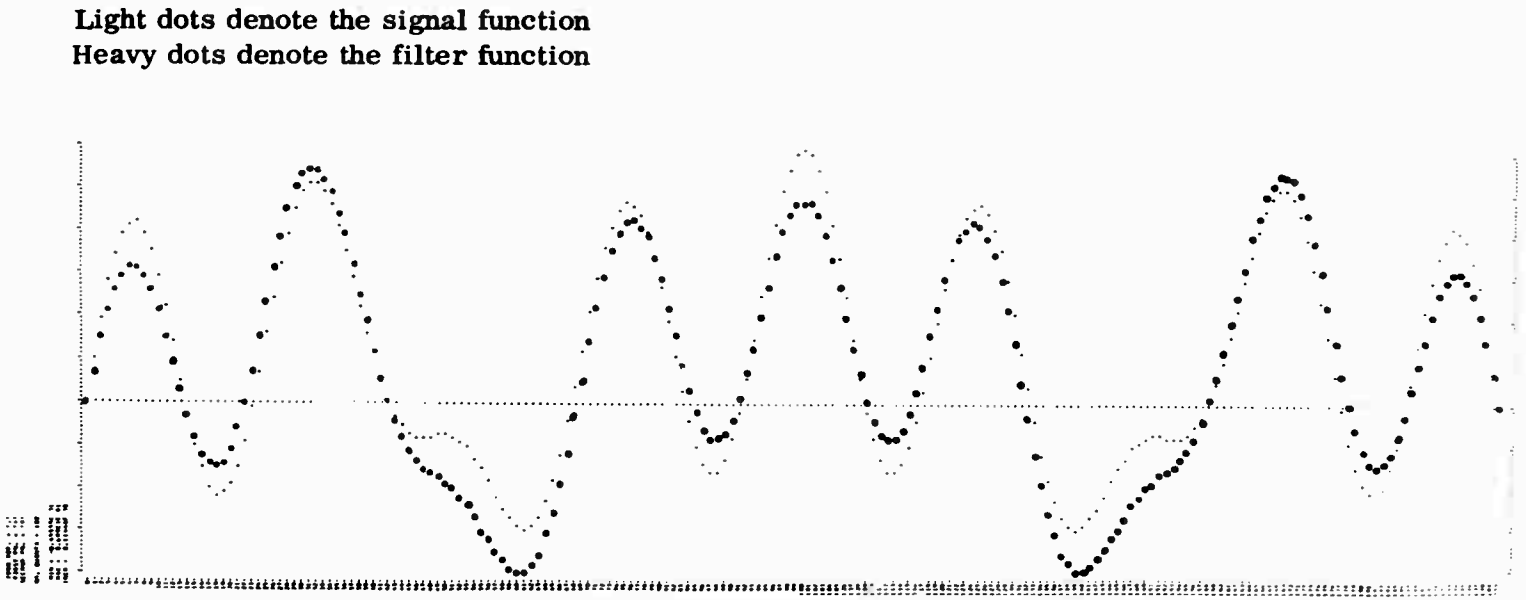

Figure 6.1. Locally Optimum Signal-Filter Pair for Range Resolution.

Delay (tau)

-.025	-.020	-.015	-.010	-.005	0.000	.005	.010	.015	.020	Doppler factor (s)
0.016425	0.036920	0.084340	0.033978	0.013634	0.158353	0.517358	0.260005	0.026623	0.051906	.90
0.068156	0.048333	0.088636	0.074336	0.064667	0.238378	0.625950	0.072886	0.007856	0.029592	.92
0.099103	0.066306	0.097262	0.118225	0.142817	0.407349	0.631191	0.122699	0.085830	0.048703	.94
0.091157	0.065710	0.087434	0.136003	0.209369	0.646160	0.470450	0.199790	0.149289	0.111550	.96
0.045400	0.034697	0.042673	0.097598	0.197763	0.867577	0.192917	0.133772	0.122158	0.098065	.98
0.019841	0.017987	0.030143	0.000270	0.069473	0.962847	0.068358	0.000202	0.030353	0.017951	1.00
0.077771	0.068592	0.101774	0.118268	0.161043	0.881891	0.215093	0.107630	0.057280	0.068439	1.02
0.106402	0.093036	0.137048	0.196792	0.411399	0.680597	0.234396	0.142725	0.094047	0.108709	1.04
0.097811	0.061395	0.118371	0.187074	0.586887	0.455948	0.176089	0.117788	0.080338	0.095310	1.06
0.060103	0.043300	0.058458	0.085184	0.641334	0.280181	0.101618	0.071216	0.047064	0.058765	1.08

Figure 6.2. Cross-Ambiguity Function of the Waveforms in Figure 6.1.

Light dots denote the signal function
Heavy dots denote the filter function

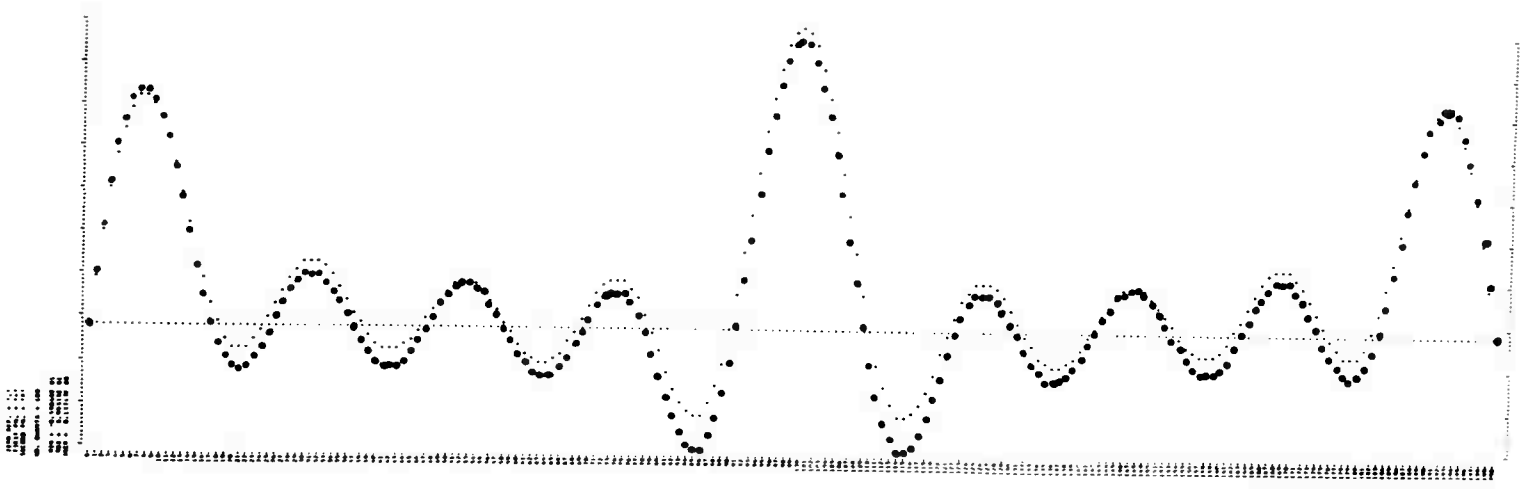

Figure 6.3. Locally Optimum Signal-Filter Pair for Range Resolution.

Delay (tau)

-.025	-.020	-.015	-.010	-.005	0.000	.005	.010	.015	.020	Doppler factor (s)
0.024611	0.050848	0.040993	0.073021	0.068329	0.161752	0.519324	0.270936	0.079375	0.067150	.90
0.039689	0.062588	0.050318	0.078442	0.102640	0.258323	0.623338	0.084980	0.050036	0.055133	.92
0.049258	0.077867	0.071255	0.098794	0.154660	0.425801	0.639766	0.118526	0.056520	0.028300	.94
0.036049	0.074615	0.079857	0.111035	0.200076	0.660763	0.486867	0.197141	0.125215	0.099490	.96
0.003258	0.040593	0.053991	0.081979	0.181516	0.886003	0.207044	0.129543	0.096913	0.091743	.98
0.055415	0.016446	0.006331	0.000238	0.051687	0.985459	0.051269	0.000286	0.006460	0.016484	1.00
0.097898	0.071822	0.074938	0.106596	0.178785	0.897654	0.189951	0.095951	0.073608	0.064724	1.02
0.111115	0.098298	0.114282	0.178331	0.430654	0.693173	0.207471	0.122752	0.101073	0.102756	1.04
0.088843	0.082606	0.100668	0.163964	0.599249	0.477029	0.160196	0.101325	0.083450	0.093419	1.06
0.041529	0.033481	0.041827	0.057074	0.640269	0.313441	0.105608	0.070946	0.053553	0.064762	1.08

Figure 6.4. Cross-Ambiguity Function of the Waveforms in Figure 6.3.

Light dots denote the signal function.
Heavy dots denote the filter function.

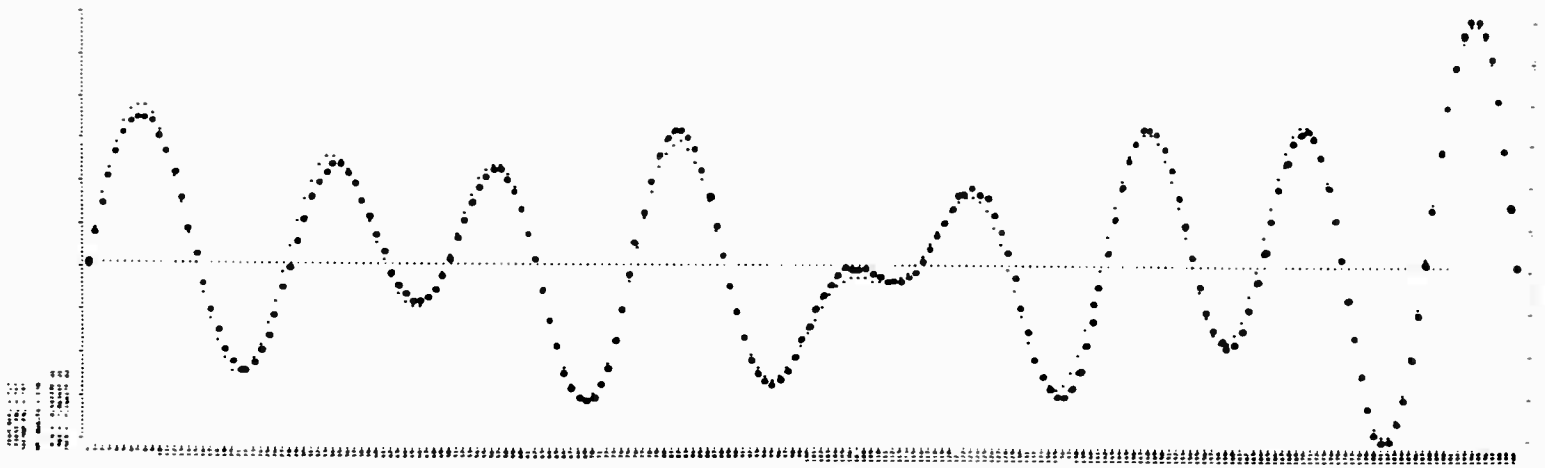

Figure 6.5. Locally Optimum Signal-Filter Pair for Velocity Resolution.

Delay (tau)

-.025	-.020	-.015	-.010	-.005	0.000	.005	.010	.015	.020	Doppler factor (s)
0.013768	0.168442	0.241194	0.027136	0.056806	0.084779	0.018801	0.265937	0.173294	0.090610	.90
0.124798	0.004677	0.164842	0.055692	0.033922	0.110026	0.355114	0.009736	0.122120	0.166298	.92
0.201940	0.184335	0.015047	0.088009	0.094526	0.076736	0.599711	0.429453	0.210209	0.039727	.94
0.171569	0.270166	0.167404	0.284911	0.387303	0.280410	0.426206	0.537195	0.431982	0.258983	.96
0.037074	0.211442	0.175061	0.355878	0.617770	0.758063	0.087702	0.252484	0.333701	0.243462	.98
0.145744	0.039492	0.016899	0.199988	0.562799	0.996274	0.529716	0.147657	0.045272	0.016002	1.00
0.296634	0.148800	0.213234	0.117544	0.197063	0.803455	0.626236	0.360586	0.169579	0.212908	1.02
0.351649	0.248285	0.366992	0.400616	0.265367	0.369615	0.416803	0.305985	0.170211	0.270593	1.04
0.296633	0.208878	0.342378	0.462646	0.525279	0.003237	0.130882	0.117965	0.014920	0.148956	1.06
0.174347	0.065577	0.155684	0.265063	0.462097	0.121113	0.027194	0.016510	0.137457	0.032680	1.08

Figure 6.6. Cross-Ambiguity Function of the Waveforms in Figure 6.5.

Light dots denote the signal function.
Heavy dots denote the filter function.

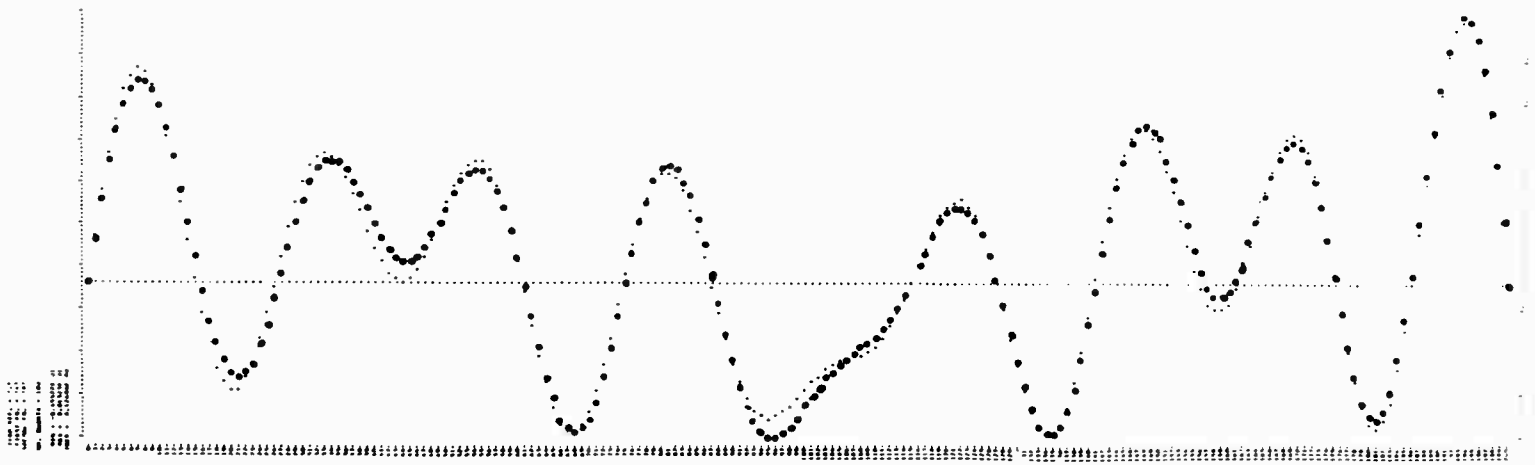

Figure 6.7. Locally Optimum Signal-Filter Pair for Volume Clearance.

Delay (tau)

-.025	-.020	-.015	-.010	-.005	0.000	.005	.010	.015	.020	
0.140203	0.148024	0.249214	0.093693	0.039362	0.194256	0.241975	0.329622	0.100028	0.138187	.90
0.243531	0.010055	0.218331	0.058290	0.003255	0.110495	0.485562	0.093650	0.078064	0.222234	.92
0.285720	0.169045	0.110357	0.127514	0.083185	0.186254	0.644336	0.245653	0.160160	0.102734	.94
0.240666	0.258747	0.012089	0.226882	0.257302	0.473042	0.495814	0.362098	0.341479	0.042936	.96
0.118690	0.245945	0.000463	0.246208	0.371088	0.825110	0.098748	0.192450	0.311273	0.042297	.98
0.035359	0.153246	0.085259	0.128182	0.285156	0.994693	0.254191	0.078042	0.145716	0.094871	1.00
0.163812	0.045468	0.208969	0.077699	0.036193	0.851669	0.369436	0.241430	0.017346	0.226358	1.02
0.223645	0.009375	0.278306	0.241409	0.350198	0.534360	0.268753	0.236391	0.020600	0.231495	1.04
0.207689	0.019123	0.234084	0.245056	0.540093	0.257998	0.103170	0.145194	0.117191	0.103854	1.06
0.146531	0.106117	0.094607	0.072709	0.497251	0.142547	0.008821	0.087220	0.199577	0.069006	1.08

Doppler factor (s)

Figure 6.8. Cross-Ambiguity Function of the Waveforms in Figure 6.7.

Light dots denote the signal function.
Heavy dots denote the filter function.

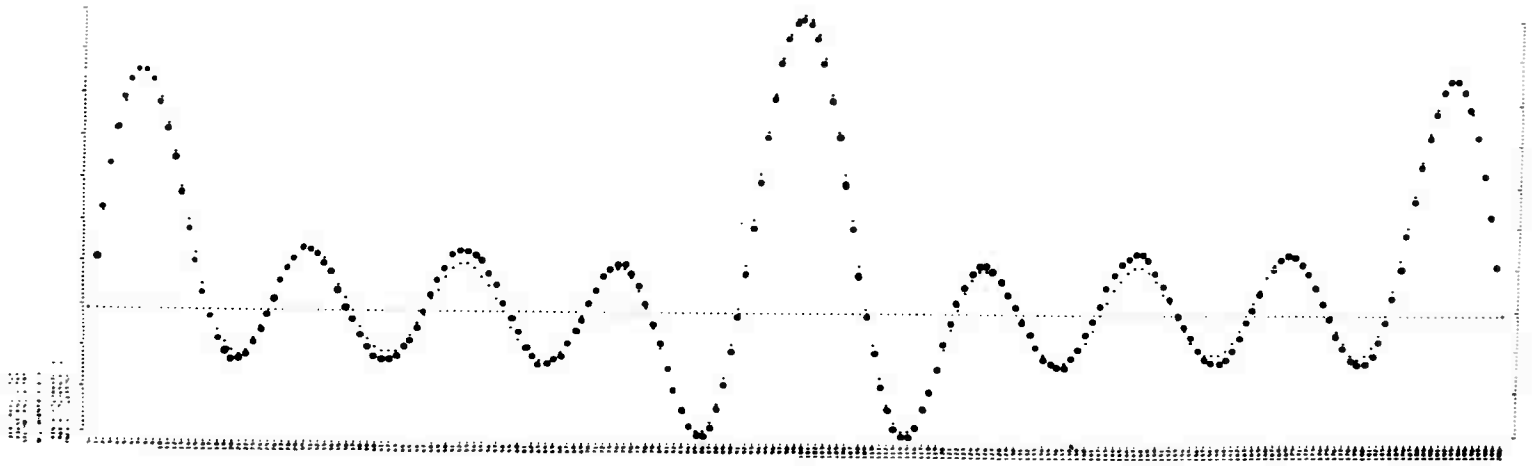

Figure 6.9. Locally Optimum Signal-Filter Pair for Volume Clearance.

Delay (tau)

-.025	-.020	-.015	-.010	-.005	0.000	.005	.010	.015	.020	
0.054982	0.091251	0.054780	0.065026	0.080244	0.121187	0.490228	0.231804	0.101322	0.065881	.90
0.070623	0.105667	0.079314	0.078455	0.121764	0.210056	0.602954	0.031271	0.050531	0.038456	.92
0.072488	0.127973	0.118015	0.115678	0.193707	0.382925	0.618663	0.180834	0.079280	0.071588	.94
0.041438	0.119375	0.136881	0.144662	0.267229	0.638576	0.445350	0.244596	0.151153	0.156263	.96
0.022853	0.066003	0.104269	0.120286	0.271671	0.888306	0.133601	0.141557	0.099710	0.132983	.98
0.100094	0.019366	0.025811	0.024014	0.146956	0.998249	0.146536	0.023940	0.025692	0.019444	1.00
0.159805	0.102456	0.070281	0.111343	0.098553	0.898027	0.283369	0.138227	0.130922	0.101635	1.02
0.176972	0.146479	0.132527	0.214907	0.375117	0.667310	0.278367	0.159991	0.161443	0.162010	1.04
0.144870	0.133261	0.127949	0.222306	0.562340	0.427031	0.201614	0.119337	0.127320	0.151595	1.06
0.078499	0.073370	0.062464	0.121407	0.607473	0.252002	0.123947	0.069197	0.073363	0.105429	1.08

Doppler factor (s)

Figure 6.10. Cross-Ambiguity Function of the Waveforms in Figure 6.9.

Light dots denote the signal function.
Heavy dots denote the filter function.

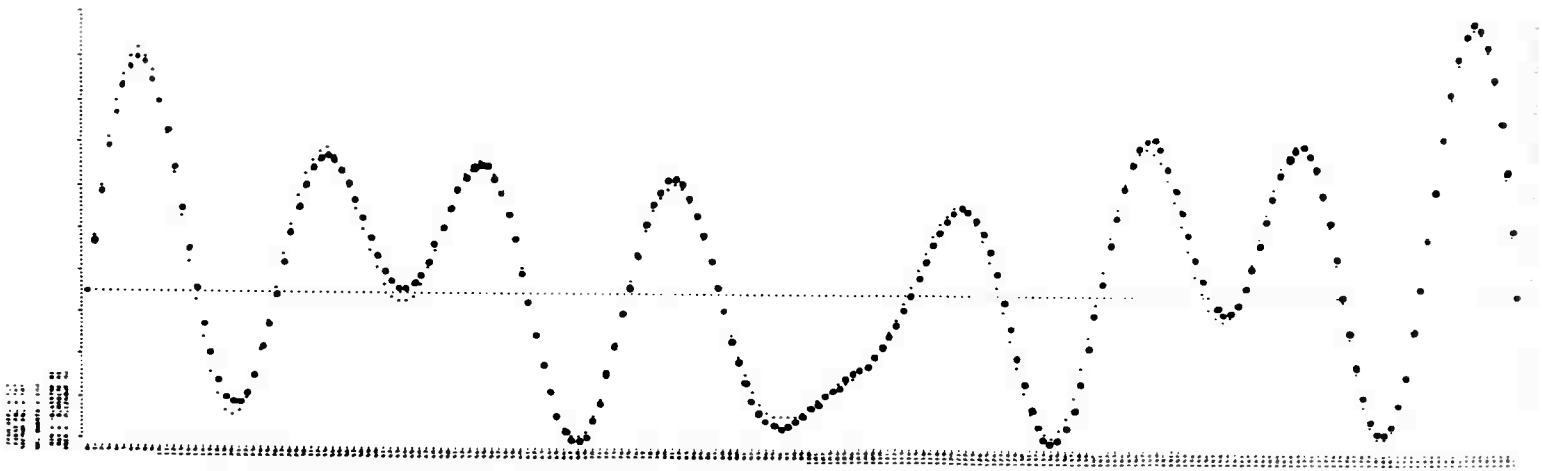

Figure 6.11. Locally Optimum Signal-Filter Pair for Combined Range-Velocity Resolution.

Delay (tau)

-.025	-.020	-.015	-.010	-.005	0.000	.005	.010	.015	.020	Doppler factor (s)
0.100212	0.140315	0.225413	0.105218	0.080106	0.224041	0.184360	0.303658	0.078888	0.083130	.90
0.192499	0.006905	0.190242	0.078084	0.043567	0.140615	0.416902	0.092380	0.083173	0.194492	.92
0.221323	0.144877	0.091440	0.147328	0.133740	0.213762	0.573062	0.232168	0.135541	0.104552	.94
0.168719	0.211504	0.012648	0.235345	0.304151	0.491383	0.435258	0.353944	0.321758	0.037744	.96
0.051393	0.183851	0.020095	0.237758	0.409715	0.832135	0.053539	0.198039	0.312253	0.060563	.98
0.084663	0.091098	0.116379	0.106522	0.318541	0.497654	0.294875	0.070153	0.158700	0.051836	1.00
0.186735	0.002707	0.237327	0.103633	0.028890	0.861059	0.418781	0.249247	0.018857	0.182207	1.02
0.220534	0.036852	0.294741	0.264828	0.310370	0.551300	0.328615	0.266771	0.006063	0.213459	1.04
0.187098	0.009654	0.237369	0.265564	0.500086	0.274270	0.162946	0.188085	0.065310	0.122660	1.06
0.121146	0.105575	0.089757	0.094150	0.463382	0.149808	0.055430	0.124576	0.140850	0.023211	1.08

Figure 6.12. Cross-Ambiguity Function of the Waveforms in Figure 6.11.

Light dots denote the signal function.
Heavy dots denote the filter function.

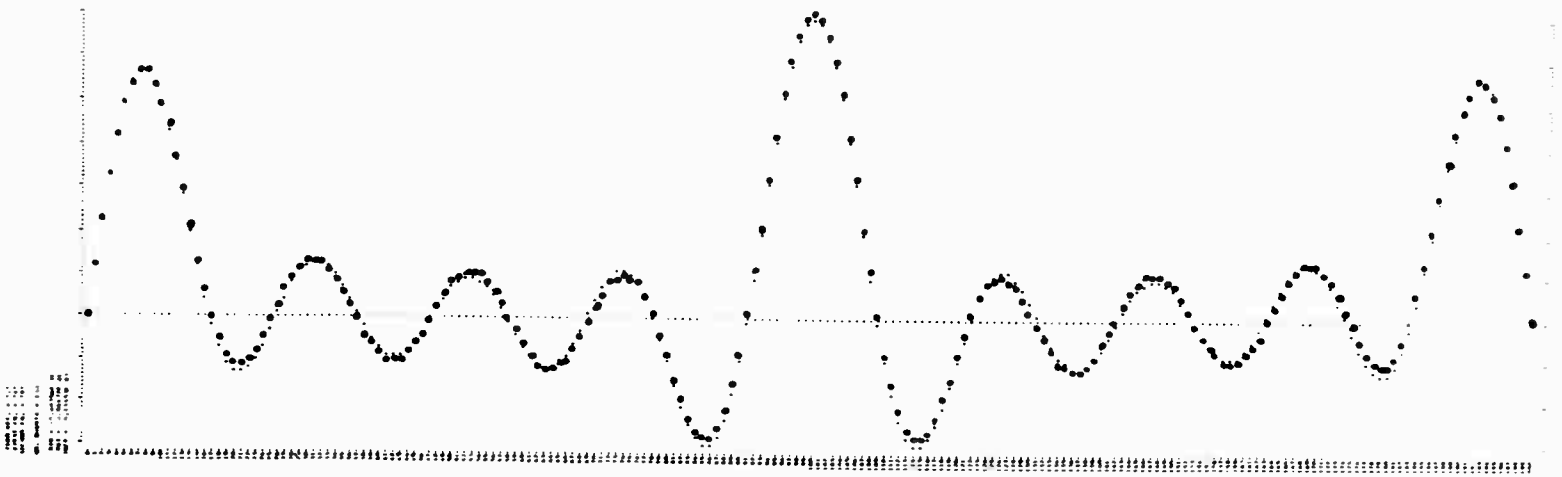

Figure 6.13. Locally Optimum Signal-Filter Pair for Combined Range-Velocity Resolution.

Delay (tau)

-.025	-.020	-.015	-.010	-.005	0.000	.005	.010	.015	.020	Doppler factor (s)
0.038596	0.048735	0.060824	0.076076	0.095407	0.117285	0.505118	0.233657	0.117783	0.071104	.90
0.057281	0.063159	0.071425	0.087281	0.142990	0.213245	0.617610	0.026941	0.070252	0.057284	.92
0.068362	0.080899	0.094252	0.114668	0.214624	0.391866	0.630516	0.192594	0.063032	0.041243	.94
0.051935	0.076236	0.101020	0.130059	0.240919	0.648267	0.454539	0.265071	0.147709	0.126142	.96
0.004898	0.035597	0.066708	0.094418	0.275057	0.894018	0.140896	0.169534	0.115514	0.118683	.98
0.056624	0.031184	0.007820	0.005925	0.142602	0.998839	0.142187	0.006037	0.007931	0.031249	1.00
0.106178	0.094957	0.091194	0.137317	0.104535	0.895792	0.284420	0.114550	0.089111	0.064527	1.02
0.121216	0.124155	0.139303	0.232103	0.377182	0.665055	0.286223	0.149627	0.124650	0.110495	1.04
0.094978	0.103775	0.124297	0.231038	0.558543	0.425592	0.214665	0.124398	0.106059	0.100571	1.06
0.039972	0.044374	0.054534	0.125825	0.599458	0.250034	0.137823	0.085997	0.071302	0.066918	1.08

Figure 6.14. Cross-Ambiguity Function of the Waveforms in Figure 6.13.

Light dots denote the signal function.
Heavy dots denote the filter function.

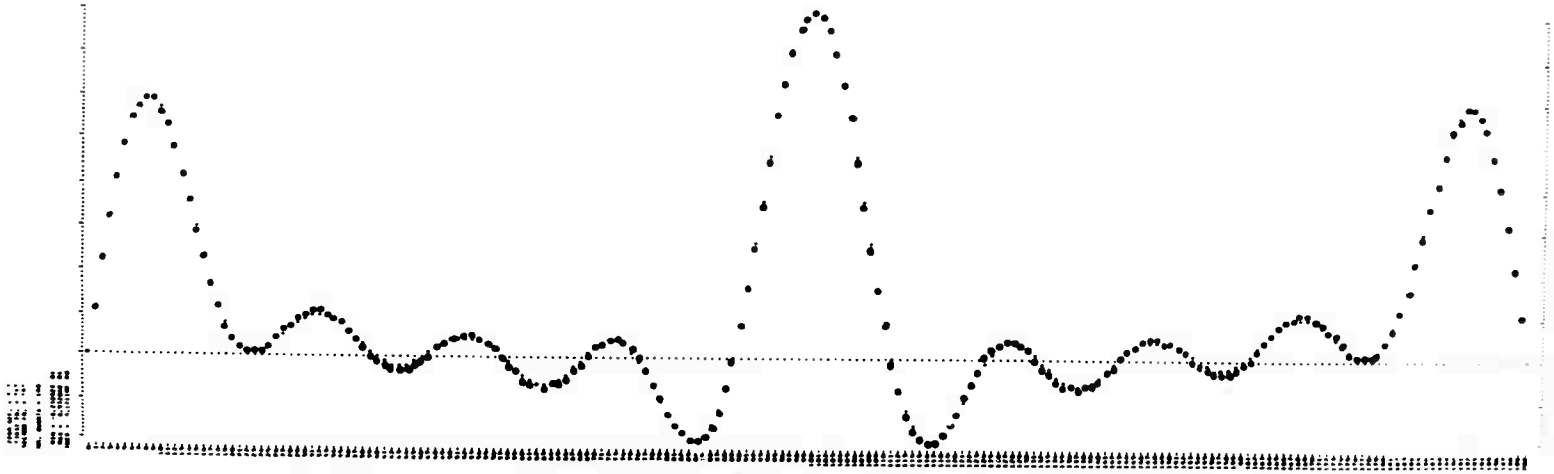

Figure 6.15. Locally Optimum Signal-Filter Pair for Clutter in Opposite Quadrants.

Delay (tau)

-.025	-.020	-.015	-.010	-.005	0.000	.005	.010	.015	.020	
0.012770	0.006391	0.008838	0.033664	0.037242	0.321455	0.667570	0.433365	0.005889	0.016184	.90
0.007544	0.001471	0.001501	0.019836	0.036182	0.440060	0.745825	0.273915	0.050975	0.031505	.92
0.003633	0.004624	0.001224	0.009632	0.025242	0.593535	0.756713	0.081413	0.023953	0.014629	.94
0.011548	0.008094	0.001982	0.001464	0.006549	0.773698	0.646391	0.046471	0.017291	0.010417	.96
0.010511	0.005078	0.003983	0.022456	0.083908	0.932640	0.437712	0.080043	0.030898	0.016989	.98
0.001614	0.004646	0.017431	0.053633	0.223942	0.999831	0.224318	0.053609	0.017499	0.004646	1.00
0.008697	0.014402	0.029667	0.077858	0.412389	0.936763	0.072030	0.015302	0.000717	0.009430	1.02
0.013113	0.015588	0.028314	0.066869	0.597856	0.789648	0.008102	0.009430	0.009183	0.013205	1.04
0.008240	0.004311	0.008163	0.000512	0.715908	0.624191	0.038563	0.020874	0.009576	0.009514	1.06
0.003348	0.015233	0.021929	0.119003	0.742150	0.481183	0.046458	0.028397	0.010562	0.008487	1.08

Doppler factor (s)

Figure 6.16. Cross-Ambiguity Function of the Waveforms in Figure 6.15.

figures referenced in the table depict the best signal and filter found for a given clutter distribution, as well as the associated cross-ambiguity function magnitude, $|\chi_{uv}^{(2)}(\tau,s)|$, sampled at the grid points.

From Table 6.1 and Figures 6.3, 6.9, 6.13 (and 6.15) it is noted that some of the locally optimum waveforms for situations Ia, IIIa, IVa (and to an extent, Va) are nearly identical. The resulting waveforms resemble three pulses, one pulse at the center of the time interval and the other two at the ends. Since the grid only covers a quarter of the possible tau-duration of the autocorrelation function, it is apparent that the end-pulses, which will produce large sidelobes on a more complete map of the ambiguity function, have no effect on the grid region. So for range resolution, volume clearance, and combined range-velocity resolution, it is reasonable to concentrate signal energy near the endpoints of the interval (for the grid as defined above). This effect is also seen (to a less extreme degree) in Figures 6.7 and 6.11.

The comparatively large values of $\alpha_u^{(1)}$ and η^2 associated with clutter distribution II (velocity resolution) are in accord with the origin properties of Chapter III. Large values of η^2 and $\alpha_u^{(1)}$ imply a sharp peak of the ambiguity function at $s = 1$ on the $\tau = 0$ axis.

Relatively large values of λ^2 associated with clutter distribution I (tau resolution) are also to be expected from second derivative properties at the origin.

The choice of basis components was somewhat unfortunate in that, for all situations, $\lambda^2 >> \eta^2$. Therefore the λ^2 -term swamps out η^2 considerations in the determination of average curvature at the origin. It was hoped that average curvature would be accentuated as an important parameter in both volume clearance (III) and combined range-velocity resolution (IV). But because $\lambda^2 >> \eta^2$, the results are generally inconclusive so far as curvature is concerned.

Lincoln remarked that "this is a world of compensation". If the component choice makes $\lambda^2 >> \eta^2$, then perhaps there are situations for which such a choice is advantageous. Clutter distribution V would appear to be just such a case. The two excellent SIR's obtained for V are both characterized by comparatively small values of η^2, $\alpha_u^{(1)}$, and $\alpha_u^{(2)}$. Indeed, the type of ambiguity function encouraged by distribution V would have the ridge or razor blade shape associated with the doppler tolerant bat-like signals derived in Chapter IV. The waveforms of Chapter IV were derived by minimizing η^2. It is to be expected, then, that basis components which make η^2 comparatively small a priori will foster the sort of waveform that gives large SIR's for clutter of type V.

Another strong basis dependence is observed for the tilt parameter, γ. In the only two situations for which component set c gives a comparatively large SIR (clutter pdf II), the associated values of γ are on the order of

half the values that appear in the rest of Table 6.1. That the small value of γ is associated with component set rather than clutter density becomes apparent when one considers the first case for clutter pdf II, where basis b is used and γ is large.

It would seem that SIR maximization with clutter distribution II (velocity resolution) leads to unusually large carrier frequencies. This correspondence may be explained in terms of the narrowband theory of Section 3.11; such an explanation would require that the centralized bandwidth λ^2 be comparatively small (as well as ω_o large). This requirement is indeed satisfied, as shown in Table 6.1.

Also associated with distribution II are exceptionally large values of T_W and D_t^2. It is possible that these parameters are large by virtue of the standard uncertainty relation (Appendix C). On the other hand, the signals are so non-Gaussian in character that there is probably considerable difference between the product $D_t^2 D_\omega^2$ and its lower bound. For the waveforms under consideration, then, it does not necessarily follow that smaller bandwidth implies larger timewidth. The large values of T_W and D_t^2 associated with wideband velocity resolution therefore may imply a property of $|\chi_{uu}^{(2)}|$ that has yet to be derived. A <u>large</u> required value of T_W is especially interesting, since T_W has been associated with range resolution and volume reduction, for which it should generally be made <u>small</u>.

6.9 Clutter Suppression for Distributed Targets.

If a distributed target's impulse response c(t) has been estimated (or is known a priori), it is possible to design a signal which provides a maximum response (of $\chi_{uu}^{(6)}$) to the target echo while minimizing response to spurious point reflectors. If r(t) is the received waveform, then it is here assumed that the processor forms the function

$$|\chi_{uu}^{(6)}(0,1,c_h,c)|^2 = \left|\int \left\{ \int u(x)c_h(t-x)\,dx \right\} r^*(t)\,dt\right|^2. \qquad (6.94)$$

If $r(t) = \int u(y)c_h(t-y)\,dy$, then the correlator response should be large. But if $r(t) = u(t)$, the echo from a spurious point target, then correlator output should be kept small. Notice that the clutter is here considered to be coincident with the target in both range and velocity - an impossible problem for the point target SIR technique.

If $r(t) = \int u(y)c_h(t-y)\,dy$, then

$$|\chi_{uu}^{(6)}(0,1,c_h,c)|^2 = \left|\int \left[\int u(x)c_h(t-x)\,dx\right] \left[\int u(y)c_h(t-y)\,dy\right]^* dt\right|^2$$

$$= \left|\int u(x) \left[\int u(y)R_{c_h}(x-y)\,dy\right]^* dx\right|^2. \qquad (6.95)$$

If $r(t) = u(t)$, then

$$|\chi_{uu}^{(6)}(0,1,c_h,c)|^2 = \left| \int u(x) \left[\int u(y) c_h(t-y)\, dy \right]^* dx \right|^2. \qquad (6.96)$$

The unit energy signal that makes (6.95) large while constraining (6.96) to be zero can be found by using the constrained Schwarz inequality discussed in Section 6.3.3. The solution is:

$$u(t) = k \left[\int u(x) R_{c_h}(t-x)\, dx - \lambda \int u(x) c_h(t-x)\, dx \right]$$

$$= k \left\{ \int u(x) \left[R_{c_h}(t-x) - \lambda c_h(t-x) \right] dx \right\} \qquad (6.97)$$

where the multiplier λ is found by substitution of (6.97) into (6.96) when (6.96) equals zero.

CHAPTER VII.

CONCLUSIONS AND SUGGESTIONS FOR FURTHER STUDY

7.1 Summary of Results.

The foregoing chapters have attempted to extend and generalize radar/sonar signal design to the point where meaningful theoretical solutions can be obtained for many nonideal, but realistic, situations.

The signal: Using a simple constant velocity point target model, previous restrictions upon signal bandwidth and carrier frequency were removed by considering the wideband ambiguity function. If the signal has very short time duration, target trajectory during reflection can be approximated by a straight line. But, by using trajectory diagrams and taking account of acceleration, it became possible to consider signals of comparatively long duration without the necessity of assuming constant velocities. The set of admissible signals for accurate radar-sonar analysis was thus increased considerably, in both permissible bandwidth and time duration.

The target: Target motion was generalized to nonlinear trajectories. This was done by trajectory diagram construction techniques and by Kelly-Wishner theory. Very high velocities can also be dealt with. Finally, the point target idealization was generalized to distributed targets. This was done partly out of necessity, for it would appear that many wideband signals are more sensitive to target configuration than their narrowband counterparts. It was found that, unlike point target reflections, the power and energy

of distributed target echoes are dependent upon the transmitted signal. Implications of this finding for clutter discrimination were examined. It was shown that a priori knowledge of general target shape, when available, can be very useful in the design of efficient radar-sonar systems.

The environment: For narrowband signals and point targets, waveform design for optimal signal to interference ratio in a cluttered environment has already become well established. Here the procedure was generalized to include wideband signals and distributed targets. Implications of the SIR algorithm for two-way wideband communication systems were briefly discussed.

Results of special interest are the properties of the wideband point target ambiguity function (Chapter III), the inscribed diamond construction technique for finding doppler tolerant (and, occasionally, distribution tolerant) waveforms (Chapters IV and V), the derivation of signals very similar to bat cruising pulses as optimally doppler (and acceleration) tolerant waveforms (Chapter IV and V), the distributed target ambiguity function and its maximization by signals that provide maximum returned energy (Chapter V), the derivation of waveforms for distribution tolerance and target description ability (Chapter V), and the SIR method of wideband waveform design for optimal resolution properties (Chapter VI).

7.2 General Conclusions.

When the narrowband assumption is discarded in favor of a more general approach to radar-sonar signal design, the existing theory is affected

in the following ways:

1. A generalized point target ambiguity function must be defined.
2. Targets which once could be represented as point reflectors must now be considered to be distributed in range and velocity. A corresponding ambiguity function must be defined.
3. Narrowband algorithms for clutter suppression must be revamped for wideband analysis.
4. Trajectory diagrams, which do not depend upon bandwidth assumptions, remain applicable.

In this dissertation, contributions have been made to each of the four basic ideas given above. Undoubtedly, further analytical refinements await discovery, making the ideas (and their associated methods) even more potent. The advances that have been made, however, render the four approaches (point target wideband ambiguity function, distributed target ambiguity function, clutter suppression algorithm, and trajectory diagram) applicable to many practical problems.

Whenever the methods overlap, i.e., whenever more than one approach can be applied to the same problem, significant insight has been acquired. The doppler tolerance problem, for example, allowed straightforward application of the point target wideband ambiguity function, the trajectory diagram, and, to a lesser extent, the clutter suppression algorithm. Each of the methods provided insight into the others; the result of each method was consistent with

that of the others. Finally, the less obvious (but important) relevance of the doppler tolerance property to the distributed target ambiguity function was revealed.

A similar overlapping of methods with consequent gain in understanding occurred for the distribution tolerance problem.

The generalized signal design methods were found to reinforce and interpret each other's conclusions, but the final evidence for the utility of a given result often came from nature, in the form of bat signals. Waveform synthesis techniques may thus be used to enhance man's understanding of animal echolocation. Conversely, a knowledge of animal sonar transmissions (and the conditions under which they are used) can shed new light on theoretical methods and results. A fifth approach (of some historical interest [57]) to wideband signal design is thus the study and interpretation of animal sonar signals.*

7.3 Suggestions for Further Study.

There are many opportunities for further study implicit in this dissertation. Among them:

1. Application of the integral transformation between wideband and narrowband ambiguity functions. A great deal is already known about the narrowband ambiguity function. All this

---

* "...in problems of analysis the best method is that which sets out from the results and arrives at the premises." - Bertrand Russell [60].

information should now (theoretically) be available to wideband designers by virtue of the integral transformation in Chapter III. A good start would be a cheap computer algorithm to realize the transformation.

2. The theoretical derivation of more animal echolocation signals. Porpoises, seals, and penguins are possibilities. More experimental data should be converted into the type of pictures taken by J. J. G. McCue and D. A. Cahlander [22]; such beautifully encapsulated representations of animal signals are quite rare, as far as the author can tell. The widespread practice of representing animal sounds via sonagrams may be useful for some applications, but without the more exact plots of period and amplitude versus time, the author might not have realized that some bats use doppler tolerant waveforms.

3. Extension of the SIR algorithm to many grid points and many orthonormal components via the fast Fourier transform. Also needed is a procedure for picking an optimal starting vector to avoid unnecessary iterations and to arrive at a globally maximum SIR. At the very least, one should have a measure of distance between starting vectors from the viewpoint of the algorithm, so that significantly different starting vectors can be tried in attempts to find the best signal-filter pair. Also needed is a measure of the sensitivity of the SIR

to the slight imperfections that will result when a system is actually built.

4. Application of wideband radar theory to two-way communication links. The SIR algorithm, particularly, seems to be a viable method of signal-filter design for two-way multipath channels. An interesting representation of a multipath channel would consist of a stochastically time varying distributed target whose changing interference patterns result in the well-known fading phenomenon.

5. There is a whole class of optimization problems to be solved in connection with high resolution. One should maximize average curvature at the origin or $\eta^2 \lambda^2$ product of the wideband ambiguity function. It is important to find meaningful constraints for this problem, such as the D_t^2 constraint in the doppler tolerance discussion. The SIR results suggest that T_W is an important parameter for both range and velocity resolution. Pulse-train results would be highly relevant.

6. The implications of the narrowtime signal property discussed in Chapter III should be further investigated. Mathematically, the property suggests a dependence upon time origin, a suspicious implication from a physical standpoint. (As evidenced by Equation (3.127), the narrowband ambiguity function is unaffected by a shift of time origin.)

7. The significance of unmatched signal-filter pairs.

Let $v(t) = u(t) - \eta(t)$, where $u(t)$ is the optimal signal and $v(t)$ the optimal filter of an SIR maximization procedure. Correlating both sides with $s^{1/2}\, u\,[s(t+\tau)]$ gives

$$\chi^{(2)}_{vu}(\tau, s) = \chi^{(2)}_{uu}(\tau, s) - \chi^{(2)}_{\eta u}(\tau, s) \quad . \tag{7.1}$$

Conjecture: $\eta(t)$ is such that $\chi^{(2)}_{\eta u}(\tau, s)$ makes $\chi^{(2)}_{vu}(\tau, s)$ small over those regions where $|\chi^{(2)}_{uu}(\tau, s)|$ cannot be small. For a specific set of basis vectors, a study of $\chi^{(2)}_{\eta u}(\tau, s)$ for various $\eta(t)$'s and clutter distributions may therefore reveal pairs of points (τ_1, s_1), (τ_2, s_2) such that $\chi^{(2)}_{uu}(\tau_1, s_1)$ and $\chi^{(2)}_{uu}(\tau_2, s_2)$ cannot simultaneously be made small. This concept, if sufficiently generalized, could lead to a wideband version of Woodward's narrowband volume invariance. That is, one could have reciprocal areas on the ambiguity plane such that, if the ambiguity height over one given area is small, then the height over another area must be large; "pushing down" the ambiguity function in one particular place may result in its "popping up" somewhere else. From the SIR results (especially for clutter distribution V, Section 6.8) one may conject that such reciprocal areas (if they exist) are frequently to be found in adjacent quadrants of the (τ, s) plane.

8. New correlator implementations.

a. The Oppenheim filter

For s = 1, equation (5.40) may be written:

$$R_{u*v,u*v}(\tau) = R_{uu}(\tau) * R_{vv}(\tau) \ . \qquad (7.2)$$

Another property of the autocorrelation function $R_{uu}(\tau)$ is that if c is a scalar constant, then

$$c\ u(ct) \Rightarrow c\ R_{uu}(c\ \tau) \qquad (7.3)$$

since

$$\int c\ u(ct)\ c\ u^*\left[c\,(t+\tau)\right] dt = c\ R_{uu}(c\,\tau) \ .$$

Equation (7.2 may be written in the more general form:

$$\phi\left[u(t)\ o\ v(t)\right] = \phi\left[u(t)\right]\ o\ \phi\left[v(t)\right] \qquad (7.4)$$

where the transformation ϕ corresponds to autocorrelation and the operation "o" is convolution.

If the transformation c u(ct) is described by the symbol ":", i.e.,

$$c{:}u(t) = cu(ct) \qquad (7.5)$$

then by (7.3),

$$\phi\left[c{:}u(t)\right] = c{:}\,\phi\left[u(t)\right] \ . \qquad (7.6)$$

A. V. Oppenheim has pointed out that if the general equations (7.4) and (7.6) hold true, then the operation ϕ may be interpreted as an algebraically linear transformation between vector spaces [58]. The autocorrelation transformation is then a form of generalized linear filtering (as one would suspect from its matched-filter implementation). But according to Oppenheim, a transformation ϕ that satisfies (7.4) and (7.6) can be implemented as a cascade of three systems (see [58] for details). This idea suggests the possibility that a new type of correlation receiver can be built. The implementation should be studied in detail.

b. Phase-locked oscillator for simulation of the doppler effect.

If a matched filter receiver is not used, one must simulate hypothetical (time-scaled) versions of the received signal for correlation processing. There are two well known methods for time scaling a waveform: (1) A time delay that varies linearly with time (as suggested by the trajectory diagram, which is a representation of the effects of a time variable delay) and (2) optical systems which translate time to spatial coordinates (as conceived in Section 4.2 of this dissertation or by Papoulis [36], p. 203 et seq).

A third process for synthesizing doppler compressed versions of a transmitted waveform is particularly applicable to the two signal types discussed in Chapter V (Table 5.1). This method multiplies or divides instantaneous frequency by using a phase-locked loop (Figure 7.1).

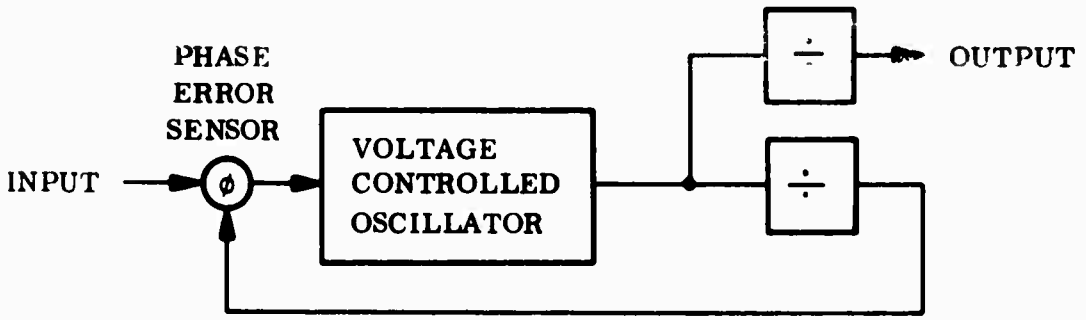

Figure 7.1. Phase-Locked Loop.

For an instantaneous period that varies in any of the ways shown in Figure 7.2, frequency multiplication (or division) using the phase-locked oscillator (or just a frequency divider) will produce an output signal that correlates strongly with a doppler scaled version of the original (constant amplitude) waveform.

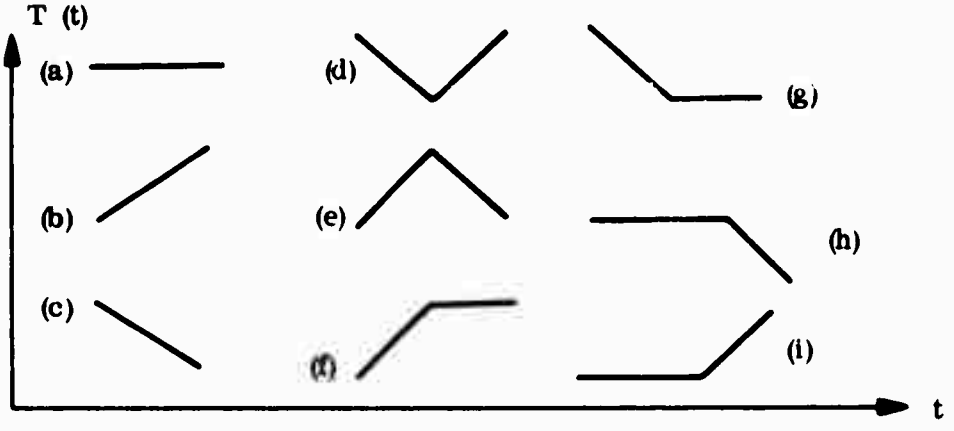

Figure 7.2. Instantaneous Period Modulations for Detection with Phase-Locked Loop.

It remains to be seen whether the phase-locked loop process can be applied to the time scaling of a more general class of signals.

9. Clutter as distributed target:

It was remarked in Chapter VI that the uncorrelated-point-target model of clutter may be somewhat unrealistic. It would seem to this author that for some situations one might do well to model clutter as a distributed target with some stochastic parameters. The surface of the sea on a windy day, for example, may be regarded as a random distribution of moving uncorrelated point scatterers. But the eye is quick to pick out a pattern of waves and troughs moving in a comparatively non-random fashion. Hence the ocean surface may sometimes be viewed as a moving distributed target (or, rather, clutter). Such a thought should no longer seem analytically intractable in view of the ideas of Chapter V.

A given environment might then consist of some deterministic distributed clutter configurations, combined with a group of uncorrelated point targets. The problem is still the same: Maximize the response of the receiver to the target echo while keeping the response to clutter and noise as small as possible.

In this situation it is possible to eliminate some of the clutter response before it ever reaches the correlator. This is because the clutter-as-distributed-target gives rise to an echo whose possible components are known a priori.

If $q_i(t)$ are the impulse responses of the various possible deterministic distributed clutter arrays present in an environment, then the echo from the target's surroundings is partially given as

$$r_q(t) = \sum_i p_i \sigma_i \int u(x)\, q_i(t-x)dx \qquad (6.94)$$

where σ_i is a function of the relative strength or cross-section of each environmental component. p_i is a likelihood factor ($\sum_i p_i = 1$) indicating the existence of a priori knowledge concerning the probability that a given q_i is really present. (In sonar, for example, a strong, constant wind at k knots might overwhelmingly favor the clutter configuration with impulse response $q_k(t)$). For radar, the time of day correlates with some ionospheric effects in a known fashion. Such factors would then be used to determine the a priori probabilities of the different possible deterministic components of clutter response.)

The basic idea is to set up a predetector which is much the same as a standard M-ary detection scheme [2]. This

predetector would test for the presence and strength of various possible clutter distributions. Having detected the presence and estimated the strength of the clutter distributions, the detector would then generate a signal composed of these same distribution responses, weighted according to their strengths. This signal would be subtracted from the (delayed) incoming signal. The result should approximate the target response (if present) added to white noise and the response from uncorrelated point targets. The SIR algorithm would then be used to design an appropriate correlating filter. A diagram of this scheme is shown in Figure 7.3.

In Figure 7.3, the input is correlated with possible clutter returns via matched filtering through systems with impulse responses $r_i(-t)$. After squaring, threshold detectors indicate whether a particular $r_i(t)$ is indeed present. (As in ordinary M-ary detection, the i^{th} threshold is a function of p_i, the a priori probability of receiving $r_i(t)$.) Once it is decided that a clutter return is present, its strength is indicated by how much it exceeds the threshold. A pulse of the proper strength is then generated, and this pulse causes an output $r_i(t)$ from another linear filter. The sum of the clutter returns $\sum_i r_i(t)$ is then subtracted from the delayed input. The resulting signal is, ideally, free of all interference save that of uncorrelated noise

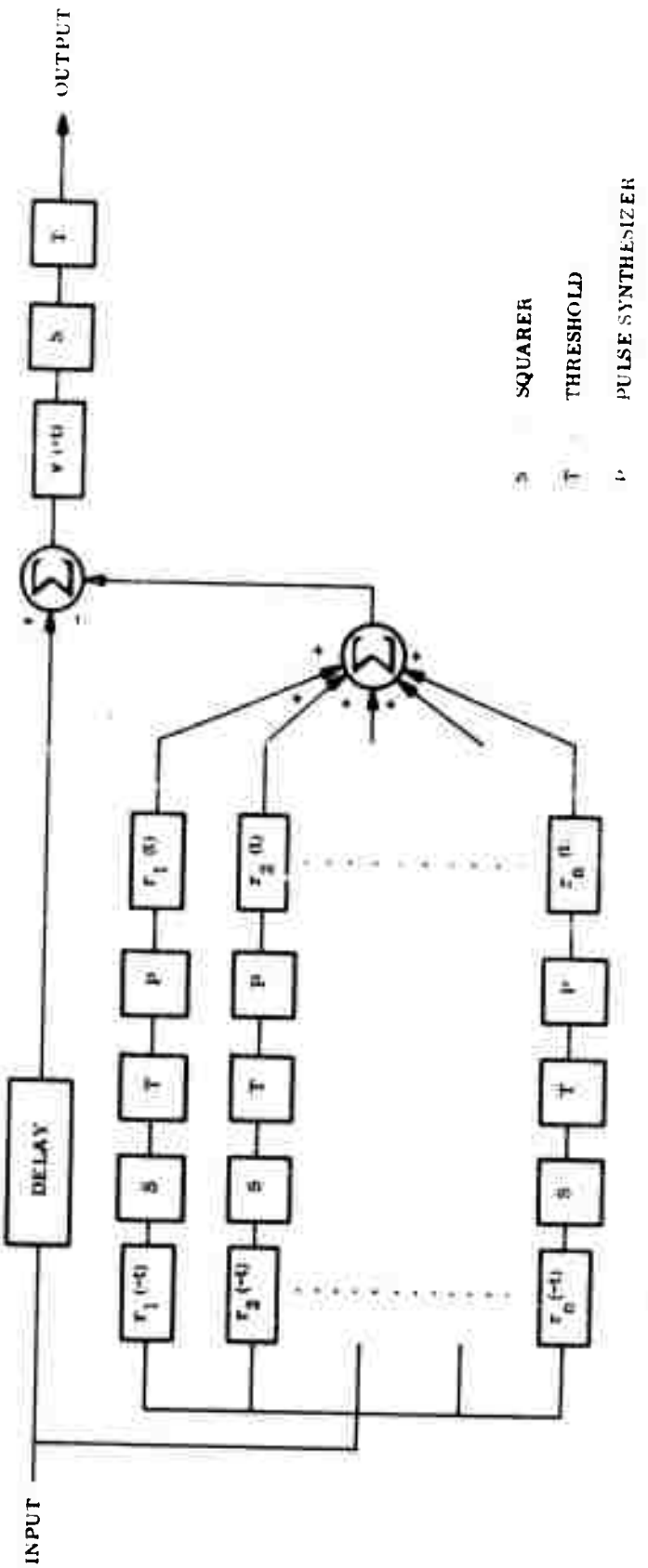

Figure 7.3. Clutter Suppression Scheme when Some Components of Clutter Response are Predictable.

and uncorrelated point target clutter. The final matched filter v(t) is designed to maximize the conventionally defined SIR.

It is interesting to compare Figure 7.3 with a detector that discriminates against colored noise, illustrated in Figure 4.39 of Van Trees' book [2].

10. Optimal control formulation.

The Rhinolophus signals discussed in Section 5.7 have some interesting implications for radar-sonar system design. Suppose that two or more different signals are transmitted in tandem, one immediately following the other, and that the processor consists of matched filters for each of the transmitted signals. For a given total energy (and time duration) the energy weighting (or time sharing) of each signal will be dictated by a cost function which seeks to optimize the acquisition of certain information. The problem can thus be formulated in terms of optimal control theory. Indeed, a frequent result of optimal control theory is the "bang-bang" solution, which in this case would cause all the energy (or transmission time) to be given to one waveform. In other words, the bang-bang solution is the usual transmission of a single waveform. However, other more uniform energy (or time) weightings may be optimal under certain conditions.

11. An immediate application of distribution describing signals.

The theory of Chapter V would seem to be of some use for the ultrasonic identification of objects by blind people. A device that uses ultrasonic sonar transmissions to aid the blind is already in existence [61]. L. Kay, inventor of the device (which he calls "ultrasonic spectacles"), made the following statement in 1966:

"The step which has yet to be taken to produce the true ultrasonic localization may be technically difficult, but the result is not so difficult to visualize...Each object should appear to make characteristic sounds which can be recognized. Since it will be unlikely for two objects to produce exactly the same sound at any one time, the observer should then be able to distinguish one from the other and therefore appreciate their relative positions. In a cluttered environment it is still difficult to accept the possibility of being able to appreciate sufficient detail from which to reconstruct the spatial pattern. The behavior of the bat suggests that it can do this using a similar sensing process. It must, for example, require more than simple object detection when catching insects among foliage." [62]

BIBLIOGRAPHY

1. P. M. Woodward, Probability and Information Theory with Applications to Radar, Oxford: Pergamon, 2nd ed., 1964.

2. H. L. Van Trees, Detection, Estimation, and Modulation Theory, Part I, New York: Wiley, 1968.

3. G. L. Turin, "An Introduction to Matched Filters," IRE Trans., v. IT-6 (1960), pp. 311-329.

4. C. E. Cook and M. Bernfeld, Radar Signals, New York: Academic Press, 1967.

5. E. J. Kelly and R. P. Wishner, "Matched-Filter Theory for High-Velocity, Accelerating Targets," IEEE Trans., v. MIL-9 (1965), pp. 56-69.

6. A. W. Rihaczek, Principles of High-Resolution Radar, New York: McGraw-Hill, 1969.

7. R. L. Gassner and G. R. Cooper, "Note on a Generalized Ambiguity Function," IEEE Trans., v. IT-13 (1967), p. 126.

8. D. A. Swick, "A Review of Wideband Ambiguity Functions," Naval Research Laboratory Report 6994 (Dec. 30, 1969).

9. J. M. Speiser, "Wideband Ambiguity Functions," IEEE Trans., v. IT-13 (1967), pp. 122-123.

10. D. Gabor, "Theory of Communications," J. IEE (London), v. 93 (1946), pp. 429-457.

11. A. B. Carlson, Communication Systems, New York; McGraw-Hill, 1968, pp. 104-110.

12. C. H. Wilcox, "The Synthesis Problem for Radar Ambiguity Functions," U.S. Army Math. Res. Cntr., Univ. of Wisconsin, Tech. Rept. No. 157, April, 1960.

13. E. F. Beckenbach and R. Bellman, Inequalities, Berlin: Springer-Verlag, 1965, p. 45.

14. E. L. Titlebaum and N. DeClaris, "A Signal Design Philosophy for High Resolution Radar," IEEE International Convention Record, 1966.

15. E. C. Titchmarsh, The Theory of Functions, London: Oxford Univ. Press, 2nd ed., 1939, p. 433.

16. E. F. Beckenbach and R. Bellman, op. cit. (Ref. 13), p. 167 (beware of misprints).

17. B. v. Sz.-Nagy, "Über Integralungleichungen zwischen einer Funktion und ihrer Ableitung," Acta Sci. Math., Szeged, v. 10 (1940-43), pp. 64-74.

18. W. M. Siebert, "Studies of Woodward's Uncertainty Function," Quart. Progress Rept., MIT, Cambridge, Mass., April 1958, pp. 90-94

19. E. L. Titlebaum, "Transformations for Radar Ambiguity Functions," Cornell Univ. EE Res. Lab. Rept. EERL 28 (1964).

20. J. M. Speiser, "Ambiguity Functions and Continuous Groups," presented at the 1969 IEEE Internat'l Symp. on Info. Theory, Ellenville, N.Y.

21. J. M. Speiser, op. cit. (Ref. 9).

22. D. A. Cahlander, "Echolocation with Wide-band Waveforms: Bat Sonar Signals," MIT Lincoln Lab Tech Rept. 271 (1964), Clearinghouse for Fed. Sci. and Tech. Info. no. AD 605322.

23. R. Courant and D. Hilbert, Methods of Mathematical Physics, v. I, New York: Interscience (1953).

24. I. M. Gelfand and S. V. Fomin, Calculus of Variations, Englewood Cliffs, N. J.: Prentice-Hall (1963), Chap. 1, pp. 14-15, Chap. 5, pp. 101-105.

25. E. L. Titlebaum, "Optimization Methods for Signal Design and Processing," Supplement to IEEE AES Trans., v. AES-3, no. 6 (1967), pp. 543-551.

26. E. Jahnke and F. Emde, Tables of Functions with Formulas and Curves, New York: Dover, 8th ed., 1945.

27. A. Erdelyi, et al, Tables of Integral Transforms, Vol. 2, New York: McGraw-Hill, 1954, Chap 19, pp. 333-364.

28. T. M. Apostol, Mathematical Analysis, Reading, Mass: Addison-Wesley, 1960, p. 96.

29. A. Papoulis, The Fourier Integral and its Applications, New York: McGraw-Hill, 1962, pp. 73, 74.

30. J. H. H. Chalk, "The Optimum Pulse-Shape for Pulse Communication," Proc. IEE (London), v. 97, Radio Section, (1950), pp. 88-92.

31. J. Irving and N. Mullineux, Mathematics in Physics and Engineering, New York: Academic Press (1959), pp. 760-767.

32. F. Smithies, Integral Equations, Cambridge: Cambridge Univ. Press, 1965.

33. D. R. Griffin, "Discriminative Echolocation by Bats," Animal Sonar Systems, R.-G. Busnel, ed., Jouy-en-Josas, France: Laboratoire de Physiologic Acoustique, 1966, vol I, pp. 273-300.

34. C. M. Johnson, "Ballistic Missile Defense Radars," IEEE Spectrum, v. 7, no. 3 (1970), pp. 32-41.

35. V. V. Ol'shevskii, Characteristics of Sea Reverberation, New York: Consultants Bureau, 1967.

36. A. Papoulis, Systems and Transforms with Applications in Optics, New York: McGraw-Hill, 1968, pp. 185-189.

37. A. J. F. Siegert, "Properties of Radar Targets," Radar System Engineering, L. N. Ridenour, ed., New York: Dover, 1965, Sec., 3.3, pp. 64, 65.

38. L. J. Spafford, "Optimum Radar Signal Processing in Clutter," Ph.D. dissertation, Polytech. Inst. Brooklyn, N. Y., June 1967.

39. C. A. Stutt, "A 'Best' Mismatched Filter Response for Radar Clutter Discrimination," G. E. Research and Dev't Center, Schenectady, N.Y., Rept. 66-C-020. March, 1966.

40. C. A. Stutt and L. J. Spafford, "A 'Best' Mismatched Filter Response for Radar Clutter Discrimination," IEEE Trans., v. IT-14, no. 2 (1968), pp. 280-287.

41. W. D. Rummler, "Clutter Suppression by Complex Weighting of Coherent Pulse Trains," IEEE Trans., v. AES-2, no. 6 (1966), pp. 689-699.

42. D. F. DeLong, Jr. and E. M. Hofstetter, "On the Design of Optimum Radar Waveforms for Clutter Rejection," IEEE Trans., v. IT-13 (1967), pp. 454-463.

43. D. F. DeLong, Jr. and E. M. Hofstetter, "The Design of Clutter-Resistant Radar Waveforms with Limited Dynamic Range," IEEE Trans., v. IT-15 (1969), pp. 376-385.

44. C. W. Helstrom, Statistical Theory of Signal Detection, New York: Pergamon, 1960, pp. 50, 55.

45. R. J. Urick, Principles of Underwater Sound for Engineers, New York: McGraw-Hill, 1967.

46. J. S. Thompson, "Radar Signal Design Using the Ambiguity Function," Ph.D. dissertation, Univ. of Rochester, Rochester, N.Y., 1967.

47. R. de Buda, "Signals that can be Calculated from their Ambiguity Function," IEEE Trans., v. IT-16, no. 2 (1970), pp. 195-202.

48. J. C. Holtzman and J. S. Thorpe, "Optimum Signals for Radar," IEEE Trans., v. AES-5, no. 6 (1969), pp. 898-905.

49. C. E. Shannon and W. Weaver, The Mathematical Theory of Communication, Urbana, Ill.: Univ. of Illinois Press, 1964.

50. H. -U. Schnitzler, "Discrimination of Thin Wires by Flying Horseshoe Bats (Rhinolophidae)," Animal Sonar Systems, R.-G. Busnel, ed., Jouy-en-Josas, France: Laboratoire de Physiologie Acoustique, 1966, Vol. I, pp. 69-87.

51. W. M. Brown and L. J. Porcello, "An Introduction to Synthetic-Aperture Radar," IEEE Spectrum, v. 6, no. 9 (1969), pp. 52-62.

52. J. J. Kroszczynski, "Pulse Compression by Means of Linear-Period Modulation," Proc. IEEE, v. 57, no. 7 (1969), pp. 1260-1266.

53. S. A. Kramer, "Doppler and Acceleration Tolerances of High-Gain, Wideband Linear FM Correlation Sonars," Proc. IEEE, v. 55, no. 5 (1967), pp. 627-636.

54. J. J. G. McCue, MIT Lincoln Laboratory, private correspondence.

55. G. A. Bliss, Lectures on the Calculus of Variations, Chicago: Univ. of Chicago Press, Phoenix edition, 1946.

56. D. Gabor, "Theory of Communications,"

57. H. Maxim, "The Sixth Sense of the Bat. Sir Hiram's Contention. The Possible Prevention of Sea Collisions.", Scientific Amer. Suppl., September 7, 1912, pp. 148-150.

58. A. V. Oppenheim, R. W. Schafer, and T. G. Stockham, "Nonlinear Filtering of Multiplied and Convolved Signals," Proc. IEEE, v. 56, no. 8 (1968), pp. 1264-1291.

59 J. W. Cooley, P. A. W. Lewis, P. D. Welch, "The Fast Fourier Transform and its Applications," IEEE Trans. on Education, v. 12, no. 1 (1969), pp. 27-34.

60. B. Russell, "Philosophical Importance of Mathematical Logic," Monist, v. 22, no. 4 (1913), pp. 481-493.

61. D. C. MacFarland, Chief, Division for the Blind and Visually Handicapped, U.S. Department of Health, Education, and Welfare, private communication (June 29, 1970).

62. L. Kay, "Enhanced Environmental Sensing by Ultrasonic Waves," Animal Sonar Systems, R.-G. Busuel, ed, Jony-en-Josas, France: Laboratoire de Physiologie Acoustigue, 1966, vol. II, pp. 757-781.

APPENDIX A.

ORIGIN PROPERTIES

Consider a two-dimensional Taylor series expansion of $|\chi_{uu}^{(2)}(\tau,s)|^2$ around the point $s = 1$, $\tau = 0$:

$$|\chi_{uu}^{(2)}(\tau,s)|^2 = |\chi_{uu}^{(2)}(0,1)|^2 + \left[\tau \left.\frac{\partial|\chi|^2}{\partial\tau}\right|_{0,1} + (s-1)\left.\frac{\partial|\chi|^2}{\partial s}\right|_{0,1}\right]$$

$$+ 1/2\left[\tau^2 \left.\frac{\partial^2|\chi|^2}{\partial\tau^2}\right|_{0,1} + 2\tau(s-1)\left.\frac{\partial^2|\chi|^2}{\partial\tau\partial s}\right|_{0,1}\right.$$

$$\left. + (s-1)^2 \left.\frac{\partial^2|\chi|^2}{\partial s^2}\right|_{0,1}\right]$$

$$+ \text{higher order terms}. \qquad (A-1)$$

With $\int_{-\infty}^{\infty} u(t)u^*(t)dt \equiv 1$ and $\chi_{uu}^{(2)}$ defined as in (2.8), one has

$$|\chi_{uu}^{(2)}(0,1)|^2 = 1 \text{ and}$$

$$\left.\frac{\partial|\chi|^2}{\partial\tau}\right|_{0,1} = \int u(t)u^{*\prime}(t)dt + \int u^*(t)u^{\prime}(t)dt \quad . \qquad (A-2)$$

In this and subsequent equations, unspecified limits of integration are taken as $(-\infty, \infty)$. Primes denote differentiation of a function with respect to its argument. Assuming $|u(t)|^2\Big|_{-\infty}^{\infty} = 0$ and integrating by parts:

$$\left.\frac{\partial |\chi_{uu}^{(2)}|^2}{\partial \tau}\right|_{0,1} = 0. \tag{A-3}$$

$$\left.\frac{\partial |\chi|^2}{\partial s}\right|_{0,1} = 1 + 2\mathrm{Re}\left\{\int tu(t)u^{*\prime}(t)\,dt\right\}.$$

Assuming $t|u(t)|^2\Big|_{-\infty}^{\infty} = 0$ and integrating by parts:

$$\left.\frac{\partial |\chi|^2}{\partial s}\right|_{0,1} = 0. \tag{A-4}$$

$$\left.\frac{\partial^2 |\chi|^2}{\partial \tau^2}\right|_{0,1} = 2\,\mathrm{Re}\left\{\int u(t)u^{*\prime\prime}(t)\,dt\right\} + 2\left|\int u(t)u^{*\prime}(t)\,dt\right|^2$$

Assuming that $u^{*\prime}u\Big|_{-\infty}^{\infty} = 0$ and integrating the first term by parts:

$$\left.\frac{\partial^2 |\chi|^2}{\partial \tau^2}\right|_{0,1} = -2\left\{\int |u^{\prime}(t)|^2 dt - \left|\int u(t)u^{*\prime}(t)\,dt\right|^2\right\}. \tag{A-5a}$$

By invoking Parseval's theorem, this equation may be rewritten in terms of $U(\omega)$, the Fourier transform of u(t):

$$\left.\frac{\partial^2 |\chi|^2}{\partial \tau^2}\right|_{0,1} = -2 \left\{(1/2\pi) \int \omega^2 |U(\omega)|^2 d\omega - \left[(1/2\pi) \int \omega |U(\omega)|^2 d\omega\right]^2 \right\}. \qquad \text{(A-5b)}$$

Making the definitions:

$$(1/2\pi) \int \omega^2 |U(\omega)|^2 d\omega = D_\omega^2 = \text{mean square bandwidth [10]}$$

$$(1/2\pi) \int \omega |U(\omega)|^2 d\omega = \omega_o = \text{carrier frequency [11,12]}$$

(A-5b) becomes

$$\left.\frac{\partial^2 |\chi|^2}{\partial \tau^2}\right|_{0,1} = -2 \left\{D_\omega^2 - \omega_o^2\right\} \qquad \text{(A-5c)}$$

Notice that the definition of carrier frequency only makes sense for analytic signals. If u(t) were considered to be strictly real, it would follow that $U(\omega) = U^*(-\omega)$, and ω_o would be zero by definition. On the other hand, if u(t) is complex and if the real and imaginary parts of u(t) are Hilbert transforms of each other, then $U(\omega) = 0$ for $\omega < 0$ [10,11] and ω_o is the centroid of the resulting one-sided spectrum. It is therefore assumed that $u(t) = a(t)\exp[j\theta(t)]$, where

$$a(t)\cos\theta(t) = H\left[a(t)\sin\theta(t)\right] , \tag{A-6}$$

the H denoting Hilbert transformation.

Returning to the evaluation of derivatives,

$$\left.\frac{\partial^2|\chi|^2}{\partial s^2}\right|_{0,1} = 4\,\mathrm{Re}\left\{\int tu(t)u^{*\prime}(t)\,dt\right\} + 2\,\mathrm{Re}\left\{\int t^2u(t)u^{*\prime\prime}(t)dt\right\}$$

$$+ 2\left|\int tu(t)u^{*\prime}(t)dt\right|^2 .$$

It has already been established (in connection with equation 3.8) that $\mathrm{Re}\left\{\int tu(t)u^{*\prime}(t)dt\right\} = -1/2$. Assuming that $t^2u(t)u^{*\prime}(t)\Big|_{-\infty}^{\infty} = 0$ and integrating by parts gives

$$\mathrm{Re}\left\{\int t^2u(t)u^{*\prime\prime}(t)dt\right\} = 1 - \int t^2|u'(t)|^2dt .$$

Therefore

$$\left.\frac{\partial^2|\chi|^2}{\partial s^2}\right|_{0,1} = -2\left\{\int t^2|u'(t)|^2dt - \left|\int tu(t)u^{*\prime}(t)\,dt\right|^2\right\} . \tag{A-7a}$$

Again using Parseval's theorem:

$$\left.\frac{\partial^2|\chi|^2}{\partial s^2}\right|_{0,1} = -2\left\{(1/2\pi)\int \omega^2|U'(\omega)|^2 d\omega - \left|(1/2\pi)\int \omega U(\omega)U^{*\prime}(\omega)d\omega\right|^2\right\}. \tag{A-7b}$$

Finally,

$$\left.\frac{\partial^2|\chi|^2}{\partial s\,\partial \tau}\right|_{0,1} = 2\,\mathrm{Re}\left\{\int tu(t)u^{*\prime\prime}(t)dt\right\} + 2\,\mathrm{Re}\left\{\int u^*(t)u'(t)dt\cdot\int tu(t)u^{*\prime}(t)dt\right\}.$$

Integrating the first term by parts gives:

$$\left.\frac{\partial^2|\chi|^2}{\partial s\,\partial \tau}\right|_{0,1} = -2\left[\int t|u'(t)|^2 dt - \mathrm{Re}\left\{\int u'(t)u^*(t)\,dt\int tu(t)u^{*\prime}(t)\,dt\right\}\right]. \tag{A-8a}$$

Using Parseval's theorem:

$$\left.\frac{\partial^2|\chi|^2}{\partial s\,\partial \tau}\right|_{0,1} = -2\left[\mathrm{Im}\left\{(1/2\pi)\int \omega^2 U(\omega)U^{*\prime}(\omega)d\omega\right\} - (1/2\pi)\int\omega|U(\omega)|^2 d\omega \cdot \mathrm{Im}\left\{(1/2\pi)\int \omega U'(\omega)U^*(\omega)\,d\omega\right\}\right]. \tag{A-8b}$$

It can be shown that exactly the same derivatives are obtained for $\chi^{(3)}_{uu}(\tau, s)$.

APPENDIX B.

AN INEQUALITY OF B.v.SZ.-NAGY [16,17]

Let y(t) be a function defined over $(-\infty,\infty)$, for which the integrals

$$J_a = \int_{-\infty}^{\infty} |y|^a dt, \quad K_p = \int_{-\infty}^{\infty} \left|\frac{d}{dt} y(t)\right|^p dt \tag{B-1}$$

exist for some $a > 0$ and some $p \geq 1$. Then

$$\max_{-\infty < t < \infty} |y| \leq (r/2)^{1/r} J_a^{(p-1)/pr} K_p^{1/pr} \tag{B-2}$$

where $r = 1 + a(p-1)/p$; further, for $b > 0$,

$$J_{a+b} \leq \left[\frac{r}{2} H\left(\frac{r}{b}, \frac{p-1}{p}\right)\right]^{b/r} J_a^{1+b(p-1)/pr} K_p^{b/pr} \tag{B-3}$$

where

$$H(u,v) = \frac{(u+v)^{-(u+v)} \Gamma(1+u+v)}{u^{-u} \Gamma(1+u)\, v^{-v} \Gamma(1+v)}, \quad H(u,0) = H(0,v) = 1. \tag{B-4}$$

The inequalities are proven by using Holder's inequality.

The relation (B-2) becomes an equality when $y(t) = cy_{pa}(|dt+e|)$, where c,d,e are arbitrary constants ($d \neq 0$) and

$$\text{for } a < p: \quad y_{pa}(t) = \begin{cases} (1-t)^{p/(p-a)} & \text{for } 0 \le t \le 1 \\ 0 & \text{for } t > 1 \end{cases}$$

$$\text{for } a = p: \quad y_{pa}(t) = e^{-t} \quad \text{for } t \ge 0 \tag{B-5}$$

$$\text{for } a > p: \quad y_{pa}(t) = (1-t)^{p/(p-a)} \quad \text{for } t \ge 0.$$

The relation (B-3) is an equality when $p > 1$ and $y(t) = cy_{pab}(|dt+e|)$ where $y_{pab}(t) = u$ is defined by the equation (for $t \ge 0$):

$$t = \int_u^1 \frac{ds}{\left[s^a(1-s^b)\right]^{1/p}} \qquad (0 \le u \le 1)\ . \tag{B-6}$$

y_{pab} is monotone decreasing with time. For $a \ge p$ it is always positive; for $a < p$, $y_{pab}(t) = 0$ for $t > t_o$, where

$$t_o = \int_0^1 \frac{ds}{\left[s^a(1-s^b)\right]^{1/p}}\ . \tag{B-7}$$

Sz.-Nagy has given an example: $a = b = 1$, $p = 2$. In this case he claims that

$$y_{211}(t) = \begin{cases} \cos^2(t/2) & \text{for } 0 \le t \le \pi \\ 0 & \text{for } t > \pi \end{cases}\ . \tag{B-8}$$

The values of t are seen to satisfy (B-7). To satisfy (B-6), the function must be the solution of the differential equation:

$$\frac{du}{dt} = -\left[u^a(1-u^b)\right]^{1/p} \quad . \tag{B-9}$$

For $a = b = 1$, $p = 2$, one sees that $\cos^2(t/2)$ is indeed a solution of (B-9)

A case of interest to this dissertation is $a = b = p = 2$. For this case (B-9) becomes:

$$u' = -u(1-u^2)^{1/2} \quad . \tag{B-10}$$

A solution of (B-10) is:

$$u(t) = \text{Sech } t \; . \tag{B-11}$$

Since $a = p$, this function yields equality in (B-3) for all $t \geq 0$. Also, since p is an even number and Sech t is even in t, J_{a+b}, J_a, and K_p are all even in t, so if equality in (B-3) holds for $0 \leq t < \infty$, it must hold for $-\infty < t \leq 0$, i.e., for all t. Hence, the hyperbolic secant function for $-\infty < t < \infty$ or $t \geq 0$ (and any scaled or translated version thereof) makes (B-3) an equality if $a = b = p = 2$. The Sech function, incidentally, has another interesting property. Like the Gaussian, it is an eigenfunction of the Fourier transform.

APPENDIX C.

THE ALPHA MOMENT

It would appear that the moment

$$\alpha_u^{(1)} = \int t^2 |u'(t)|^2 \, dt = (1/2\pi) \int \omega^2 |U'(\omega)|^2 \, d\omega \qquad \text{(C-1)}$$

is of some importance as a signal parameter in the design of wideband waveforms for radar and sonar (Chapter III). E. L. Titlebaum has thus investigated some of this moment's properties. Having found these properties, Titlebaum realized that they were the same as those of time-bandwidth product. That is, the alpha moment has the same characteristics as the $D_\omega^2 D_t^2$ product used to express the standard uncertainty principle for a function and its Fourier transform. One might have expected such a result because of the two different ways of writing the Schwarz inequality for the moment:

$$\int tu(t)u^{*\prime}(t)dt = (1/2\pi) \int \omega U'(\omega)U^*(\omega) \, d\omega \, . \qquad \text{(C-2)}$$

That is,

$$\left|(1/2\pi) \int \omega U^*(\omega)U'(\omega) \, d\omega\right|^2 \leq \begin{cases} (1/2\pi) \int \omega^2 |U'|^2 d\omega \cdot (1/2\pi) \int |U|^2 d\omega \\ (1/2\pi) \int \omega^2 |U|^2 d\omega \cdot (1/2\pi) \int |U'|^2 d\omega \end{cases}$$

or, for unit energy signals,

$$\left|(1/2\pi)\int \omega U^*(\omega)U'(\omega)\,d\omega\right|^2 \le \begin{cases}\alpha_u^{(1)} \\ D_\omega^2 D_t^2\end{cases} . \qquad \text{(C-3)}$$

If $u(t) = a(t)e^{j\theta(t)}$, then

$$\int tu(t)u^{*\prime}(t)\,dt = \int ta(t)a'(t)\,dt - j\int t\theta'(t)a^2(t)\,dt$$

where $\int taa'dt = -\int taa'dt - 1$, or $\int taa'dt = -1/2$,

so that the left side of (C-3) becomes

$$\left|(1/2\pi)\int \omega U^*(\omega)U'(\omega)d\omega\right|^2 = 1/4 + \left[\int t\theta'(t)a^2(t)\,dt\right]^2 . \qquad \text{(C-4)}$$

E. L. Titlebaum's results are as follows:

If u(t) has unit energy, and $\alpha_u^{(n)} = \int t^{2n}\left|u^{(n)}(t)\right|^2 dt$, then

1. $\alpha_u^{(n)} \ge (n - 1/2)^2 \alpha_u^{(n-1)} \ge 1/4$.

2. $\alpha_u^{(n)}$ has time-frequency symmetry:

$$\int t^{2n}\left|u^{(n)}(t)\right|^2 dt = (1/2\pi)\int \omega^{2n}\left|U^{(n)}(\omega)\right|^2 d\omega .$$

3. $\alpha_u^{(n)}$ is invariant under the transformation $u(t) \rightarrow s^{1/2} u(st)$.

The properties for $\alpha_u^{(1)}$ follow trivially from (C-1) to (C-4). But the generalized properties for $\alpha_u^{(n)}$ are more difficult to derive. As already mentioned, these properties also apply to the time-bandwidth product $D_\omega^2 D_t^2$.

The $\alpha_u^{(1)}$ moment is also indicative of narrowtimeness and narrowbandedness (the implications of which are discussed in Chapter III). Defining

$$y(t) = tu(t) , \tag{C-5}$$

one finds that

$$J_2 \equiv \int |y|^2 dt = D_t^2 \tag{C-6}$$

and

$$K_2 \equiv \int |y'|^2 dt = \alpha_u^{(1)} \tag{C-7}$$

so that Sz.-Nagy's inequality gives:

$$\alpha_u^{(1)} \geq \frac{\left[\max_t |tu(t)|\right]^4}{D_t^2} . \tag{C-8}$$

Similarly, if $y(\omega) = \omega U(\omega)/(2\pi)^{1/2}$, (C-9)

then $J_2 = D_\omega^2$

$$K_2 = \alpha_u^{(1)} \tag{C-11}$$

and Sz.-Nagy's inequality gives:

$$\alpha_u^{(1)} \geq \frac{\left[\max_\omega |\omega U(\omega)|\right]^4}{(2\pi)^2 D_\omega^2} \quad . \tag{C-12}$$

The quantities on the right-hand sides of (C-8) and (C-12) are indicative of narrowtimeness and narrowbandedness, respectively. To demonstrate this, one can assume a band limited signal with support only on the interval $[\omega_o - W/2, \omega_o + W/2]$, for which

$$D_\omega^2 = (1/2\pi)\int \omega^2 |U(\omega)|^2 d\omega \leq (1/2\pi)\left[\max_\omega |\omega U(\omega)|\right]^2 W$$

$$\text{or} \quad \frac{\left[\max_\omega |\omega U(\omega)|\right]^2}{D_\omega^2} \geq 2\pi/W. \tag{C-13}$$

$$\text{Thus} \quad \alpha_u^{(1)} \geq \frac{\left[\max_\omega |\omega U(\omega)|\right]^2}{2\pi W} \quad . \tag{C-14}$$

But by the Schwarz inequality,

$$\omega_o^2 \equiv \left[(1/2\pi)\int \omega |U(\omega)|^2 d\omega\right]^2$$

$$\leq (1/2\pi)\int \omega^2 |U(\omega)|^2 d\omega \cdot (1/2\pi)\int |U(\omega)|^2 d\omega$$

$$\leq (1/2\pi)\left[\max_\omega |\omega U(\omega)|\right]^2 W \tag{C-15}$$

or

$$\alpha_u^{(1)} \geq \frac{\left[\max_{\omega} |\omega U(\omega)|\right]^2}{2\pi W} \geq \left[\frac{\omega_o}{W}\right]^2 \quad . \tag{C-16}$$

For a time-limited signal with support only on the interval $[t_o - T/2, t_o + T/2]$, the same sort of argument shows that

$$\alpha_u^{(1)} \geq \left[\frac{t_o}{T}\right]^2 \quad . \tag{C-17}$$

If a signal has large carrier-to-bandwidth ratio (narrowband) or large mean-time-to-time-duration ratio (narrowtime), then $\alpha_u^{(1)}$ must be large. A large $\alpha_u^{(1)}$ is thus a necessary condition for a signal to be narrowbanded or narrow in time.

APPENDIX D.

FLOW CHARTS FOR THE SIR MAXIMIZATION ALGORITHM

1. Generation and Storage of $X_{mk}(\tau, s)$.

Having defined the grid points τ_i, s_j and the orthonormal components $\varphi_n(t)$, one wishes to generate and store all possible inner products at each grid point:

$$X_{mk}(\tau_i, s_j) = \int_{\max\{0, s\tau\}}^{\min\{T, s(T+\tau)\}} \varphi_k^*(t)\, \varphi_m[(t/s_j) - \tau_i]\, dt$$

$$= XX(I,J,M,K) \ . \qquad \text{(D-1)}$$

In all cases considered here,

$$\varphi_n(t) = (2/T)^{1/2} \sin(n\pi t/T) \ . \qquad \text{(D-2)}$$

For a large number of grid points and/or components, the XX(I,J,M,K) are best generated via the fast Fourier transform. But since the examples here are meant merely as simple prototypes, the problem was restricted to only five basis components and a hundred grid points. The routine consists of 2500 integrations (25 possible inner products between the five components at each of 100 grid points). The results were stored on 250 cards, to be used in the main SIR optimization program with different clutter distributions. The approximate cost of this part of the routine was $9.00.

2. Main SIR Routine.

Flow Chart:

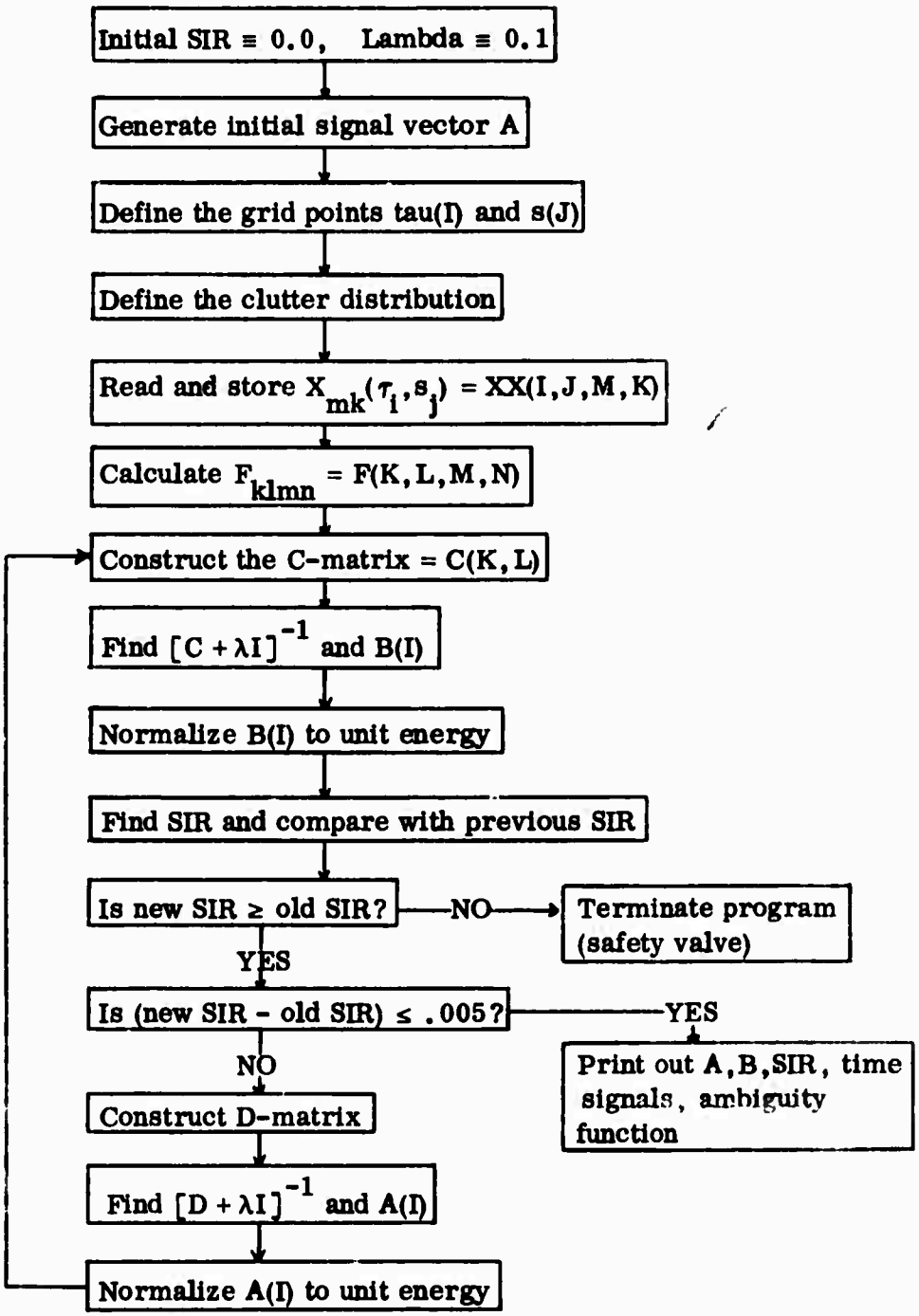

In order to graphically display the time signals, the program used line printer routine TWOPL, written by Dr. H. Voelcker, Electrical Engineering Department, University of Rochester. Other borrowed subroutines were MATEQ and SIMP, University of Rochester library programs adapted from IBM subroutines for matrix inversion and integration.

Approximate cost for each clutter distribution: $2.00.

3. Generation of the Analytic Signal's Moments.

Flow Chart:

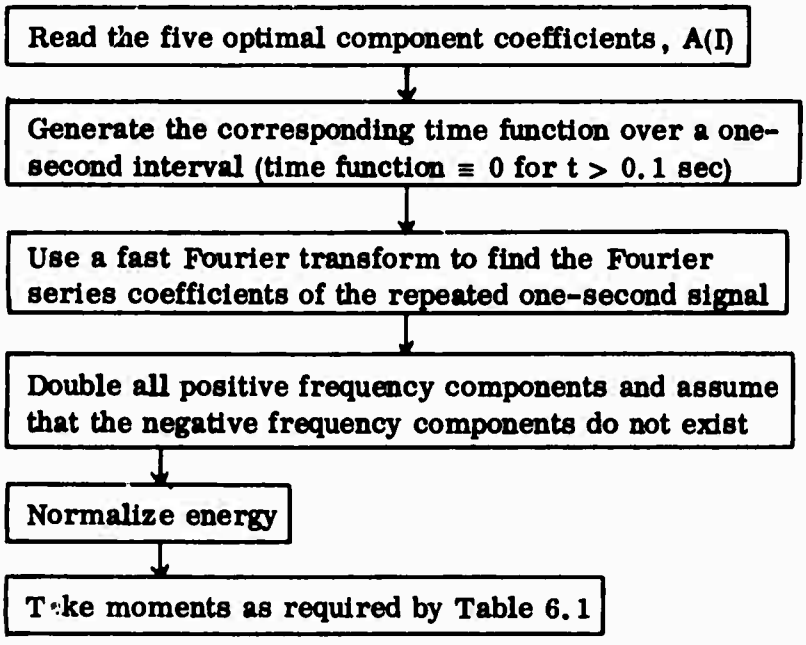

The FFT routine was written by A. Requicha, a graduate student in the Electrical Engineering Department, University of Rochester. It is based on an algorithm by Cooley, et al [59]. Advice on the fine points of the FFT was obtained from L. R. Morris. Approximate cost: $0.65.

Security Classification

DOCUMENT CONTROL DATA - R & D

(Security classification of title, body of abstract and indexing annotation must be entered when the overall report is classified)

1 ORIGINATING ACTIVITY *(Corporate author)*

University of Rochester
Department of Electrical Engineering
Rochester, New York

2a. REPORT SECURITY CLASSIFICATION

Unclassified

2b. GROUP

3 REPORT TITLE

Methods of Wideband Signal Design for Radar and Sonar Systems

4. DESCRIPTIVE NOTES *(Type of report and inclusive dates)*

Dissertation

5. AUTHOR(S) *(First name, middle initial, last name)*

Richard A. Altes

6 REPORT DATE	7a. TOTAL NO. OF PAGES	7b. NO. OF REFS
1970	269	

8a. CONTRACT OR GRANT NO.	9a. ORIGINATOR'S REPORT NUMBER(S)
66001-69-C-1510	
b. PROJECT NO.	
c.	9b. OTHER REPORT NO(S) *(Any other numbers that may be assigned this report)*
d.	

10. DISTRIBUTION STATEMENT

11. SUPPLEMENTARY NOTES	12. SPONSORING MILITARY ACTIVITY
Descriptors: Sonar Signals, Radar Signals, Optimization Techniques, Doppler Effect	NASA and Naval Undersea Research and Development Center, San Diego, California

13. ABSTRACT

DD FORM 1 NOV 65 1473 (PAGE 1)

S/N 0101-807-6801

Security Classification

Security Classification

14 KEY WORDS	LINK A		LINK B		LINK C	
	ROLE	WT	ROLE	WT	ROLE	WT

DD FORM 1 NOV 65 1473 (BACK)

(PAGE 2)